Single-end Reflectometric Measurements of Polarization - Mode Dispersion in Single-Mode Optical Fibres

Samuel Kofi Fosuhene

Submitted to the Faculty of Science, Nelson Mandela Metropolitan University in Fulfilment of the requirements for the degree of

PHILOSOPHIAE DOCTOR

Promotor: Prof. Andrew. W.R. Leitch

Optical fibre Research Unit, Department of Physics

Nelson Mandela Metropolitan University

South Campus

Lower Ground, Building 13

6031, Port Elizabeth

SOUTH AFRICA

SEPTEMBER 2012

DECLARATION

I, **Samuel Kofi Fosuhene** with student number **208090658**, hereby declare that this thesis for the award of the Ph.D. qualification is my own work and that it has not previously been submitted for assessment to another university or for another qualification.

Signature:…….

Date:……..

To all members of the Fosuhene Family: Past, present and generations to come.

ACKNOWLEDGEMENTS

I would first of all thank Prof. Andrew W.R. Leitch, first of all for accepting me as his PhD student and for all his support and assistance. Next I would like to thank Dr. T.B Gibbon and Dr. D. Waswa for their encouragements and direction. I also owe a debt of Gratitude to Prof. P.K. Buah-Bassuah of University of Cape Coast Ghana for showing interest in my academic development. Many thanks to Prof. Andrea Galtarossa and Dr. Luca Palmirei for the warm reception and academic insight offered me during my research visit to the Department of Information Engineering, University of Padova in 2009. I thank also Ms. Alter Beer of the dean's office for her great assistance.

I would like to thank all my Colleagues here at the OFRU, Romeo and Kennedy, many thanks. I thank former colleagues, Vitalis Musara , Winston Irreeta and Jesman Changundega for their kindness and support during their stay with us,

Family is very important. I therefore thank my father Nana Fosuhene, my mother Martha Fosuhene, my sisters, Emelia, Patrica and Eleanora and finally my brother Frank. I thank you for your love, prayers and support.

For financial support, I acknowledge: African Laser Centre (ALC), Telkom South Africa (Pty) Ltd., National Laser Centre (NLC), National Research Foundation (NRF), the Technology and Human resources for Industry Program (THRIP), Dartcom (Pty) Ltd and Research Capacity Office NMMU.

My stay here in Port Elizabeth here would have been impossible without friends and Family. I acknowledge the Osei Family of Humewood, Mr. Osei Ofosu, Jacqueline Ofosu and Kwame Ofosu. I would also like to thank my friends Eric Akuffo, George Oppong, Fuseina Mohammed, Evelyn Badasu and Fred Charway.

Last, but not the least Special thanks to Harriet Adwoa Kyerewaa Ofori for her patience, love and prayers.

Samuel Kofi Fosuhene

Port Elizabeth

(s208090658@live.nmmu.ac.za)

SUMMARY

In this thesis two novel single-end methods are applied to measure and characterize polarization mode dispersion in single mode optical fibres. Polarization mode dispersion (PMD) is an important factor negatively affecting the successful implementation of high speed long haul optical fibre networks operating at bit rates of 10Gb/s and above. PMD measurements are thus important for quality control during manufacturing and cabling processes. It is also useful for network operators planning to upgrade bitrates in existing networks to 10Gb/s and beyond. In an optical fibre link, sections with particularly high PMD may act to increase the entire PMD of the link. Identifying and replacing such sections can greatly reduce the PMD of the link.

PMD measurements can be forward or single-end. In forward measurements, both ends of the fibre are used for input and detection. In single-end configuration, only one end of the fibre is used. For this reason, single-end measurements are more practical for the field where fibre ends are situated several kilometres apart. Single-end techniques can be implemented with a continuous wave for non-local PMD measurements (by Fresnel reflection). If a pulsed wave is used, local measurements can be achieved (by total power due to Rayleigh scattering).

Two single-end schemes, one based on Fresnel reflection and the other due to Rayleigh scattering have been applied to measure non-local and local PMD of standard single mode optical fibres. For the non-local PMD measurements, the general interferometric technique (GINTY) was modified to operate in a round-trip configuration. In this configuration, the fibre was treated as a concatenation of two identical fibre segments. Three different sets of fibres were investigated, each set representing a particular mode coupling regime. For polarization maintaining fibres, (PMFs), with no mode coupling, a factor of two was found between forward and single-end measurements. For long single mode fibres in the long length regime, the factor was 1.4. For a combination of PMF and single mode fibres, a factor of 1.6 was obtained. The method which is accurate, repeatable, low cost and robust is very suitable for field applications.

The second method is the polarization optical time domain reflectometric (P-OTDR) technique. This technique performs local birefringence measurements by measuring the evolution of the states of polarization (SOP). The birefringence information from such measurements was extracted and analysed to characterise four different fibres. Beat lengths and correlation lengths extracted from the P-OTDR were used to calculate the differential

group delay (DGD) of the fibres. Next an expression for the root-mean-square differential group delay was derived and applied to the birefringence measurements to calculate the DGDs at a single wavelength. This method which operates at a single wavelength has a huge advantage. Firstly it is able to measure completely all the fibre characteristic parameters. Secondly it can measure mean DGD, root mean square DGD and instantaneous DGD. A plot of instantaneous DGD vs. length enables one to identify and eliminate sections with particularly high DGD. Finally since the P-OTDR system operates with a single wavelength, real time monitoring of PMD is possible via multiplexing. The results obtained are repeatable, accurate and are in good agreement with the standard Jones Matrix Eigenanalysis (JME) technique.

Table of Contents

CHAPTER 1

INTRODUCTION

It has always been the desire of humans to communicate and do so in the fastest and most efficient way possible. This need has always driven scientists and engineers to conduct research into various ways and methods of communication- from fire, electricity, through microwave, radio and currently light. The motivation is to increase speed, capacity/size of information to be transmitted in the shortest time possible. The desire also is to send the information to the furthest distance at minimum loss and cost.

A long standing observation is that the industrial development of a country is closely dependent on the country's communications infrastructure (Androuchko *et al.*, 1990). According to Hardy (1980) and Hudson (1987) while economic growth contributes to telecommunications investment, telecommunications growth also makes a small but significant contribution to economic growth. The clear implication is that investment in telecommunications should facilitate economic growth. Investment in the communications infrastructure of a nation also implies the modernization of the transmission systems that form the existing communication networks.

Every communication system is made up of three parts, a transmitter, a medium of transmission and a receiver. The invention of the laser in the 1960s aroused the interest of scientists and engineers to explore its coherent nature for optical communication. Following this development there was the need to develop a low loss waveguide to carry the light signal, as well as detectors and other passive optical components. One major problem for developing practical optical communications systems was the lack of a good transmission medium. Many approaches for optical systems were suggested, such as sending laser through air, confocal optical waveguides with regularly spaced lenses, hollow optical waveguides made of reflective pipes, and dielectric optical fibres (Ming-Jun *et al.*, 2008, 2009). Kao and Hockham (1966) proposed for the first time that glass fibre could be a good medium for the transmission of information. They predicted that the fundamental limit for practical optical communication for transparent glass was 20dB/km. The optical fibre, which is a thin, transparent, cylindrical dielectric material (mostly made from silica) was identified as a carrier waveguide for optical communications. Kapron *et al* (1970), produced a low loss glass fibre with a 20dB/km attenuation in 1970. Following this development, optical fibre

technology advanced rapidly. In 1979, Miya *et al.* demonstrated that an attenuation of 0.2dB/km in fibres was possible.

The rapid evolution of optical fibre over the past three decades has been closely linked with developments in optical components and transmission systems. It therefore stands to reason that the driver for the evolution would alternate between fibre capabilities and system performance. A key example of this linkage is the development of light sources, modulation formats and detectors. Optical fibres have developed from multimode in the 1970s, single - mode in the 1980s and 1990s to bend insensitive fibres today (Li 2008). Optical sources have evolved from Light emitting diodes (LEDs) and semiconductor lasers to vertical-cavity surface-emitting lasers (VCSLs) and distributed feed-back (DFB) lasers, corresponding to ordinary binary non-return-to-zero (NZR) and return-to-zero (RZ) to more advanced forms such as carrier-supressed-return-to-zero (CSRZ) and dense-quadrature-phase-shift-keying (DQPSK). Another major milestone was the development of the (EDFA) erbium-doped fibre amplifier (Mears, 1987). This made it possible to increase carrier capacity and transmission distance. More channels can now be transmitted through dense wavelength division multiplexing (DWDM). Transmission rates of 10 and 40Gb/s are now in operation with next generation systems expected to run at 100Gb/s and beyond. Indeed, transmissions of 432GB/s over a distance of 400km in a standard single-mode fibre have been recently reported (Dong, *et al.* 2011).

The above developments have been driven by demand for high speed high capacity transmission by network operators and customers for many applications. Optical communication is the choice because it satisfies these demands and even more. It offers transmission rates close to the speed of light, high bandwidth, adequate security as well as lower attenuation rates per kilometre compared to other communication systems. Optical communication has been embraced with applications ranging from data, internet, voice and live video just to mention a few. Long haul applications have brought the world closer. Today people can run companies and attend board meetings from any part of the globe via video conferencing. Internet lectures for educational purposes, mobile and internet banking as well as live video streaming for entertainment are but a few of the benefits of optical communications.

In the developed world, the systems mentioned above are already in place. The challenge now is for the developing world and Africa in particular to tap into this technology to harness its full benefits. In order to catch up, developing countries might be thought of as requiring four types of optical systems (Androuchko, 1990):

- High capacity systems for junction networks between exchanges in cities or large towns where explosive population growth is producing high demand for communications.

- High capacity systems from exchanges to link other systems such as radio and satellite earth stations sited some distance away from the exchange station to attain the best transmission path.

-High capacity systems for trunk networks where installation costs are not prohibitive and the large traffic density ensures competitiveness of fibre optics over other media.

-Low capacity, long distance systems for use in urban and rural areas of low population density. These would offer a better quality service with the possibility of expansion to higher density or enhanced service, but with a considerable initial cost.

Like any communication system, optical communications systems must meet certain basic criteria including network upgradability. Upgradability of optical communications systems has posed many challenges. In the early years the challenge was signal attenuation and chromatic dispersion. The problem of chromatic dispersion has been addressed by the introduction of dispersion shifted fibres (DSFs) and dispersion compensating fibres (DCFs). Signal attenuation has also been addressed by improvements in laser technology and components as stated in the previous paragraphs.

Today, the major challenge limiting network upgradability of long haul optical fibre transmission systems for operations at 10Gb/s and beyond is polarization mode dispersion (PMD). This phenomenon has become important because most existing optical fibre networks especially in Africa include legacy fibres (ITUT-G.652, G.653 and G.655) which were laid a few years ago when demand for bandwidth was low and fibre manufacturing systems were not advanced enough. Although fibre manufacturing technologies have again been used to reduce polarization mode dispersion to below 0.1ps/km$^{1/2}$, it is expensive to replace legacy fibre plants. It has therefore fallen on network designers and operators to study and manage the effect of PMD.

Under ideal conditions, a pulse of light entering a perfectly circular fibre splits into two polarization states which are expected to travel with the same speeds through the fibre. This however does not happen in reality and the two polarization modes propagate with different speeds. The difference in arrival times, which is known as the differential group delay is the magnitude of polarization mode dispersion (PMD). PMD causes the spreading of the optical pulse and the consequent distortion of transmitted data at the receiver. Polarization mode dispersion originates from random birefringence and mode coupling. Birefringence causes a variation of refractive index in a waveguide with a corresponding variation in the propagation speed of light. Birefringence may be caused by several random intrinsic and extrinsic factors. An example of an intrinsic cause of birefringence is core asymmetry which may happen during manufacturing. External stress due to bending and twists during cabling and deployment are some of the causes of extrinsic birefringence. Within the optical fibre, there may exist random perturbation points where interchanges between the two propagation modes of previous segments may occur. This phenomenon known as mode coupling also contributes to PMD. Environmental factors such as temperature and vibrations caused by wind especially on aerial fibres may also cause birefringence resulting in PMD.

To increase capacity on legacy fibres, methods including PMD compensation have been proposed and implemented (Gibbon, 2008). Most PMD compensation schemes require monitoring of the states of polarization of the propagating pulse. These rates of evolution of the principal states may occur at speeds which may be difficult to track. For these and other reasons PMD compensation schemes are difficult to achieve and implement.

It is known that, the total polarization mode dispersion of an optical fibre link may be affected by sections within the link with particularly high contributions (Visser *et al*. 2003). Locating and replacing such ‘bad’ sections offers a more practical and cost effective solution to the problem.

This thesis addresses the problem of PMD by applying practical single-end reflectometric techniques. The aim is to characterize fibre PMD and identify the factors that cause it. Single-end techniques are advantageous because they make use of only one end of the fibre and both the transmitter and detector are located at the same point. This makes them practical and cost effective, especially for the field where fibre ends are usually separated by several kilometres. The thesis discusses two single-end methods for characterizing PMD, which are

suitable for both the laboratory and the field measurements of PMD. The first method, which is a variation of the standard generalized interferometric method (GINTY), is capable of measuring the mean DGD of an entire optical fibre link.

The second method, is the polarization sensitive reflectometric (P-OTDR) technique, and is able to completely characterize an optical fibre. By measuring the round-trip birefringence of a fibre as a function of distance, the total information about the fibre is derived. It is able to measure fibre parameters such as beat length, correlation length and differential group delay can be measured from a single P-OTDR trace. Mean DGD, instantaneous DGD and root mean square DGD are measured at a single wavelength. Distributed measurements of instantaneous DGD as a function of distance provides information about sections of the fibre where PMD is particularly high.

This thesis is organized as follows:

Chapter 2 describes the nature of light and propagation through an optical fibre including concepts of polarization, Stokes and Jones vectors, birefringence and loss mechanisms, such as dispersion and nonlinear effects. In chapter 3 polarization mode dispersion and birefringence effects are discussed. The chapter also considers the fundamental principles underlying various PMD measurement techniques. Chapter 4 introduces the concepts of reflectometric measurement techniques. A theoretical overview of reflectometric measurement techniques and their advantages are presented. The main experimental results of this research are presented in chapters 5 to 7. In chapter 5, a single-end interferometric technique for measuring the total PMD of an entire link is presented. In the chapter, three different fibre types namely, polarization maintaining fibres, spooled and cabled fibres are analysed using the single-end inteferometric technique. In chapter 6 characterization of optical fibres using P-OTDR is presented. In the chapter, four optical fibres are completely characterized in terms of beat length, correlation length and DGD. Measurements of instantaneous and root mean square differential group delay using P-OTDR are presented in chapter 7. The concluding remarks of this research work are presented in chapter 8.

CHAPTER 2

LIGHT PROPAGATION AND OPTICAL FIBRE CHARACTERISTICS

2.1 Nature of light

Light is an electromagnetic wave which propagates as a vector field, with the electric and magnetic fields vibrating in a direction perpendicular to the direction of the advancing wave (figure 2.1). The relationship between the propagating electric and magnetic fields is given by a set of equations known as Maxwell's equations. For a linear, isotropic, lossless dielectric with no charges and currents, the set of Maxwell's equations are given by,

$$\nabla \times \boldsymbol{E} = -\frac{\partial \boldsymbol{B}}{\partial t} \tag{2.1}$$

$$\nabla . \boldsymbol{D} = 0 \tag{2.2}$$

$$\nabla \times \boldsymbol{H} = \frac{\partial \boldsymbol{D}}{\partial t} \tag{2.3}$$

$$\nabla . \boldsymbol{B} = 0 \tag{2.4}$$

where $\boldsymbol{D} = \epsilon \boldsymbol{H}$ and $\boldsymbol{B} = \mu \boldsymbol{H}$, $\boldsymbol{\epsilon}$ is the permittivity or dielectric constant and μ is the permeability of the medium. Equation 2.3 shows that an alternating electric field gives rise to a magnetic field. Equation 2.2 indicates the absence of magnetic charges while equation 2.4 asserts the absence of static electric field.

These equations can be decoupled to obtain new equations in terms of only magnetic and electric field by applying vector calculus to yield (Keiser, 2000);

$$\nabla^2 \boldsymbol{E} = \epsilon \mu \frac{\partial^2 \boldsymbol{E}}{\partial t^2} \tag{2.5}$$

$$\nabla^2 \boldsymbol{H} = \epsilon \mu \frac{\partial^2 \boldsymbol{H}}{\partial t^2} \tag{2.6}$$

Equations 2.5 and 2.6 are similar to the three dimensional standard wave equation of the form;

$$\nabla^2 \boldsymbol{\rho} = \frac{1}{v^2} \frac{\partial^2 \boldsymbol{\rho}}{\partial t^2} \tag{2.7}$$

where $v = c/n$ is the propagation velocity in the medium of refractive index n with c being the speed of light in vacuum.

Comparing terms of equation 2.7 with equations 2.5 and 2.6, implies that an electromagnetic wave propagates in a medium with a velocity given by,

$$v = \frac{1}{\sqrt{\epsilon\mu}} \tag{2.8}$$

Considering a waveguide with a varying refractive index n in the x and y directions (but fixed in the z-direction of propagation), the solutions to equation 2.5 for a propagating electromagnetic wave is of the form:

$$E(r,t) = e^{i(\beta z - \omega)t} \tag{2.9}$$

where $\beta(\omega) = \frac{\omega}{c} n(\omega)$ is the propagation constant and ω is the angular frequency of the propagating light.

Substituting equation 2.9 into 2.5 and simplifying yields:

$$\left(\frac{\partial^2}{\partial x^2} + \frac{\partial^2}{\partial y^2}\right) E(x,y) + KE(x,y) = 0 \tag{2.10}$$

where, $K = (\epsilon\mu\omega^2 - \beta^2)$.

Equation 2.10 is a scalar three dimensional equation whose solution may either be exponential or sinusoidal varying depending on the sign of the factor K. According to eq.2.10, the frequency of the propagating light and the refractive index profile of a waveguide are important parameters, since they determine the sign of K. This analysis will be applied later in section 2.3.2 to explain the concept of guided modes in an optical fibre.

2.2 Polarization concepts

The inclination of the directions of the vibration of an electromagnetic field is called its polarization. The interaction between light and a medium may cause a change in the characteristics of the medium and the light itself. These changes can be observed by observing the difference in the polarization properties of the light before and after the interaction. It is therefore important to describe light in terms of its polarization.

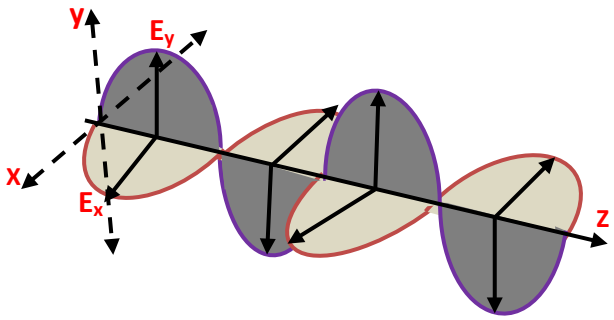

Figure 2.1: Plane wave propagating as a superposition of two orthogonal components E_x and E_y.

As depicted in figure 2.1, the electric field of a plane polarized light wave $E(z,t)$ propagating in the z direction may be represented by the superposition of the two orthogonal sinusoidal time varying components, E_x and E_y given by,

$$E(z,y) = E_x(z,t) + E_y(z,t) \tag{2.11}$$

The two orthogonal electric field components in the x and y directions are given by,

$$E_x(z,t) = E_{ox}\cos(\beta(\omega)z - \omega t + \delta_x)\hat{x} \tag{2.12}$$

$$E_y(z,t) = E_{oy}\cos(\beta(\omega)z - \omega t + \delta_y)\hat{y} \tag{2.13}$$

where E_{ox} and E_{oy} are the amplitudes and δ_x and δ_y represent the phase angles respectively.

From equations 2.12 and 2.13, the equation of the path traced out by the tip of the electric field vector z=constant can be deduced. To achieve this we substitute $\beta(\omega)z - \omega t = \tau$ into equations 2.12 and 2.13 to yield;

$$E_x(z,t) = E_{0x}(cos\tau cos\delta_x - sin\tau sin\delta_x) \tag{2.14}$$

$$E_x(z,t) = E_{0x}(cos\tau cos\delta_x - sin\tau sin\delta_x) \tag{2.15}$$

Simplifying and rearranging eq. 2.14 and 2.15 gives;

$$\left(\frac{E_x}{E_{ox}}\right)^2 + \left(\frac{E_y}{E_{oy}}\right)^2 - 2\frac{E_xE_y}{E_{ox}E_{oy}}\cos(\delta_y - \delta_x) = sin^2(\delta_y - \delta_x) \tag{2.16}$$

where $\delta = \delta_y - \delta_x$ is the relative phase difference between the two orthogonal electric field vectors E_x and E_y.

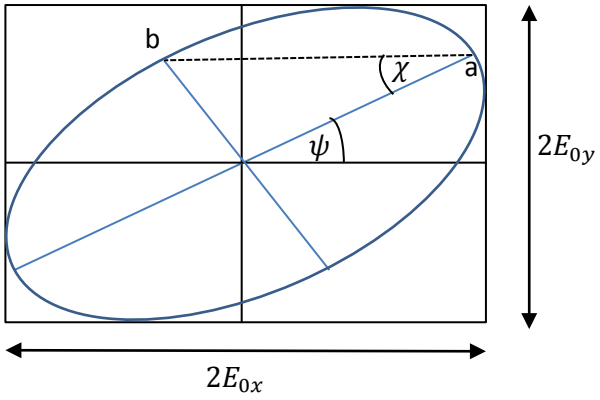

Figure 2.2: Polarization ellipse for which the states of polarization are determined by χ and ψ.

Figure 2.2 shows the behaviour of equation 2.16. It represents an ellipse inscribed in a rectangle with sides $2E_{ox}$ and $2E_{oy}$ on the x and y axes respectively. Hence in the general case, the tip of the electric field of a propagating monochromatic light wave traces out an ellipse in the x-y pane (z=constant). Such a wave is called an *elliptically* polarized wave.

The orientation of the electric field is known as the *state of polarization* (SOP) of the light. The nature of the polarization ellipse depends on the amplitudes E_{ox} and E_{oy} and the relative phase difference, $\delta = \delta_y - \delta_x$ between the two orthogonal components. For an isotropic medium, as ωt varies between $0 - 360^o$, the phase difference δ, causes the shape of the ellipse to change. While tracing the elliptical path, the tip of the electric field vector rotates either clockwise or anticlockwise. These two cases are defined as *right-handed polarization* (clockwise when facing the light source) and *left-handed polarization* (anticlockwise when facing the source). These directions are defined by the sign of the relative phase difference δ. For $0 < \delta < 180^o$, the light exhibits *right-handed polarization*. Similarly, the light exhibits *left-handed polarization* for the interval $180^o < \delta < 360^o$. For integral multiples of the relative phase difference, ($\delta = 180^o m,\ m = 0, \pm 1, \pm 2, ...$) the light is *linearly polarized*. A special case of *circular polarization* occurs when the amplitudes E_{ox} and E_{oy} are equal (E_{ox}=E_{oy}) and the relative phase difference $= 180^o\ m/2$, m= ±1,±3, ±5.. (Akhmanov 1997).

The various states of polarization are illustrated in figures 2.3-2.5, where the amplitudes E_{ox} and E_{oy} have been set to unity for simplicity.

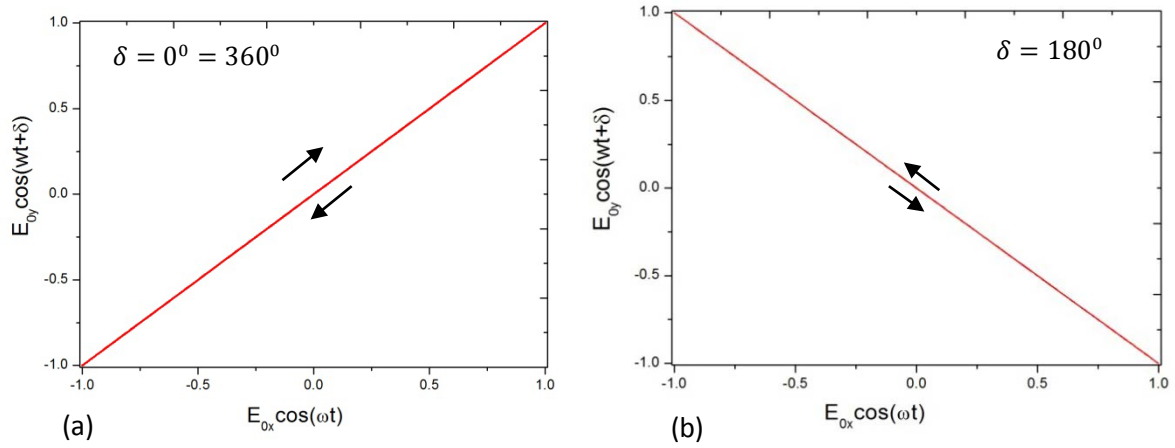

Figure 2.3: (a) Linear states of Polarization for even integral multiples of the relative phase, and (b) odd multiples.

Figure 2.3 shows two cases of linear polarization. In figure 2.3(a), the relative phase difference between the two orthogonal components, $\delta = 0^0 = 360^0$ while in (b), $\delta = 180^0$. For $\delta = 180^0 m$, where m= ± 1, ± 2,.., the path traced by the tip of the electric field is linearly polarized and its orientation is like that of figure 2.3 (a) if m is even. If m is odd, the path traced out is linear and its orientation is like that of figure 2.3(b).

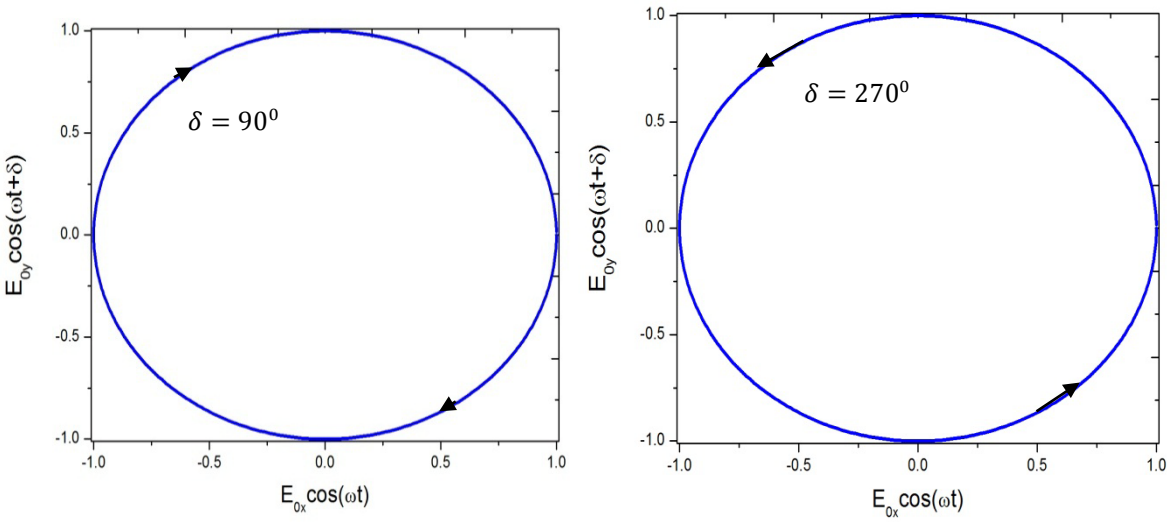

Figure 2.4: Circularly polarized light; (a) right circular polarization, (b) left circular polarization

Figure 2.4 shows two cases of circular polarization, (a) right circular polarization and (b) left circular polarization. The polarization is right circular if $\delta = 90^0 + 2m(180^0)$ and left circular, if $= -90^0 + 2m(180^0)$, m = ± 1, ±3, ±5…

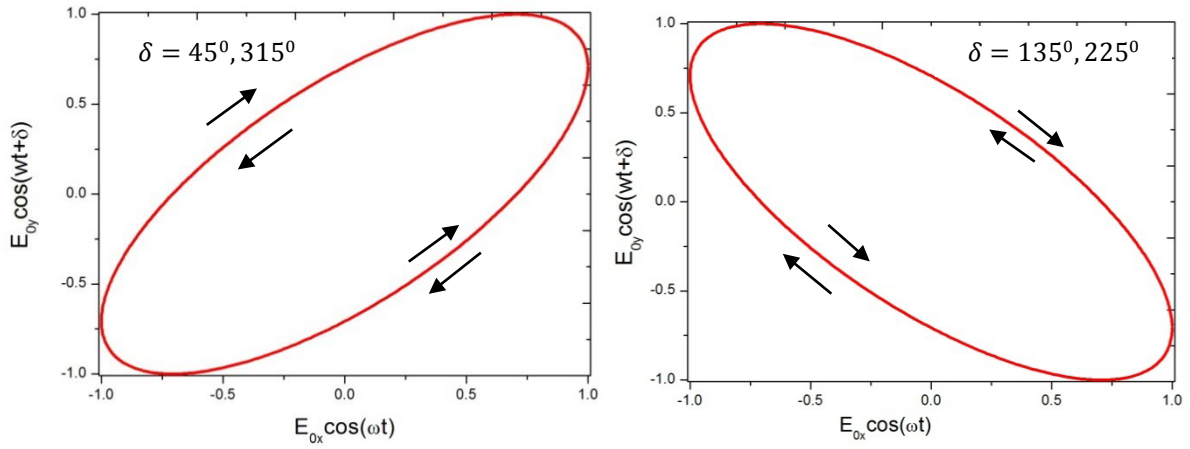

Figure 2.5: Elliptical polarization states; (a) clockwise of the electric field for $\delta = 45^0$ and anticlockwise rotation for $\delta = 315^0$, (b) clockwise rotation of the electric field for $\delta = 135^0$ and anticlockwise rotation for $\delta = 225^0$.

Figure 2.5 depicts the general case of the paths traced by the electric field. The path is generally elliptical for any other relative phase differences between the two orthogonal electric fields. Figure 2.5(a) shows selected examples elliptical polarization states, for $\delta = 45^0, 315^0$ and $135^0, 225^0$. The orientation of the ellipses for the phase angles $\delta = 45^0, 315^0$ are the same but their directions of rotation different, clockwise for 45^0, and anticlockwise for 315^0. The same situation occurs for phase angles 135^0 (clockwise rotation) and 225^0 (anticlockwise rotation).

The concept of polarization ellipse is therefore useful for describing light in all the possible polarization states. It has been shown in the examples above that the light traces out an ellipse in the x-y plane (z=0) as it propagates in the z-direction. The ellipse is defined by the magnitudes of the orthogonal electric fields and their phase difference.

2.2.1 Jones vector formalism

The concept of polarization has been dealt with in an isotropic medium. However in many real life situations, such as an optical fibre, light propagation may be complex. The refractive index of the fibre may vary along the fibre length. It is therefore prudent to use simplified

mathematical formalisms that accounts for the changes in polarization of the light as it propagates through the medium.

Equations 2.11-2.13 can be rewritten in an exponential complex forms as:

$$E(z,t) = \hat{e}_x E_x(z,t) + \hat{e}_y E_y(z,t) \tag{2.16}$$

where the two orthogonal time dependent components of the electric field are given by;

$$E_x = E_{0x} e^{i(\beta(\omega)z - \omega t + \delta_x)} \tag{2.17}$$

$$E_x = E_{0y} e^{i(\beta(\omega)z - \omega t + \delta_y)} \tag{2.18}$$

In equations 2.16-2.18 $\hat{e}_x$ and $\hat{e}_y$ are unit vectors in the x and y directions respectively, E_{0x} and E_{0y} represents the amplitude, and δ_x and δ_y are the phase angles. The z and t dependence on E have been dropped for simplicity.

Substituting equations 2.17 and 2.18 into equation 2.16 yields

$$E = \left[\hat{e}_x E_{0x} e^{i\delta_x} + \hat{e}_y E_{0y} y\right] e^{i(\beta(\omega)z - \omega t)} = E_0 e^{i(\beta(\omega)z - \omega t)} \tag{2.19}$$

where E_0 is the complex amplitude for the polarized wave. The states of polarization are completely described by the relative amplitudes and the phases of the two orthogonal components. According to equation 2.19, the complex amplitude can be written in normalized vector form as (Jones, 1941);

$$E_0 = \begin{bmatrix} E_{0x} \\ E_{0y} \end{bmatrix} = \frac{1}{\sqrt{E_{0x}^2 + E_{0y}^2}} \begin{bmatrix} E_{0x} e^{i\delta_x} \\ E_{0y} e^{i\delta_y} \end{bmatrix} \tag{2.20}$$

Jones vector notation may be used to describe different linear states of polarization. An example is horizontally polarised light for which $E_{0x} = A, E_{0y} = 0$ and $\delta_x = 0$; in this case, the Jones vector is given by $E_0 = A \begin{bmatrix} 1 \\ 0 \end{bmatrix}$.

The transmission properties of a two port optical system can be described by a two-by-two Jones matrix which relates the input and output Jones vectors. The Jones formalism can be used to measure polarization dependent effects on optical systems by measuring three output Jones vectors in response to three known input stimulus linear polarizations (Derickson 1998). Jones vector formalism is limited to the description of fully polarized light.

2.2.2 Stokes vector formalism and the Poincaré sphere

It is difficult to measure the electric field of a light wave but it is easy to measure the intensity. The Stokes formalism is another method for representing the states of polarization of light in terms of its intensity. Unlike the Jones vector, it deals with both partially and totally polarized light. As indicated in figure 2.2, each polarization ellipse may be described in terms of the two angles, $0 \leq \psi \leq \pi$ and $-\pi/4 \leq \chi \leq \pi/4$. The state of polarization of a light wave with intensity E^2, having orthogonal components with amplitudes E_{0x}, E_{0y} and relative phase δ can be written in terms of the ellipse angles χ and ψ (Born, 1999). The four Stokes parameters can then be written as;

$$s_o = \frac{E^2}{E_0^2} \tag{2.21}$$

$$s_1 = \frac{E_{0x}^2 - E_{0y}^2}{E_0^2} = cos2\chi cos2\psi \tag{2.22}$$

$$s_2 = \frac{2E_{0x}E_{0y}cos\delta}{E_0^2} = cos2\chi sin2\psi \tag{2.23}$$

$$s_3 = \frac{2E_{0x}E_{0y}cos\delta}{E_0^2} = sin2\chi \tag{2.24}$$

where $E_0^2 = E_{0x}^2 + E_{0y}^2$ is the intensity of the polarized component of the light wave.

The Stokes parameters s_1 , s_2 and s_3 describe a point on the surface of a unit sphere as shown in fig. 2.6. The sphere is known as the Poincaré sphere and the three dimensional space is known as the Stokes space. The Stokes space provides a geometrical representation of the states of polarization (SOPs). Each point on the sphere represents a unique SOP. The poles represent circular polarization, while linear polarization lies on the equator. Left-handed polarization is located in the southern hemisphere while right-handed polarization is located in the northern hemisphere. For fully polarized light, $E = E_0$ and so,

$$s_o^2 = s_1^2 + s_2^2 + s_3^2 \tag{2.25}$$

For partially polarized light, $E < E_o$ and the degree of polarization (DOP) is given by,

$$DOP = \frac{\sqrt{s_1^2 + s_2^2 + s_3^2}}{s_0} \tag{2.26}$$

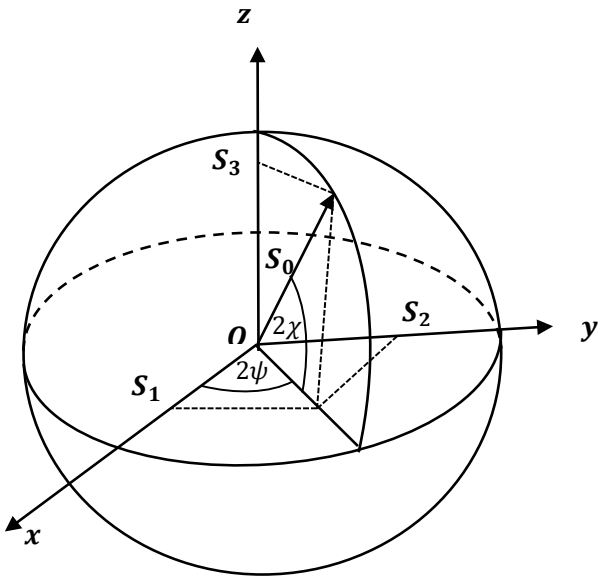

Figure 2.6: Stokes' parameters representation on the Poincaré sphere.

In agreement with equation 2.26, the light wave can exhibit various degrees of polarization. The $DOP = 1$ when the light is fully (100%) polarized. The light exhibits partial (less than 100%) polarization when the $DOP < 1$. When the $DOP = 0$, the light is not polarized (depolarized). In the case of normalized Stokes vectors, (s_1/s_o , s_2/s_o , s_3/s_0), fully polarized light will be located by a point on the surface of the Poincaré's sphere. Partially polarized light will be represented within the Poincaré sphere. The DOP is the distance between the point and the origin (O) of the Stokes space. The relationship between Stokes space and Jones space can be found in appendix A of this thesis.

2.3 The optical fibre

The optical fibre is a cylindrical waveguide usually made of silica (i.e, Glass) or plastic. It consists of a central core region surrounded by an outer cladding that has a slightly different refractive (n_1) index from that of the core (n_2) as shown in figure 2.7.

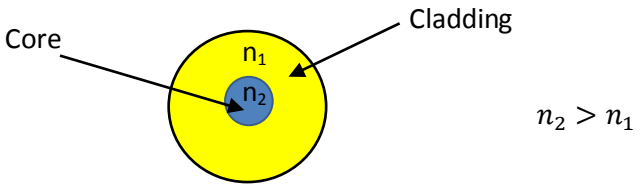

Figure 2.7: An optical fibre cross-section

The core is doped with germanium to make its refractive index slightly higher than that of the surrounding cladding. Germanium is used as a dopant because of its absorption characteristics. It absorbs less energy at 1300nm and 1500nm, which are the operating wavelengths of most optical communication systems. The difference in refractive index enables the fibre to confine light to the core for transmission according to the principles of total internal reflection.

2.3.1 Fibre geometry and light guiding requirements

Fibre types are specified and characterised by their refractive index (RI) profiles. This depends on the variation of the RI from the centre of the core to the core cladding boundary as well as the dimensions of the core and the cladding.

The propagation of light through an optical fibre can be described in terms of a set of guided electromagnetic waves known as modes of the waveguide (Keiser, 2000, p. 35). Each guided mode is a pattern of electromagnetic and magnetic field distributions that is repeated along the fibre at specific intervals. Only a certain discrete number of modes are allowed according to the homogeneous wave equation and the boundary conditions at the core cladding interfaces.

The number of allowed modes is related to the dimensions of the fibre and the operating wavelength of the fibre. In terms of the mode concept, optical fibres can be classified into single mode and multimode fibres. Ideally, single mode fibres as the name suggests transmit only one mode while multimode fibres transmit many modes. Standard single mode fibres have core diameters of 9µm and cladding diameters of 125µm (Hecht, 1999). A typical multimode fibre has a core diameter of 100µm and a cladding diameter of 140µm. Fibre transmission characteristics are also dictated by their refractive index profiles. On this basis, fibres can be classified into step index and graded index according to the refractive index variation in the core (figure 2.8). Other special fibres such as dispersion shifted (DSF) and large effective area fibres LEAF have more complex RI profiles (Li *et al*, 2008).

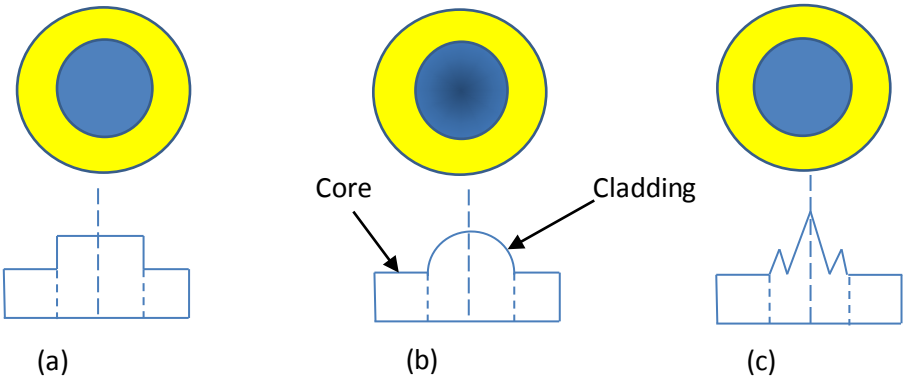

Figure 2.8: Refractive index profiles of optical fibre; (a) Step index, (b) Graded index, and (c) Dispersion shifted.

Figure 2.8 show the RI profile of some fibres. The basic difference is how the RI varies from the centre of the core to the cladding. For a step index profile as in Figure 2.8 (a), the RI is constant and changes abruptly at the core-cladding interface. For a graded index profile, the RI changes gradually from the centre of the core to the core-cladding interface as shown in Figure 2.8 (b). The graded index fibres are used to reduce material dispersion. The RI profile of the dispersion shifted fibre has been modified in the core as shown in figure 2.8 (c). Dispersion shifted fibres were developed to reduce the effects of chromatic dispersion.

2.3.2 Transmission characteristics of an optical fibre

Light is confined and transmitted in the core of an optical fibre based on the principle of total internal reflection. This is due to the difference in the refractive index of the core and the cladding, with the core having a slightly higher index than the cladding. Using the ray model and Snell's law (Ghatak, 2000), light entering the core at a critical angle θ_c will undergo multiple reflections at the core-cladding interface and hence continue to propagate in the core according to the relation;

$$\theta_c = sin^{-1}\left(\frac{n_1}{n_2}\right) \tag{2.27}$$

where n_2 is the core refractive index and n_1 is the cladding refractive index.

As discussed in Section 2.3.1, an optical fibre can support the transmission of many modes. The modes are special solutions to the boundary conditions and have the specific property

that their spatial distributions remain constant during propagation. An important waveguide parameter known as the normalised frequency or simply the V-number specifies the cut off conditions for single mode transmission. The V-number for a fibre of core diameter ɑ , core refractive index n_2, cladding refractive index n_1 which is operating at a wavelength λ is given by (Ghatak, 2000);

$$V = \frac{2\pi a}{\lambda}\sqrt{n_2^2 - n_1^2} \tag{2.28}$$

For single mode transmission, V < 2.405. According to equation 2.28, the fundamental HE_{11} mode has no cut off and only vanishes when the fibre core diameter, ɑ is zero. The V-parameter can also serve as a guide in fibre design since it captures all the fibre parameters as well as the operating wavelength. Essentially, if the operating wavelength and the refractive index difference $(n_2 - n_1)$, are known, then the parameter that can be varied to achieve single-mode or multi-mode transmission is the core diameter ɑ.

The mode theory can also be analysed using equation 2.10, which may be rewritten as;

$$\left(\frac{\partial^2}{\partial x^2} + \frac{\partial^2}{\partial y^2}\right) E(x,y) + [k_o^2 n^2(r) - \beta^2]E(x,y) = 0 \tag{2.29}$$

where $k_o^2 \equiv \omega^2\mu\epsilon = (2\pi/\lambda)^2$.

For the sake of mathematical simplicity, the solution to equation 2.29 can be solved for a planar wave guide and the results for the three identified regions are as follows (Yariv, 1997);

Region I (RI is n_1) $$\frac{\partial^2}{\partial y^2}E(x,y) + [k_o^2 n_1^2 - \beta^2]E(x,y) = 0 \tag{2.29a}$$

Region II (RI is n_2) $$\frac{\partial^2}{\partial y^2}E(x,y) + [k_o^2 n_3^2 - \beta^2]E(x,y) = 0 \tag{2.29b}$$

Region III (RI is n_3) $$\frac{\partial^2}{\partial y^2}E(x,y) + [k_o^2 n_3^2 - \beta^2]E(x,y) = 0 \tag{2.29c}$$

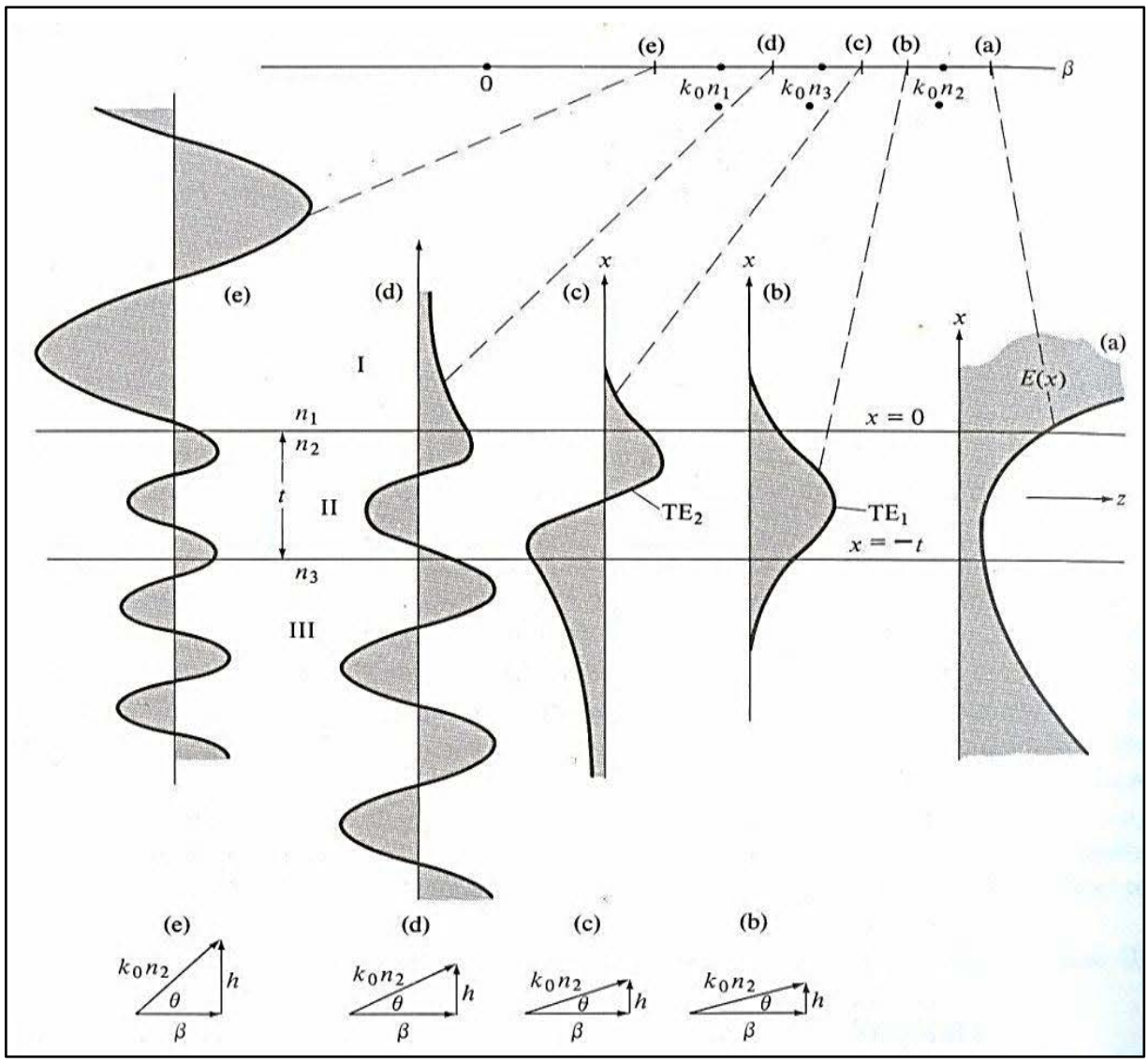

Figure 2.9: Propagating modes in a planar wave guide for the three regions (equation 2.29a-c) showing the field distributions corresponding to the different values of the propagating constant [after Yariv, 1997].

For the analysis of the planar waveguide, it is assumed that $n_2 > n_3 > n_1$. In the first instance, suppose that $\beta > k_o n_2$, then $(1/E)(\partial^2 E/\partial x^2) > 0$ everywhere, implying that $E(x)$ is exponential in all three layers (Yariv,1997). For this solution, there should be continuity at the boundary. The resulting field distribution is as shown in figure 2.9(a). This solution is not physically possible since the field keeps increasing exponentially and does not correspond to a real wave.

For $k_o n_3 < \beta < k_o n_2$, the solution is sinusoidal in region II since $(1/E)(\partial^2 E/\partial x^2) < 0$, but has an exponential solution in regions I and II. This results in two possible distributions as depicted in figures 2.9 (b and c) where the energy of the modes are confined to region II, the region with the highest index of refraction.

In the situation where $k_o n_1 < k_o n_3$, the solution is exponential in region I but sinusoidal in regions II and III as shown in figure 2.9(d). These modes are known as substrate radiation modes. Finally as illustrated in figure 2.9(e), the case where $0 < \beta < k_o n_3$, gives rise to a sinusoidal behaviour in all the regions resulting in radiation modes.

From the above analysis, it can be deduced that the allowed values of β in the propagation region $k_o n_3 < \beta < k_o n_2$ are discrete. The number of allowed confined modes depends on the thickness (t) of region II, the frequency and the refractive indices of the three regions. As the thickness t increase, the number of confined modes also increases.

2.4 Optical fibre loss mechanisms

In order to achieve optimum performance of an optical communication system, it is crucial that an optical signal propagates through a fibre with minimal distortion. In general, a signal propagating in an optical fibre experiences some losses resulting in signal degradation. The losses may occur as a result of the material make-up of the fibre, the shape of the fibre as well as the polarization properties of the propagating light signal. This section discusses fibre loss mechanisms which include attenuation, dispersion and nonlinear effects.

2.4.1 Attenuation

As light travels through a fibre, its optical power decreases exponentially with distance (z). This loss in energy is known as attenuation. If the optical power $P(0)$ is the optical power at the origin (input, $z = 0$), then the power at a distance z further down the fibre is given by (Keiser, 2000, p.92);

$$P(z) = P(0)e^{-\alpha_p z} \tag{2.30a}$$

where

$$\alpha_p = \frac{1}{z} ln \left[\frac{P(0)}{P(z)}\right] \tag{2.30b}$$

In equation 2.30b, α_p is the fibre attenuation coefficient in units of km^{-1}.

For simplicity in calculating optical signal attenuation in an optical fibre, it is conventional to express the attenuation coefficient in units of decibels per kilometre (dB/km) as;

$$\alpha(dB/km) = \frac{10}{z} log\left[\frac{P(0)}{P(z)}\right] \quad (2.30c)$$

Attenuation plays an important role in the design of an optical system because it determines the maximum transmission distance between a transmitter and a receiver. Attenuation is basically caused by absorption, scattering and radiative losses of the optical energy. Absorption losses are due to the nature of the fibre material while scattering losses may be attributed to both the fibre material and structural imperfections of the fibre. Attenuation due to radiative effects occurs as a result of perturbations (both microscopic and macroscopic) of the fibre geometry such as bending.

Absorption may occur as a result of defects in the atoms or impurities in the glass material. Atomic defects of the fibre glass occur when the fibre is exposed to radiation, which changes the internal structure of the material. The impurities become a major source of absorption. OH ion impurity in particular is known to cause high attenuation at particular wavelengths where its presence results in high absorption peaks on the wavelength-attenuation curve (Keiser 2000).

Scattering in the fibre occurs mainly as a result of variations in the material density, compositional fluctuations and structural in-homogeneities or defects which may arise during the fibre manufacturing process. Variations in the molecular density and compositional fluctuations due to the presence of oxides cause variations in the refractive index within the fibre over distances which are small compared to the order of magnitude of wavelength. The index variations causes Rayleigh scattering of the light, which has a wavelength dependence of λ^{-4}. As a result of this wavelength dependence, scattering losses decrease considerably with an increase in wavelength. Losses due to fibre geometry will be discussed in chapter 3.

2.4.2 Dispersion effects

Dispersion effects in an optical fibre distort an input optical pulse by causing a broadening of the pulse at the output. There are several dispersive effects which occur in an optical fibre, the most common being modal, chromatic and polarization mode dispersion.

In multimode fibres, modal dispersion occurs as a result of the difference in the velocities of the various modes. Modal dispersion may viewed as the dispersive effect caused by the discrete electromagnetic wave patterns travelling through different paths, hence causing a dispersion of the modes with time. This effect is minimal in single mode fibres.

Chromatic dispersion is a combination of material and waveguide dispersion. This effect occurs as a result of the group velocity being a function of wavelength. Material dispersion arises from the variation of the group velocity as a function of wavelength. Material dispersion occurs as a result of the variation of the fibre core refractive index as a function of wavelength. Since material dispersion results from the wavelength dependence of the group velocity, it follows that the pulse dispersion will still occur even if all the wavelengths contained in a propagating pulse follow the same path. Waveguide dispersion occurs as a result of fibre design. Approximately 80% of the optical power propagates in the core while the remaining 20% propagates in the cladding at a faster rate. The difference in the propagating speeds in the cladding and core results in the waveguide dispersion. Chromatic dispersion can be controlled by adjusting waveguide dispersion to cancel out the effects of material dispersion during fibre design. These kinds of fibres are known as dispersion shifted fibres.

Due to the cylindrical shape of the optical fibre, an optical pulse launched into it propagates as two identical orthogonal polarization modes. A distortion of the shape or a variation in the refractive index of the fibre may cause a delay between the two orthogonal polarization modes. The variation in the refractive index is known as optical birefringence. The time delay between the two propagating polarization modes (the differential group delay), is the magnitude of the dispersive effect known as polarization mode dispersion (PMD). The differential group delay is usually in the order of picoseconds. Effects which may vary the fibre birefringence are bending and twisting as well as environmental factors such as temperature variation and wind. The coupling of the light between fibre sections with different refractive indices (birefringence sections), is known as mode coupling. Mode coupling effects may complicate the effects of birefringence since travel times of the two orthogonal polarization modes may keep varying from one birefringence segment to the other. In line with the theme of this thesis, a more detailed background of polarization mode dispersion is presented in chapter 3.

2.4.3 Nonlinear effects

Under normal conditions, light waves or photons which propagate through an optical fibre have little interaction with each other, and do not vary much during propagation except for the changes introduced by absorption and scattering. However a phenomenon known as nonlinear effect occurs when high optical powers are concentrated at a small area of dielectric materials. The result of this effect is that output optical power and input optical power are no longer proportional. Two nonlinear effects may be identified. The first is a result of nonlinear inelastic scattering processes, while the second nonlinear effect is caused by the intensity dependent variations of the refractive index of the fibre.

Stimulated Raman scattering (SRS) and stimulated Brillouin scattering (SBS) processes are nonlinear inelastic scattering effects. These effects reduce the intensity of some channels while providing gain to others, resulting in crosstalk between wavelength channels. SRS reveals how light waves interact with the vibrational modes of the molecules. When a photon is incident on a molecule with a bond having a particular frequency, the molecule absorbs some of the energy leaving the photon with a lower energy and frequency. If an already existing frequency is the same as the new frequency, the SRS light is amplified. Hence SRS causes a reduction for shorter wavelengths and a gain for longer wavelengths.

SBS occurs as a result of scattering of light waves from acoustic waves. The resultant scattered waves propagate in a backward direction in single mode fibres (Keiser, 2000). The backscattered light gains energy from the forward propagating light, leading to a depletion of optical signal power. The frequency of the backscattered light experiences a Doppler shift that is dependent on the refractive index and the velocity of sound in the dielectric material.

Non-linear effects which occur as a result of intensity-dependent variations of the refractive index produce effects such as self-phase modulation (SPM), cross-phase modulation (XPM) and four-wave mixing (FWM). SPM and XPM alter the phase of the optical signal leading to chirping of optical signals. In general, the refractive index increases with intensity and its corresponding nonlinearity is known as the Kerr nonlinear effect. Kerr non-linear effects produce a self-phase modulation where the fluctuating optical power of the light wave is converted to phase fluctuations of the same wave. XPM converts power fluctuations in a particular channel signal to phase fluctuations in other co-propagating channel signals. When SPM and XPM spectral broadening is combined with dispersion, the effect can be a major

limitation to long haul transmission links. FWM may occur as a result of the interaction between three co-propagating frequencies. The interaction produces a new frequency, wave whose frequency is dependent on the three original frequencies. This new frequency can result in serious crosstalk. A detailed analysis of the subject of non-linear effects can be found in Keiser (2000).

In this chapter, the nature of light, including its propagation through a waveguide has been discussed. In addition some of the loss mechanisms encountered by a light wave propagating within a medium have also been treated. As the focus of this thesis, polarization mode dispersion which is a major loss mechanism is treated in detail in the next chapter.

CHAPTER 3

POLARIZATION MODE DISPERSION

3.1 Introduction

As already mentioned in Section 2.4.2, polarization mode dispersion (PMD) is a dispersive effect resulting from the combined effects of optical birefringence and mode coupling. PMD is an important concept to study because it causes serious capacity impairments including pulse broadening and signal fading in high speed digital systems as well as signal distortion in analogue systems. During data transmission the PMD of a fibre changes the polarization state of each frequency differently, adding a polarization modulation component to the signal. PMD is a stochastic phenomenon which varies randomly with time. This chapter discusses the characteristics and measurements of polarization mode dispersion.

3.2 The origin of PMD

Any arbitrary optical signal with a particular state of polarization (SOP), upon entering a single mode fibre may be regarded as a linear superposition of two fundamental HE_{11} modes (Poole, 1997). In an ideal situation, these two modes are degenerate and orthogonal and propagate with the same phase and group velocities. In real single mode optical fibres however, the effects of optical birefringence may result in a difference in phase and group velocity of the degenerate modes. The difference in phase velocity, results in a change in the SOP of the light. Group velocity changes give rise to dispersion, leading to a broadening of the output pulse as shown in figure 3.1a. The mode with a higher group velocity is known as the fast mode while the one with a lower group velocity is known as the slow mode. The magnitude of the PMD vector, known as the differential group delay (DGD), is the difference in the times of flight of the two propagating modes through the fibre. Signal fading and inter-symbol interference may occur if the DGD exceeds a significant fraction of bit period. Signal fading and inter-symbol interference lead to system or network outages.

For deployed or long single mode fibres, the magnitude and orientation of the birefringence axes vary randomly along the fibre as shown in figure 3.1b. The random changes in the birefringence axes are known as mode coupling. Environmental conditions further complicate the random variation of birefringence and mode coupling as a function of time.

The combined effects of birefringence and mode coupling are responsible for polarization mode dispersion.

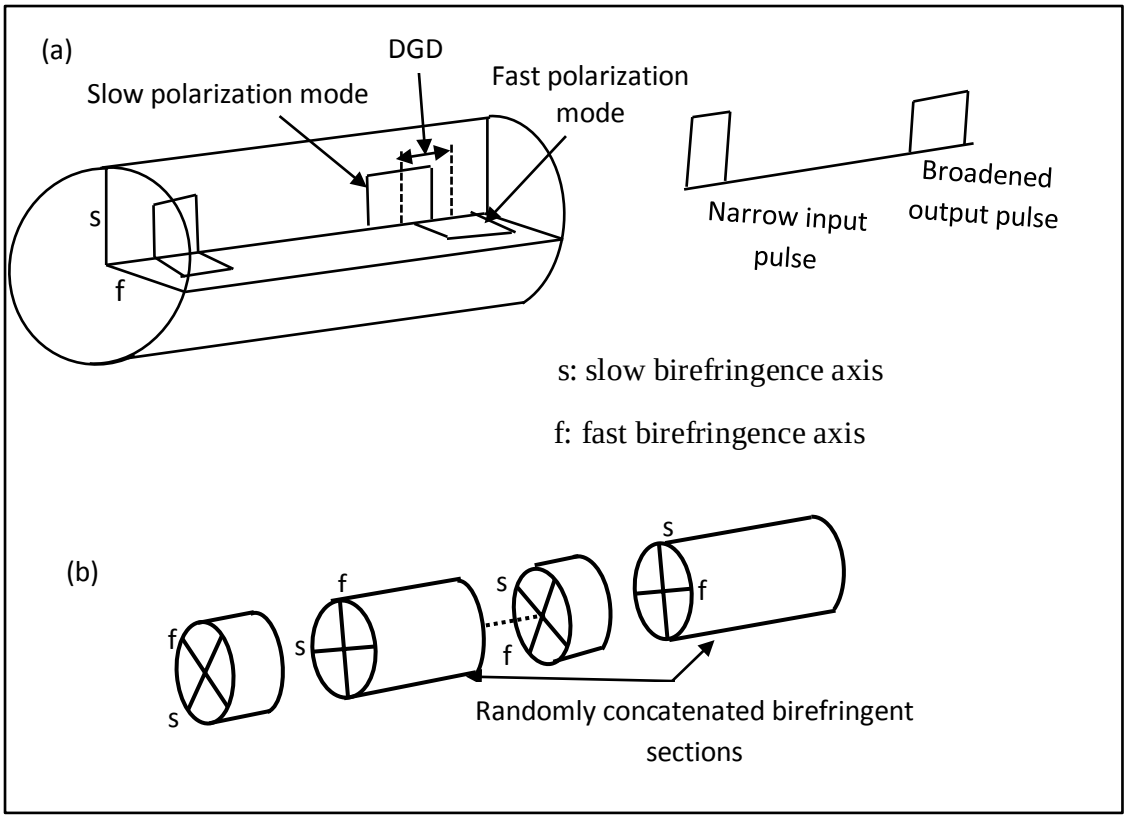

Figure 3.1: Dispersive broadening of an optical pulse in a single mode fibre due to birefringence;(b) Randomly varying birefringence sections along an optical fibre.

3.2.1 Birefringence

Birefringence in a single mode optical fibre can be caused by both extrinsic and intrinsic factors as illustrated in figure 3.2. Intrinsic factors such cause permanent characteristic features of the fibre and are accidentally introduced during the manufacturing process. These include core asymmetry and non-uniform stress in the cladding. A non-circular core is gives rise to geometrical birefringence while non-uniform stress fields result in stress birefringence (Rashleigh, 1983). During the fibre manufacturing process, the core (which is doped to slightly increase its index of refraction) attains a different thermal coefficient of expansion from that of the cladding. This difference gives rise to some significant amount of radial stress during cooling of the fibre after it has been drawn from the preform (Kaminow, 1981).

If the fibre is perfectly circular, as expected in an ideal case, then these fields would be symmetrical and would not cause any anisotropy in the fibre. However, if the core or the cladding is not circular as desired, then the fibre will have some non-uniform internal stress fields. Such stress fields introduce anisotropies in the core which result in birefringence.

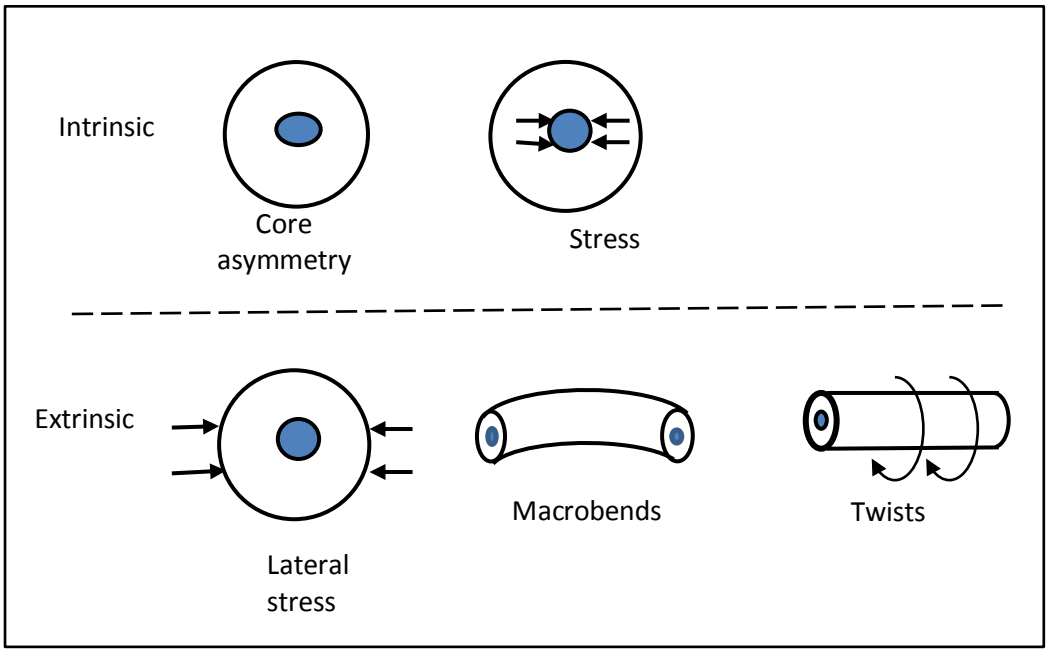

Figure 3.2: Intrinsic and extrinsic factors, responsible for birefringence.

Currently, due to improved fibre manufacturing processes, intrinsic birefringence is greatly reduced, making it possible to realise low PMD coefficients as low as 0.05ps/km$^{1/2}$ or less, in single mode fibres (Nelson, 2005). Birefringence however can be introduced by external factors during cabling and deployment. These extrinsic factors may include lateral stress, bending and twisting. Environmental factors such as temperature and wind may also cause birefringence, giving rise to PMD in deployed fibres (Cameron *et al*, 1998).

In order to understand the effect of birefringence on a light wave system, consider a single birefringent segment of a single mode fibre such as one of the concatenated segments in figure 3.1(b). Let the propagation vectors of the slow and the fast HE_{11} modes be β_s and β_f respectively. Then the birefringence can be expressed as the difference between the propagating vectors:

$$\Delta\beta = \beta_s - \beta_f = \frac{\omega \Delta n}{c} \tag{3.1}$$

where $\omega = \frac{2\pi c}{\lambda}$ is the angular frequency of the light, n_s and n_f are the indices of refraction for the slow and fast modes respectively, $\Delta n = n_s - n_f$ is the differential index of refraction and c is the speed of light in vacuum (Poole, 1997).

The induced birefringence causes a difference between the times of flight of the fast and the slow polarization modes, known as the differential group delay (DGD), $\Delta\tau$. The DGD can be expressed in terms of the angular frequency derivative of the fibre as (Kogelnik, 2002):

$$\frac{\Delta\tau}{L} = \frac{d}{d\omega}\left(\frac{\Delta n\omega}{c}\right) = \frac{\Delta n}{c} + \frac{\omega}{c}\frac{d\Delta n}{d\omega} \tag{3.2}$$

where L is the length of the fibre section. In the absence of mode coupling the DGD is wavelength independent (provided that the differential index of refraction is wavelength independent). For polarization maintaining fibres (PMFs) and short single mode fibres (no mode coupling), the DGD increases linearly with fibre length and the PMD coefficient is reported in units of ps/km.

Birefringence further acts to alter the states of polarization (SOP) of a propagating light. For an input light wave which is not aligned to any of the birefringent axes, the SOP evolves in a cyclic manner as the light propagates along the fibre.

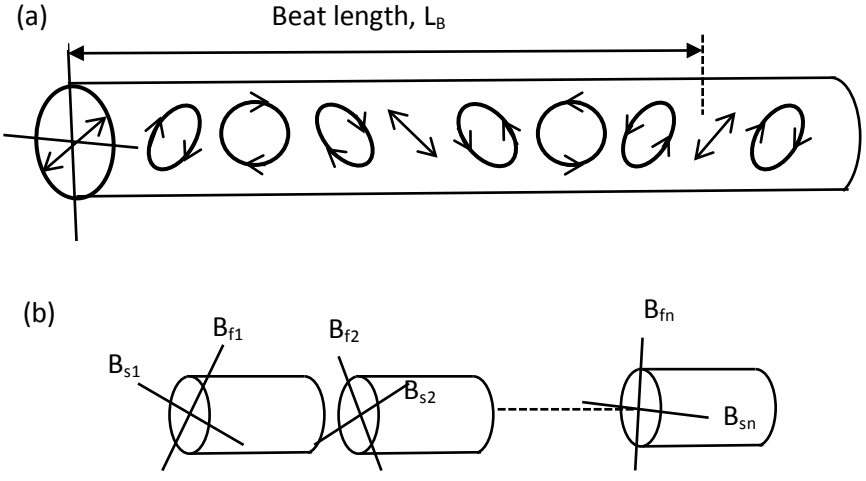

Figure .3.3: (a) Evolution of SOP of a light wave propagating through a birefringent optical fibre without mode coupling; (b) Concatenation of randomly oriented birefringent segments, representing a long length of single mode fibre with mode coupling.

Figure 3.3a illustrates how the SOP of a light wave launched midway between the two birefringent axes evolves. The propagation distance for which the phase difference equals integral multiples of 2π and the SOP repeats itself, is referred to as the beat-length (L_B). For a propagating light with wavelength λ, and differential index Δn, the beat-length is given by $L_B = \lambda/\Delta n$ (Kogelnik, 2002). Standard telecommunication fibres can have beat lengths of $\sim 10m$ (Galtarossa *et al.*, 2000). Generally the input and output SOPs of a propagating wave at a fixed wavelength will be different unless of course the fibre length is an integral multiple of the beat-length or the input light is aligned to one of the birefringent axes.

If the input SOP of a propagating wave, with a fixed wavelength, is aligned with one of the birefringent axes, then the output SOP will be independent of wavelength. Consider on the other hand, a fixed input SOP which is not aligned to the either of the birefringent axes. If the wavelength is altered, the output SOP evolves in a cyclic manner, similar to that of the evolution of the SOP of a light wave propagating along the length of a fibre. The rate of change of the output SOP with respect to change in wavelength depends on the birefringence. This is the basis of frequency domain DGD measurement techniques such as the Poincaré sphere arc and Jones Matrix Eigenanalysis (JME) methods (see sections 3.4.1 and 3.4.2).

3.2.2 Combined effects of birefringence and mode coupling

As depicted in figure 3.3(b), a long length of single mode fibre can be treated as a concatenation of many birefringent segments, each with a unique length and a birefringence. The orientation of the birefringent axes varies for each segment creating mode coupling interfaces between adjacent segments. Mode coupling may occur due to variations in fibre geometry, composition and strain. These geometric perturbations may originate from the fibre preform, during drawing, or cabling. Fibre twists and splices along a fibre link are further extrinsic sources of mode coupling (Kaminow, 1981).

The combined effects of mode coupling and birefringence are different from the case where the fibre is only affected by birefringence. With the introduction of mode coupling, the effective birefringent axes and the DGD of a fibre link become wavelength dependent. Generally the output SOP changes in response to a variation of a fixed input wavelength, however at each wavelength, there exists an orthogonal pair of input SOP whose output SOPs remain constant for small changes in the input wavelength (Poole, 1986). These input polarization states are known as the principal states of polarization (PSPs). The PSPs are

orthogonal only in the absence of polarization dependence loss (PDL). The pair of PSPs at each wavelength is analogous to the idea of slow and fast axis; the only difference is that for fibre with mode coupling, the PSPs vary with wavelength. Furthermore, the PSPs need not be linear states and the output SOP need not be the same as an input SOP aligned with a PSP (Gibbon, 2007). The DGD at a given time is defined as the difference in propagation times associated with the two PSPs at that particular wavelength.

PMD values are typically reported as either the root mean square (RMS) or the mean of the DGD over a wavelength range. PMD does not accumulate linearly in long single mode fibres. Due to the random nature of mode coupling, the individual birefringent section constituting a fibre may either add or subtract depending on the orientation of their respective birefringent axes. This idea is positively exploited in modern telecommunication fibres where mode coupling is intentionally introduced by periodically spinning the fibre preform back and forth during the drawing process (Li 2008). The spinning introduces right-handed and left-handed circular polarization states, with linear polarization states in between. Although the spinning process is imperfect, the residual PMD due to the induced mode coupling in a spun fibre is much less than the PMD without spinning. The accumulation of the PMD is analogous to a random walk process and the PMD value (RMS of the DGD) is proportional to the square root of the fibre length (Gisin *et al*, 1991). As such the PMD coefficient of a long span of single mode fibre is defined as the PMD value normalized to the square root of the fibre length, and is reported in units of ps/km$^{1/2}$.

3.3 Definition of the PMD vector and second-order PMD

Polarization mode dispersion at a specific wavelength is a vector completely defined by the DGD (its magnitude) and the PSPs (the direction). It is traditional to represent PMD to the first order with a vector in three dimensional Stokes space as:

$$\vec{\tau} = \tau\hat{q} \tag{3.3}$$

where τ is the DGD and $\hat{q}$ is a unit vector pointing in the direction of the slow PSP (Kogelnik, 2002). The notation of τ is used to represent the DGD instead of $\Delta\tau$ for simplicity. The vector $-\hat{q}$ which is oriented 180^o from $\hat{q}$ in Stokes space represents the fast PSP. There are minor variations in the definition of PMD vector in literature with regards to whether it is aligned with the fast or slow PSP. For instance Poole defined the PMD vector to point in the

direction of the fast PSP with left circular polarization in Stokes space (Poole *et al*, 1988a). The definition used here applies to right circular polarization in Stokes space, which is denoted by (001).

Polarization mode dispersion can also be affected by changes in angular frequency. This results in second-order PMD (SOPMD) which refers to the change in PMD vector with respect to optical angular frequency, expressed as:

$$\vec{\tau}_\omega = \frac{d\hat{\tau}}{d\omega}\hat{q} + \tau\frac{d\hat{q}}{d\omega} = \tau_\omega\hat{q} + \tau\hat{q}_\omega \tag{3.4}$$

A geometric vector analysis of SOPMD is shown in figure 3.4. The first term, $\tau_\omega\hat{q}$, in eq.3.4 is a vector parallel to the differential delay $\vec{\tau}$ in Stokes space. It denotes the change in DGD with wavelength and is responsible for polarization chromatic dispersion (PCD). The sign of PCD is positive when the PCD vector points in the direction of $\vec{\tau}$ and negative when it points in the opposite direction of $\vec{\tau}$. The $\tau\hat{q}_\omega$ term indicates a rotation of the PSP in Stokes space with a change in angular frequency and is referred to as the PSP depolarization term. The vector $\hat{q}_\omega$ has a magnitude of $d\phi/d\omega$, where ϕ is the angle swept through by the PMD vector with changing angular frequency.

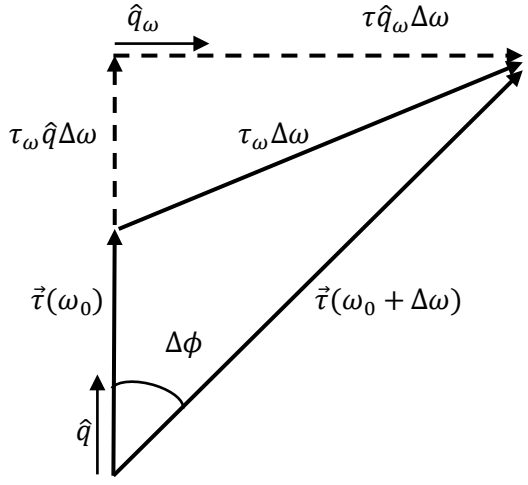

Figure 3.4: A schematic diagram of the PMD vector $\tau(\omega)$ and the second order components showing how $\tau(\omega)$ changes with frequency. Depolarization, $\tau\hat{q}_\omega$, and PCD, $\tau_\omega\hat{q}$ are the orthogonal components of the second order PMD vector $\vec{\tau}_\omega$.b [after Kogelnik,2002}

Since the PCD and the depolarization vectors are orthogonal to one another, the magnitude of the SOPMD vector is given by:

$$|\vec{\tau}_\omega| = \sqrt{|\tau_\omega \hat{q}|^2 + |\tau \hat{q}_\omega|^2} \tag{3.5}$$

It has been shown both by theory and experiment that depolarization is the more dominant SOPMD component with an expectation: $E(|\tau \hat{q}_\omega|^2) = \frac{8}{9} E(|\tau_\omega|^2)$, where E denotes the expectation operator (Foschini, 1991; Nelson , 1999). It has been shown by Nelson (1999) that high depolarization is usually associated with relatively small DGD values. Generally first-order PMD is known to pose more problems in terms of limiting network performance than SOPMD. SOPMD can however severely limit the performance of high speed networks for which the PMD varies significantly within the signal bandwidth. This is particularly the case when the DGD value is small and the depolarization is large. This is usually the case when first-order PMD is compensated for in a link with an initially high DGD before compensation (Gibbon, 2007).

3.4 PMD measurement techniques

The interaction of light with matter (a dielectric medium) may either change the properties of the light or that of the medium. In measuring polarization mode dispersion, the properties of light (frequency, phase, and polarization) before and after interaction with the fibre are very crucial. In single-mode fibres, the DGD (PMD magnitude) can also be measured as the difference between the transient times of the fast and the slow modes as they propagate through the fibre. PMD measurements can thus be classified into time domain and frequency domain measurement techniques. Frequency domain techniques includes the Jones Matrix Eigenanalysis (JME) method (Heffner, 1992, 1993), the Poincaré sphere arc method (Andersciani, 1987; Poole, 1988), the Poincaré sphere analysis (PSA) method (Cyr 1999, 1999a), the fixed analyser method (Poole, 1994; Gisin, 1994) and the Mueller matrix method (Williams 2005; Jopson, 1999). Time domain measurement techniques include the time of flight method (Williams, 2005), interferometric methods (Gisin, 1991) and polarization optical time domain reflectometric techniques (Rogers, 1981; Galtarossa, 2005). Commercial PMD instruments are available and such instruments were applied in the measurement of PMD in this thesis. This chapter gives a brief background of some of the measurement techniques mentioned above which are applied later in this thesis.

3.4.1 The Poincaré sphere arc method

Due to the effects of PMD, a light wave with a given SOP ($\hat{s}$) at the input of the fibre will vary from the output SOP ($\hat{t}$) according to the relation, $\hat{t} = R\hat{s}$, where R is a 3x3 Mueller rotation matrix describing the transformation in Stokes space. In a similar manner, a change in the wavelength of a fixed SOP ($\hat{s}$) will result in a change in the output SOP ($\hat{t}$) which can be expressed as (Nelson, 2005):

$$\hat{t}_{\omega} = \frac{d\hat{t}}{d\omega} = \vec{\tau} \times \hat{t} \tag{3.6}$$

where $\vec{\tau} \times = R_{\omega}R^{T}$ and R^{T} is the transpose of the Mueller rotation matrix.

Equation 3.6 is in accordance with the so called law of infinitesimal rotation and it describes the circular rotation of the output SOP about the PMD vector ($\vec{\tau}$) as the angular frequency/wavelength of a fixed input SOP is varied. This is illustrated in figure 3.5 for a birefringent fibre with mode coupling. As the angular frequency of a fixed SOP changes from ω_1 to ω_1 the output SOP traces out an arc about the PMD vector. Due to the effect of mode coupling, the orientation of the PMD vector changes with changing angular frequency. Hence the output SOP traces out a seemingly random trajectory on the surface of the Poincaré sphere. Any two points on the trajectory traced by the output SOP, representing a change in angular frequency ($\Delta\omega = \omega_1 - \omega_2$), is section of a circular arc about the PMD vector in accordance with the law of infinitesimal rotation.

The speed with which the output SOP rotates about the PMD vector depends on the DGD of the fibre and is expressed as:

$$\tau = \left|\frac{\Delta\theta}{\Delta\omega}\right| \tag{3.7}$$

where $\Delta\theta$ denotes the rotation angle in radians. The output SOPs rotate about the PSP axis due to an incremental change in the input optical frequency, $\Delta\omega = \omega_1 - \omega_2$ (Poole 1998). During a single measurement step, the DGD and the PSP about which the rotation occurs are determined and assigned to a particular wavelength corresponding to an angular frequency midway between ω_1 and ω_2.

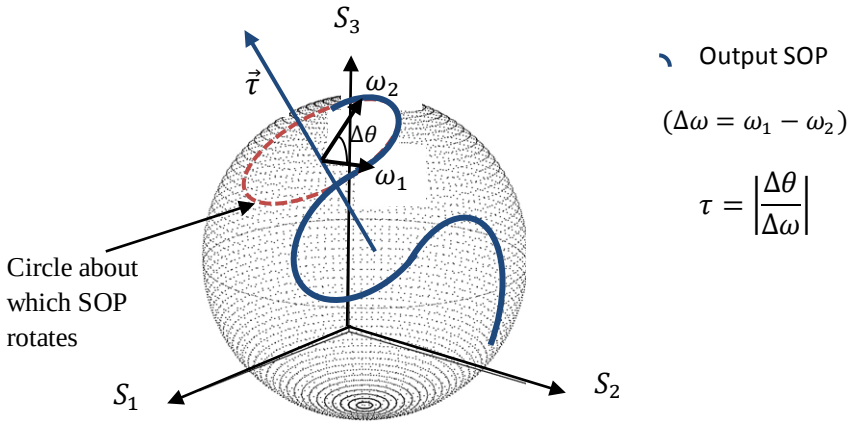

Fig.3.6: Illustration of how the PMD vector is determined using the Poincaré sphere arc method.

A systematic stepping of the angular frequency of a fixed input SOP in incremental steps over a desired wavelength range makes it possible to measure both the DGD and PSP as a function of wavelength.

The Poincaré sphere arc method works well for fibres with negligible mode coupling. In the case of random mode coupling where PSPs vary rapidly with wavelength, the method leads to inaccurate results. Errors are further introduced accidentally when an input SOP corresponds to (or close to) a PSP. In this case the output SOP remains unchanged for an incremental change in wavelength, thus introducing measurement errors. Due to these shortcomings, the JME method and PSA method are generally preferred when DGD and PSP are to be measured as a function of wavelength.

3.4.2 The Jones Matrix Eigenanalysis method (JME)

Following the results in section 2.2.3, the transmission of a monochromatic light wave through a linear medium such as an optical fibre can be represented in Jones space as $E_{out} = T(\omega)E_{in}$, where $T(\omega)$ is an independent transfer matrix that characterizes the medium. By measuring the transfer matrix of the medium, it is possible to determine the DGD and PSP of the fibre. The DGD at an angular frequency midway between the two closely spaced angular frequencies, ω_1 and ω_2, is given by:

$$\tau = \left| \frac{Arg\left(\rho_1/\rho_2\right)}{\omega_2 - \omega_1} \right| \tag{3.8}$$

where ρ_1 and ρ_2 are the eigenvalues of the matrix product $T(\omega_2)T^{-T}(\omega_1)$ and Arg is the argument function defined as; $Arg\left(ae^{i\theta}\right) = \theta$. Furthermore, the fast and the slow PSPs of the fibre are given by the two eigenvectors of $T(\omega_2)T^{-T}(\omega_1)$ (Heffner 1992, 1993).

\

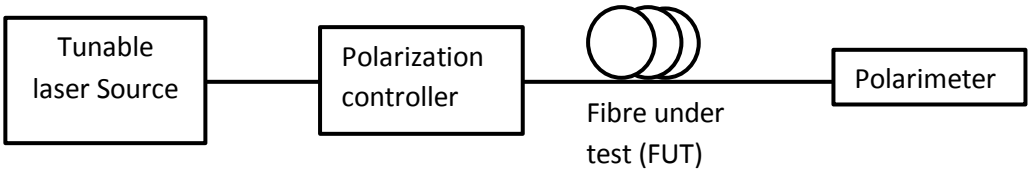

Figure 3.7: A typical experimental setup of a Jones Matrix Eigenanalysis method used to measure PMD.

Figure 3.7 shows a typical experimental setup of a JME method for determining PMD. The tunable laser is incrementally stepped across a carefully chosen wavelength range. After each step, the transmission matrix of the fibre at that wavelength is determined by measuring the output SOPs (via the polarimeter) of three known input SOPs. The calculations involved in the computation of the transfer matrix are simplified when three linear input states of polarization such as 0^0,45^0 and 90^0 are chosen. In principle any three distinct known input SOPs may be used (Derickson 1998). The DGD and PSPs at intermediate wavelengths corresponding to angular frequencies of $\left(\frac{\omega_n + \omega_{n-1}}{2}\right)$ are then determined across the measurement range from the eigenvalues and eigenvectors of $T(\omega_n)T^{-T}(\omega_{n-1})$. In addition, the PCD and depolarization can also be determined from the angular frequency derivative of the PMD vector according to equation 3.4. The JME measurement technique is a standard PMD measurement technique and it is applied later as a reference test method in chapters 6 and 7 to measure mean DGD and root mean square DGD values of four fibres.

3.4.3 Mueller matrix method

The Mueller matrix method (MMM) (Jopson *et al,* 1999) determines the PMD in a similar manner to the JME technique, with a few differences. The fundamental difference is that calculations are carried out in Stokes space for MMM while JME uses Jones space. Further, during MMM measurements the absence of PDL is assumed entirely, contrary to the JME technique which assumes the absence of PDL only during the last step when the DGD is being calculated. Because of these basic differences in measurement principle, the algorithm for the MMM is much more simplified compared to the JME technique. For the MMM the PMD vector is calculated in Stokes space using the Mueller rotation matrix instead of the Jones space where the Jones transfer matrix is used. Hence the MMM uses only two different input SOPs at each wavelength, unlike the JME method where three known input SOPs must be used. A major advantage with the MMM is that, the two input SOPs need not be known. This leads to greater measurement accuracy, making the MMM more suitable for the measurement of second-order PMD, where an accurate determination of the PMD vector is desired. The major drawback of this method is that it is susceptible to errors in the presence PDL, unlike the JME method which remains exact in the presence of PDL. The reader is referred to Jopson et al. (1999) and Williams (2004, 2005) for further details.

3.4.4 Time of flight technique

The time of flight technique is an intuitive time domain measurement technique. Figure 3.8 shows how narrow pulses of light propagate through a non-mode coupled device of DGD $\Delta\tau = \tau_s - \tau_f$, where subscripts s and f denote slow and fast. The propagation delay through the device will be τ_s (if it is polarized along the slow PSP), or τ_f (if it is polarized along the fast PSP). If the polarization state of the input pulse lies in between the slow and the fast PSP, the pulse breaks into two components with delays, τ_s and τ_f and the relative intensities weighted according to the projection of the input polarization state on the PSP.

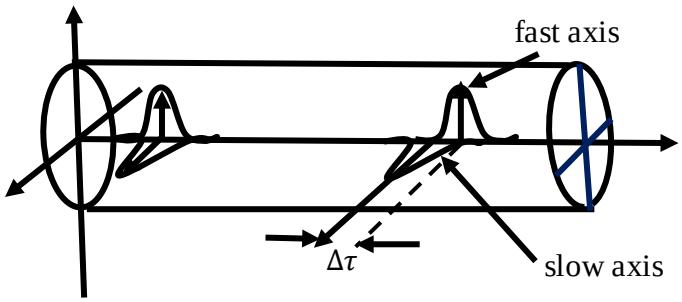

Figure 3.8: Illustration of input pulses launched simultaneously into the fast and the slow PSPs of a device. The difference in the emergence times of the pulses corresponds to the differential group delay.

Figure 3.8 shows a narrow pulse of light launched into a non-mode coupled fibre of DGD $\Delta\tau$. In this method, short optical pulses are launched into the fibre and detected at the output. A fast oscilloscope plots the arrival time of the pulses as the input polarisation state is changed. This method is commonly found in literature (Poole, 1988a; Namihira and Maeda 1992; Williams 2005), but it is impractical because the pulse width limits temporal resolution. Narrow pulse widths on the order of the desired DGD are a requirement for this technique.

3.4.5 The interferometric technique

Interferometric methods for determining PMD are similar to the time of flight method discussed in section 3.3.4, however it is more practical. The technique is very popular for field work since it facilitates the rapid and accurate determination of PMD even in the presence of fibre movements and vibrations. Furthermore, it has an advantage over polarimetric methods such as the Poincaré sphere arc method and the JME which are time consuming and requires stability of the fibre during measurements. Polarimetric techniques are thus unsuitable for measurements in the field especially in the case of aerial fibres.

Varied forms of the interferometric technique such as the traditional interferometric technique (TINTY) and the generalized interferometric technique (GINTY) are available commercially. The grounding theory behind this technique however is interferometry. In most cases, a Michelson interferometer is used. A detailed description of this technique is reported in Chapter 5 (sections 5.1 and 5.2) of this thesis where it is applied to measure PMD of different fibre types.

Apart from classification into frequency and time domain techniques, PMD measurements can also be classified into single-end and forward measurements. In forward measurements, both ends of the fibre are required. The optical source is placed at one end of the fibre and detected at the other end. In single-end measurements only one end of the fibre is required, thus the source and the detector are located at the same position. By this classification the measurement techniques discussed in this section fall under forward measurement techniques. Single-end measurement techniques make use of both Rayleigh backscattered signal within the fibre as well as the Fresnel reflection at the fibre far end.

Single-end techniques which are also known as reflectometric measurement techniques include optical time domain reflectometry, polarization sensitive optical time domain reflectometry (P-OTDR), and polarization optical frequency domain reflectometry (O-FDR). An overview of reflectometric measurement techniques is presented in chapter 4 of this thesis.

CHAPTER 4

REVIEW OF REFLECTOMETRIC MEASUREMENT TECHNIQUES

4.1 Introduction

Most standard optical fibre loss measurement techniques including polarization mode dispersion require the use of both fibre ends for input and output light in order to make measurements. These measurement techniques may be destructive, requiring a piece of the fibre to be cut off (e.g. the cut back technique). These standard methods known as forward measurements are not very practical for use in the field where fibre ends are separated several kilometres apart. Mostly fibres have to be looped in order to make measurements or monitor installed fibre. In the case of PMD these techniques only provide the total or mean value for the entire link over a range of wavelengths or frequencies. PMD may be high at specific sections of the link and measuring it on a global scale may be deceptive (Cameron 1999). In recent years single-end reflectometric measurement techniques have been developed and applied extensively to measure and characterize optical fibre including its differential group delay and birefringence. Single-end optical time domain reflectometric (OTDR) techniques were pioneered by Rogers, 1980; Brinkmeyer, 1980; Nakazawa, 1983 and Heatly, 1985. By the end of the 1990s, Corsi, 1998, 1999a,b,c; Galtarossa, 1999; Hurtner 1999 had developed polarization sensitive optical domain reflectoctometry (P-OTDR) techniques extensively. More recently (Dong, 2007; Galtarossa, 2008; Fosuhene, 2010; and Palmieri 2011) have applied the technique to measure instantaneous differential group delay and root mean square differential group delay. Some of the practical advantages of single-end measurement techniques are that:

a) they make use of only one end of the fibre during measurements;
b) they are easy to use in the field;
c) they measure local DGD as well as beat length and correlation length.

Thus the main attraction of these techniques is that they are non- destructive but yet effective for evaluating fibre characteristics. Most OTDR techniques are time-domain based such as the single pulse OTDR and the correlation OTDR. On the other hand, frequency-domain techniques (OFDRs) provide higher resolution even to the sub-centimetre level and can therefore reveal more information about the fibre in terms of its loss profile and mechanisms.

4.1.1 Basic principles

When a probe signal is launched into a fibre, a certain quantity of the signal is backscattered or reflected back towards the input end of the fibre, depending on the physical structure of its core. Since its original development, OTDR techniques have undergone many subsequent developments due to improvements in optical sources and detection techniques. It is now possible to measure several fibre parameters and characteristics from a single OTDR trace. The signal backscattered in the fibre is due mainly to two effects, Rayleigh scattering of the signal as it encounters inhomogeneous sections in the fibre as well as the Fresnel reflection at glass-air interface at the fibre end face. The basic idea is to monitor the time dependence and distribution of the attenuation signal backscattered by a short pulse of light through a fibre. These same techniques can be applied for sensing the spatial distribution of the external fields which affect the light propagation conditions such as electric, magnetic, stress, strain and temperature.

4.1.2 Theoretical description of the conventional OTDR

A basic OTDR launches a short input pulse into the fibre and measures the returned signal as a function of time. The fraction of the signal being returned is due to its interaction with both Rayleigh scattering and Fresnel reflection sites within the fibre. Measurement of the arrival time of the signal, offers the opportunity to determine the magnitudes and location of faults within the fibre link. An OTDR trace (signature) is a backscatter impulse response of the fibre response and characterizes the fibre loss profile. Figure 4.1 shows a block diagram of a conventional OTDR. It esentially consists of a pulse generation system made up of a laser diode and a pulse generator which is triggered by the signal processor to modulate the intensity of the laser. In most cases the signal is a single square pulse with width between 5ns and 10μs depending on sensitivity and spartial resolution requirements. Some OTDRs are equipped with two lasers via wavelength division multiplexing in order to probe with different wavelengths (typically 1310nm and 1550nm). The input signal is coupled into the fibre via the bidirectional coupler with a 50:50 split ratio at the measurement wavelength. In principle any other three port component such as a beam splitter, isolator or a circulator could be applied, the basic requirement being a sufficient isolation between ports.

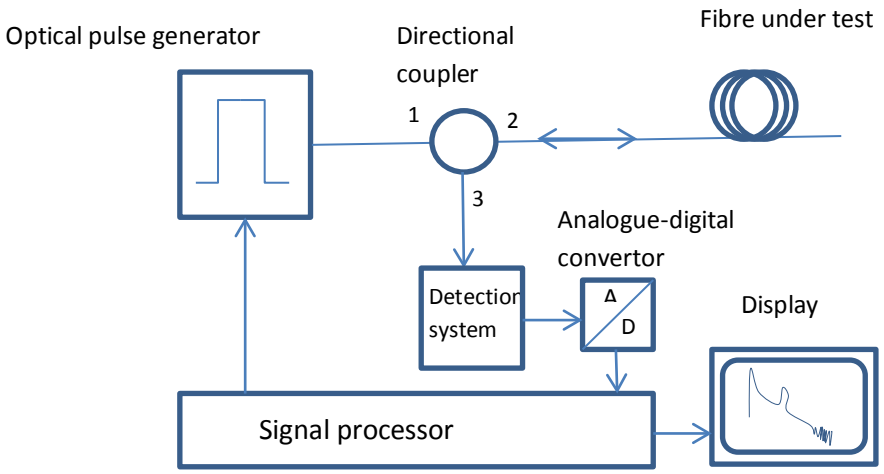

Figure 4.1: Block diagram of an OTDR measurement set-up.

The launch pulse is fed into the coupler at point 1, enters the fibre under test via point 2 of the circulator. The backscattered signal is then received at the detection system via point 3 of the circulator. The detection system consists of a photodetector and an amplifier. The detector is required to exhibit high dynamic range and sensitivity for detection of signals covering several orders of magnitude. An analogue-to-digital convertor (ADC) interfaces measured data to the processor for processing and computing after which it is displayed digitally. The function of the ADC is to provide the required sampling rates between adjacent data samples. The sampling rates determine the spatial resolution of the system.

4.1.3 OTDR backscatter signal and analysis

The total attenuation (α) that constitutes an OTDR signal includes both absorption (α_a) and Rayleigh scattering (α_s) and can be expressed as

$$\alpha = \alpha_a + \alpha_s \tag{4.1}$$

The relationship between the transmitted power P(x) and incident power P(0) at a distance x is given by,

$$P(x) = P(0).\exp(-\alpha x) \tag{4.2}$$

where α is the attenuation coefficient measured in km^{-1} units. If the attenuation coefficient is expressed in terms of dB unit as is more commonly the case for loss measurements, the above expression becomes,

$$P(x) = P(0).\,10^{\frac{-\alpha_{dB}}{10}x} \tag{4.3}$$

where

$$\alpha_{dB} = \frac{10}{ln10}\alpha \approx 4.34\alpha \tag{4.4}$$

In the above analysis the attenuation limit is bounded by $\alpha_s; 0 \leq \alpha_a \ll \alpha_s$.

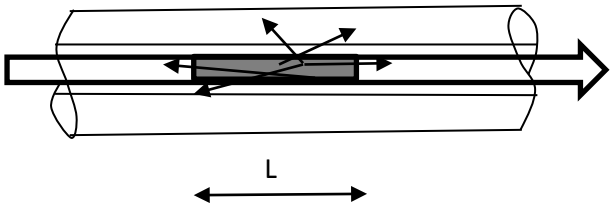

Figure 4.2: Scattering inside a fibre element of length L.

Consider a pulse with a temporal duration τ which experiences scattering in an optical fibre of elemental length L as depicted by figure 4.2. The distance L traversed by the pulse within the segment is given by

$$L = \tau v_g = \tau \frac{c}{n_g} \tag{4.5}$$

where $v_g$is the group velocity, c is the speed of light in vacuum and n_g is the group refractive index of the glass fibre.

The scattered power dP_s with respect to distance at a position x within an infinitesimally small element dx is related to the pulse power P(x) by,

$$dP_s = kP(s)dx \tag{4.6}$$

where $k = S\alpha_s$ and $\alpha_s \sim \frac{1}{\lambda^4}$ is the scattering coefficient.

The backscatter capture coefficient S which represents the fraction of light guided back into the OTDR in all directions is given by the equation (Neuemann, 1980; Brinkmmeyer, 1980 and Nakazawa, 1983),

$$S = \left(\frac{NA}{n_0}\right)^2 \frac{1}{m} \tag{4.7}$$

where NA is the numerical aperture of the fibre, n_0 is the refractive index of the fibre core and m (typically 4.55 for single mode fibres) depends on the refractive index profile (Derickson, 1998).

Now consider the backscatter response caused by a rectangular pulse of width W with a leading edge located at $L = Tv_g$ (figure 4.3a-c).

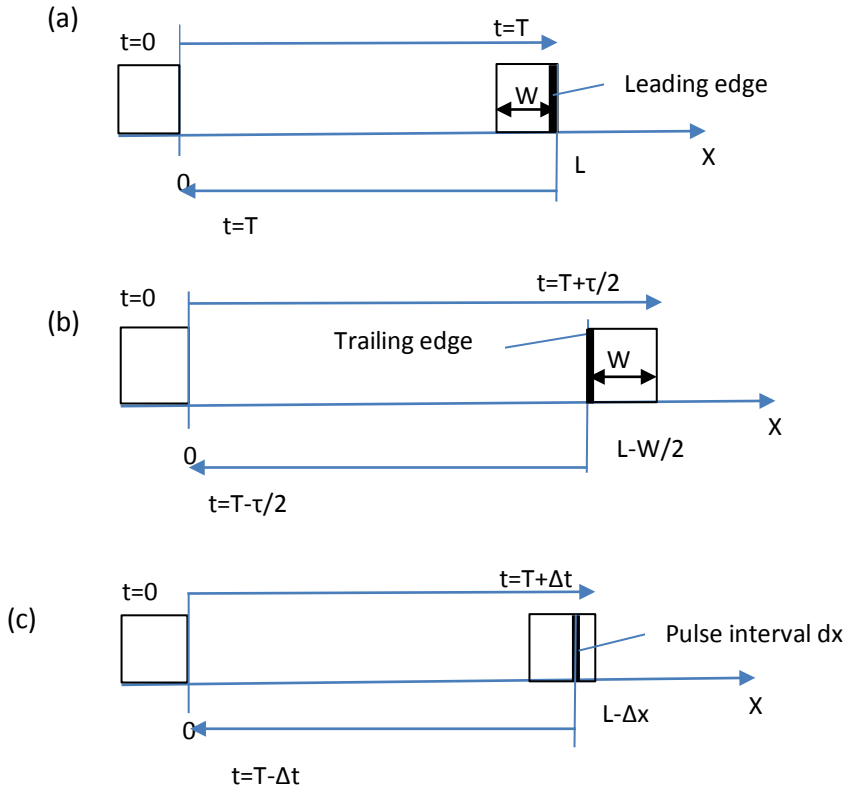

Figure 4.3: Backscatter round trip time for three different scenarios (t=2T) (after, Derickson 1998).

In figure 4.3(a) light is backscattered from the leading edge and it reaches the front point of the OTDR in a round trip time of t=2T after covering exactly the same distance. At time $t = T + \tau/2$, where the trailing edge hits the distance $L - W/2$ (figure 4.3b), the light will travel with a time of $t = T - \tau/2$ back to the input point of the OTDR covering a round-trip time of t=2T. Now consider a short ΔW lagging the pulse leading edge by 2Δx at time t=T+Δt (figure 4.3c). The backscattered light now travels with time t=T-Δt back to the OTDR input again covering a round trip time of t=2T. We can therefore generalize from the above scenarios that at any particular time t=2T, the backscattered power collected by the OTDR will be an integral sum of the backscatter signal within the interval; $L - \frac{W}{2} < x < L$ when probing with a pulse of width W.

Applying this idea to the signal power equation and taking note of attenuation and simplifying yields (Derickson, 1998);

$$P_s(L) = \int_0^W S\alpha_s P(0) exp\left(-2\alpha\left(L + \frac{x}{2}\right)\right) dx \tag{4.8}$$

$$= S\frac{\alpha_s}{\alpha} P(0) exp(-2\alpha L)(1 - \exp(-\alpha W)) \tag{4.9}$$

with $L \geq W/L$, and $t \geq \tau$

For distances within the interval [0,W/2],

$$P_s(L) = S\frac{\alpha_s}{\alpha} P(0) exp(-\alpha W)(1 - \exp(-\alpha L)) \tag{4.10}$$

The initial backscattered power P(i) can be approximately estimated for L=W/2 from the previous equation by conversions between exponential functions and polynomials yielding

$$P(i) = P_s\left(\frac{W}{2}\right) \approx S\alpha_s P(0) W \tag{4.11}$$

For short pulses ($\alpha W \ll 1$), hence,

$$P(i) = P_s\left(\frac{W}{2}\right) \approx S\alpha_s P(0) \exp(-2\alpha L) \tag{4.12}$$

The above equations indicate the important parameters for the effective operation of the OTDR. For narrow pulses, the backscatter power is proportional to the pulse duration τ.

These equations are therefore important for the selection of an appropriate pulse width in order to achieve the right accuracy in terms of resolution of a measurement.

4.1.4 OTDR fibre trace

A diagram of a generic OTDR measurement is shown in figure 4.4. The vertical scale is the back-reflected signal level in decibels (logarithmic scale), and the horizontal axis represents the distance between the OTDR and a location along the fibre. This is a linear scale and it is converted to distance from the time measurements of the backscattered data. Typically, a conversion factor of 10μs/km is used as the round trip propagation delay of light within an optical fibre. From calculations indicated above in previous equations, the accuracy depends on exact timing and the fibre's group index. There are various variations of the OTDR (Healy, 1986) depending on the detection type or the kind optical source being applied.

The backscattered response of the fibre has four major features:

1. A large initial peak resulting from Fresnel reflection at the input end of the fibre.
2. Straight lines caused by the Rayleigh scattering along the length of the fibre,
3. Steps or abrupt shifts along the straight line due to losses at fibre joints or connectors, or bends.
4. Positive spikes from Fresnel reflections at the end of the far end of the fibre, some fibre joints, breaks and imperfections.

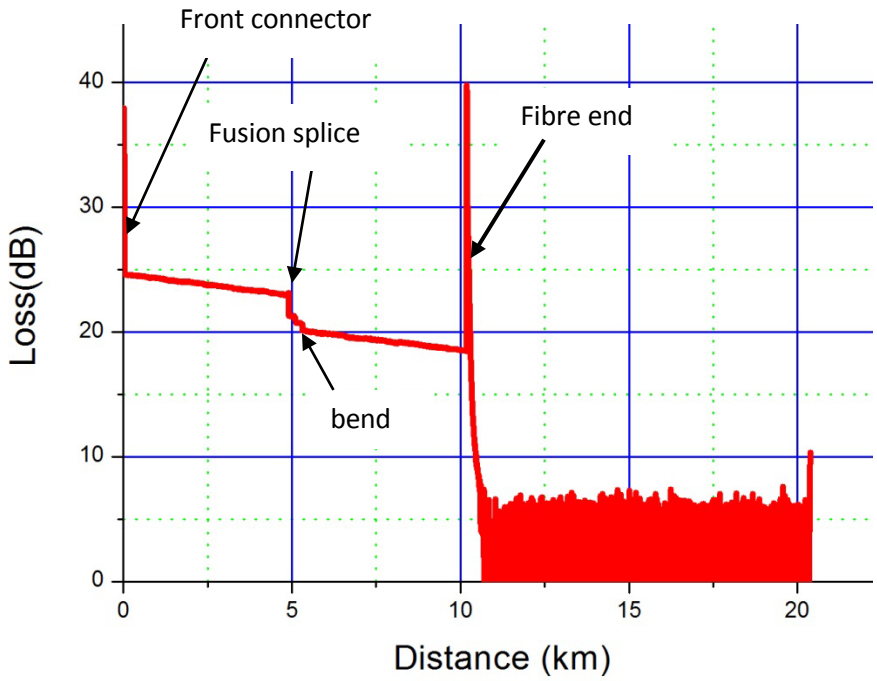

Figure 4.4: An OTDR trace of two fibre spools of lengths 5km each measured at the N.M.M.U optical fibre laboratory by the author.

The first event seen on any OTDR trace is the reflection from the connection of the instrument to the fibre input end. This Fresnel reflection is brought about when light enters a medium with a different refractive index. OTDRs are joined to the test fibre by a connector. A clean high quality connector is important to give low reflectance as some information may be hidden at the front end of the fibre. The open end of a non-terminated fibre causes strong Fresnel reflections depending on the condition of the fibre end. A perfect fibre end reflects about 4% of light incident on it. This is usually seen at the end of the OTDR fibre trace, where since no optical power is detected, the signal drops to the noise level of the detector.

The straight lines give the attenuation of the fibre in dB/km since the plot is that of power (dB) verses distance. Fusion splices causes a sudden drop in the backscattered level of the plot, and the size of the drop is the “insertion loss” of the splice. A similar drop in the power level on the plot is produced by a bend, but in this case, the drop in power level is not so sudden as opposed to the sharp drop of the fusion splice. In the case where the sudden drop in power level has a spike superimposed on it, or even on the straight portion of the trace, it is a mechanical splice, a connector or a crack in the fibre. These are known as reflective events whilst the bends and fusion splice are non-reflective events.

There are situations whereby reflective events can cause features known as “ghost’’ events. If the fibre being tested has connectors or any device along the link that gives high reflectance, echoes generated from multiple reflections from the device can give spikes at false locations on the trace. An echo pulse moving from the fibre to the OTDR is partially reflected at the front connector of the OTDR back into the fibre, thus acting as an additional delayed pulse. The repetition rate of the pulse if too fast and not adapted to the fibre, would overlap at the detector giving rise to wrong data. If connectors are clean and well maintained, the echo is too small to give “ghost” features. Ghost features are located at twice the actual reflective event if the first reflective event is taken to be at the front connector of the OTDR.

OTDRs are used as estimators of the above fibre parameters but to ensure accuracy, it is always good to measure the fibre at both ends and some averaging should be performed.

OTDRs are only good for estimating some system loss mechanisms. However for measuring the PMD, and other fibre characteristics such as beat length and coupling length, the setup needs to be improved to achieve these purposes. The next few sections deal with these issues.

4.2 Polarization sensitive optical time domain reflectometry (P-OTDR)

This is another form of the reflectometric technique but it is modified to be polarization sensitive. A.J. Rogers (1981) observed that by monitoring the evolution of the states of polarization (SOPs) backscattered by an OTDR signal, the changes in birefringence effects caused by any external perturbations can be inferred. The P-OTDR was originally designed as a sensor, but has been applied extensively to characterize single mode optical fibres (Galtarossa ,2003, 2004; Wuilpart, 2002; Dong , 2007; Palmieri *et al* 2011). The advantage of the technique is that, once the birefringence is extracted, many of the fibre’s parameters including polarization mode dispersion, correlation length, beat length and even polarization dependent loss can be deduced. Again, the measurement is spatially resolved so point to point information can be obtained from the birefringence information. Figure 4.5(a) shows a typical P-OTDR signal showing how birefringence is distributed along the fibre. Magnified sections of the same trace are shown in figures 4.5(a) and 4.5(b). Compared to the OTDR signal such in figure4.4, the P-OTDR gives more detailed information about the fibre.

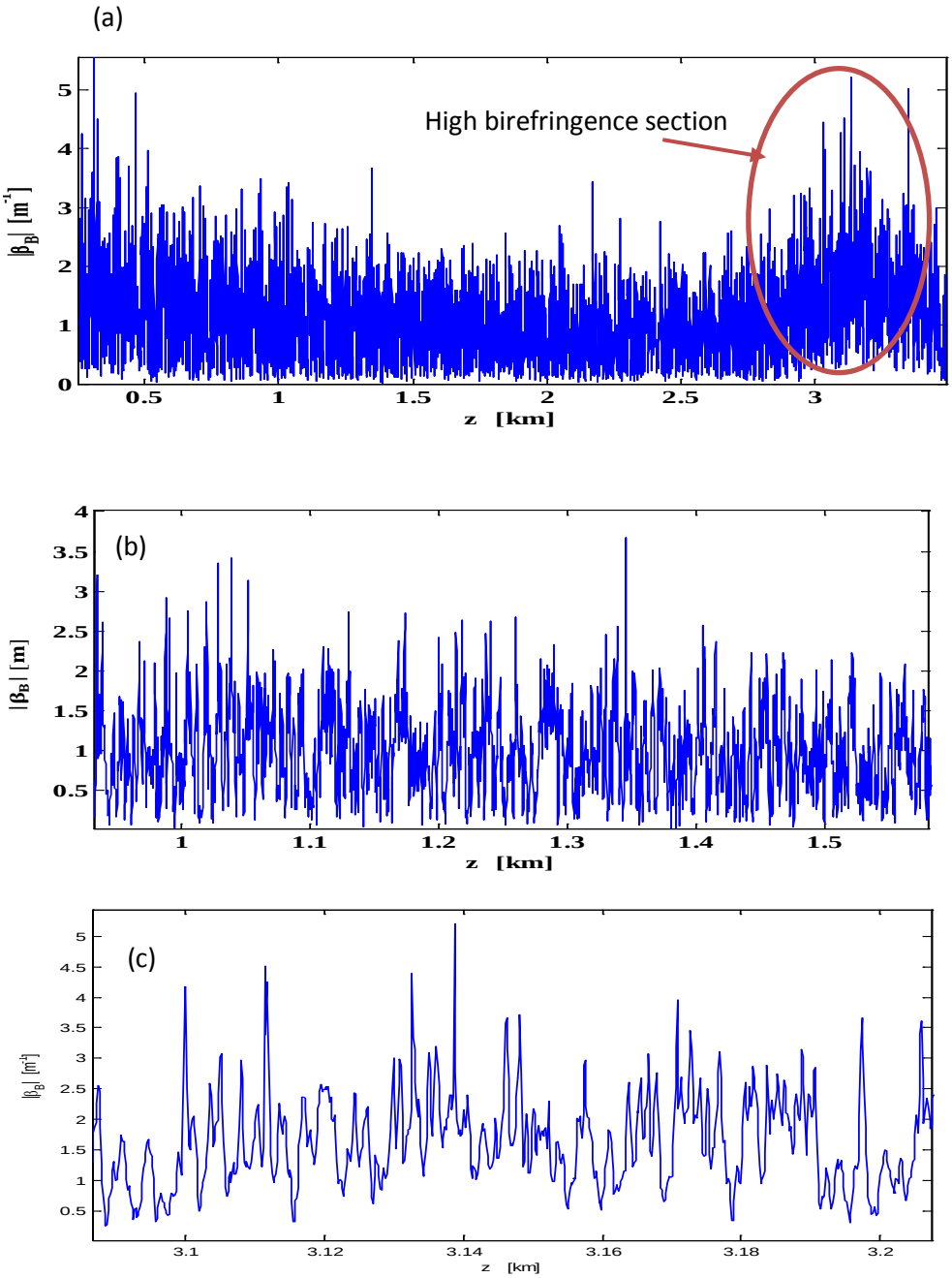

Figure 4.5: (a) A P-OTDR 7racel showing how birefringence varies with distance for a 3.5 km fibre (measured by the author in Padova, Italy June 2009); (b) first 600km of same fibre, (c) last 600m of same fibre.

Figure 4.5 indicates how birefringence which is the cause of PMD may be high at certain sections of a link giving rise to high PMD at such sections. Hence P-OTDR can be used to map out the birefringence distribution along an optical fibre link. Regions of high PMD along and optical fibre link corresponding to regions of high birefringence can thus be

identified and replaced in order to reduce the total PMD. The P-OTDR technique is thus more versatile compared to the ordinary OTDR technique.

4.2.1 Principle of measurement of a P-OTDR

Fundamentally, by measuring the evolution of the SOPs or degree of polarization (DOP) of a backscattered signal, any of the known techniques can be applied to extract the PMD. In most cases the measurements are qualitative and give an idea about places of high and low PMD sections along a link (Huttner, 1999). Figure 4.6 shows a schematic diagram of a P-OTDR setup.

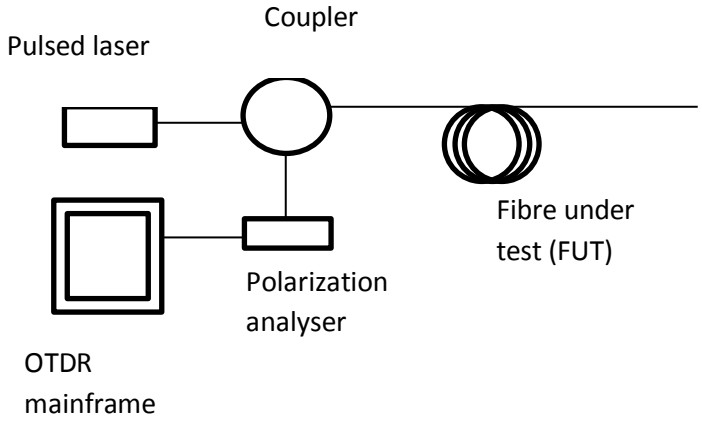

Figure 4.6: Schematic diagram of a P-OTDR setup.

Figure 4.6 depicts a typical P-OTDR setup. The main frame of the OTDR usually drives a suitable laser emitting optical pulses (10-100ns). The principle is the same as the OTDR described above except that the detected signal goes through a polarization analyser into a fast detector. The detected signals are the three Stokes parameters s_1 s_2 s_3 and the total intensity s_0 and hence the state of polarization with respect to time is obtained. In most cases (Huttner, 1999) the instrument measures only the beat-length and coupling length and extracts the PMD from them. It has been demonstrated that the degree of polarization is sometimes a more relevant parameter of the back scattered pulse due to depolarization (Hutner, 1999). Care has to be taken however not to confuse depolarization caused by the OTDR laser line-width and the temporal depolarization caused by the local birefringence of the fibre which forms the basis of the measurements.

4.2.2 Measurement of PMD through coupling length/ beat length

Rayleigh back scattered signals are retrieved by the polarization analyser as a function of distance from scattering point. This is best represented by the SOP on the evolution of a Poincaré sphere. The SOP of the light in a birefringent fibre rotates around the birefringence axis. The velocity of the rotation is equal to the local birefringence β which is related to the beat-length L_b by the relation;

$$L_b = \frac{\lambda}{\beta_c} \tag{4.13}$$

where λ is the wavelength.

The beat-length indicates the periodicity of the rotation about the axis. The distance after which the birefringence moves significantly is known as the coupling length h. The spatial correlation for the birefringence vector is given by equation 4.14, with $\vec{\beta}(z) = \beta(z)\hat{u}$ where β is the birefringence and $\hat{u}$ is the birefringence axis on the Poincare sphere;

$$\frac{1}{L}\int_0^L \vec{\beta}\,(z).\vec{\beta}(z+\Delta)dz = \bar{\beta}^2 \exp(-2\frac{|\Delta|}{h}) \tag{4.14}$$

where $\bar{\beta}$ is the root mean square average of the birefringence over a length L and is obtained by substituting $\Delta = 0$.

By plotting the SOPs on a Poincaré sphere and looking at the displacement as a function of distance, one can infer the beat length. The value of h can be derived by finding the rotation axis at all points. This involves differentiation and therefore any noise or inaccuracy in finding SOP will create difficulties in the accurate determination of h.

PMD is not a local parameter, but by measuring the parameters, which are the beat length and coupling length, for a section say l, the PMD can be calculated as (Gisin, 1991);

$$PMD = \frac{\lambda}{L_b c}\sqrt{lh} \tag{4.15}$$

For a total link of N concatenations with i sections the total PMD is given by

$$PMD = \sqrt{\sum_{i=1}^{N} PMD_i^2} \tag{4.16}$$

The above equations show that the beat length and the correlation length control the PMD in opposite ways. A high L_b means a smaller PMD while a large h means a high PMD. It is thus crucial to know these parameters separately. For most commercial fibres (including old ones), the range of the variation of these parameters is

$$0.5 \leq L_b \leq 20m$$

$$5 \leq h \leq 500m$$

It has been observed that older fibres with high PMD have longer coupling lengths than newer fibres (Huttner *et al.* 1999).

It should be noted that it is difficult to measure fibres which exhibit very high birefringence such as polarization maintaining fibres and fibres with circular birefringence. P-OTDRs can achieve spatial resolutions of about 0.5m in measurements of fibres ranging tens of kilometres.

4.3 Optical frequency domain reflectometry

Optical frequency domain reflectometry is usually applied to shorter fibres and achieves much better resolution. It permits the determination of beat-lengths of a few millimetres and was first developed for fibre component testing (Froggatt, 2006; Von der Weid, 1997). Most of the previous OFDR techniques applied Fourier transforms to calculate beat-length from the time-domain amplitude data, but currently the methods apply autocorrelation of the distributed scattered signal. The use of the distributed autocorrelation Rayleigh signal of the fibre under test (FUT) to calculate the group birefringence enhances the OFDRs, resolution. Currently these techniques have been varied to measure strain induced birefringence of optical fibres due to twist (Galtarossa, 2009).

A basic set of the technique is shown in Figure 4.6. The measurement setup consists of a tuneable laser source and a reference interferometer with polarization controller (PC1 to prevent fringe fading. The delay line L determines the sampling increments on the S and P modes. Polarization controller 2 (PC2) ensures that the reference power splits equally on the polarisation beam splitter (PBS) between the P and S modes.

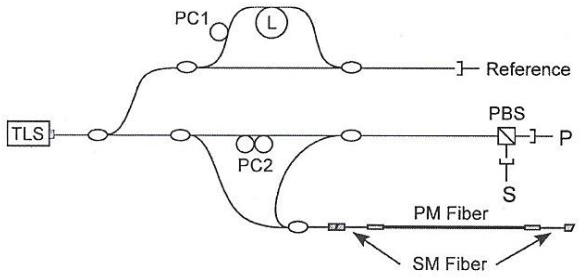

Figure 4.7: A schematic of an OFDR system (after Froggatt, 2006)

The tuneable laser sweeps over a range of wavelengths to produce high resolution. The polarization states of the backscattered signal are arbitrary so a polarization diversity detection system is employed (PC2). PC2 adjusts the polarization of the light in the path of the reference interferometer such that light is split between the two states of the reference interferometer. The reference interferometer provides a high resolution tuning of the laser resulting in high resolution transform data. A fast Fourier transform is then performed to convert the data from frequency domain into time domain. The two channels recorded for each polarization state ensure detection of the total power reflected from the DUT. The scatter profile from the core of the fibre is assumed to be a set of complex numbers, based on which beat-length measurements are constructed. Further analysis and applications of this technique can be found in Huttner, 1999 and Froggatt, 2006.

3.4 Summary

In this chapter reflectometric techniques (single-end) for characterizing optical fibre loss have been discussed. While an ordinary OTDR is limited to measuring specific losses, P-OTDR can measure and characterize almost all fibre losses. Further OFDR techniques offer better measurement resolution but for shorter fibres. In the next chapters we present experimental results based on P-OTDR techniques.

CHAPTER 5

SINGLE-END INTERFEROMETRIC THECHNIQUE

5.1 Introduction

Over the years, interferometric methods for measuring PMD have proved to be highly accurate and applicable to a wide range of fibre types (Gisin, 1991, Oberson, 1997). Due to its robustness it is very suitable for measurements in the field for both aerial and buried fibres. Interferometric techniques have proved to be simple and easy to implement. As such both traditional interferometry (TINTY) and generalized interferometric techniques (GINTY) have been extensively used to measure PMD across South Africa by the NMMU optical fibre research unit (Gibbon, 2005; Mudau, 2007 and Wu, 2006, Fosuhene, 2011). In this chapter, the ideas of low coherence interferometry are applied to make single-end measurements of polarization mode dispersion. The aim was to modify GINTY such that it can be more suitable for field measurements. The basic instrument is the EXFO-5500B PMD analyser (GINTY). A brief theory of the general measurement principles of the Michelson interferometer and the generalized interferometric technique is presented. The measurement method is applied to three sets of fibre types in different coupling regimes (nine fibres in total). A relationship is then established between measurements in forward and single-end for three different fibre types.

5.2 Background of interferometric techniques

The two standard interferometric techniques for measuring PMD, classified as time domain measurements are based on the principles of low coherence inteferometry (TIA/EIA 455-124A 2004). The traditional technique (TINTY) was the first one to be developed. Later it was modified and renamed the generalized interferometric technique GINTY (Cyr, 2004). Interferometric techniques make use of a broadband source to measure the delay between two arms of an interferometer. The accuracy of the measurement depends on the coherence time (T_c) of the source. The coherence time is the duration within which the characteristics of the source are stable and remain in a predictable phase (Hecht, 2002).

For a time domain measurement, the coherence time T_c of the source should satisfy the conditions (Williams, 2004, 2005);

$$\Delta\tau < T_c \tag{5.1}$$

$$T_c \propto \lambda^2/c\Delta\lambda \tag{5.2}$$

where, $\Delta\lambda$ is the differential group delay, λ is the centre wavelength of the optical source, c is the speed of light and $\Delta\lambda$ is the full-width at half-maximum of the coherence source.

The proportionality sign in equation 5.2 could be eliminated by multiplying the right-hand side of the equation by a factor depending on the spectrum shape - 0.44, 0.88 and 1.2 for a Lorentzian, Gaussian and rectangular spectrum respectively (Derickson, 1998). According to equation 5.2 the resolution of the measurement can be influenced by choosing an optical source with the appropriate frequency spectrum.

Figure 5.1 shows a traditional Michelson interferometer. Light from the source S is split into the two arms of the interferometer and recombine at the detector D after reflections from the stationary and movable mirrors respectively. Constructive interference occurs when light reflected from both arms of the interferometer have travelled equal path lengths.

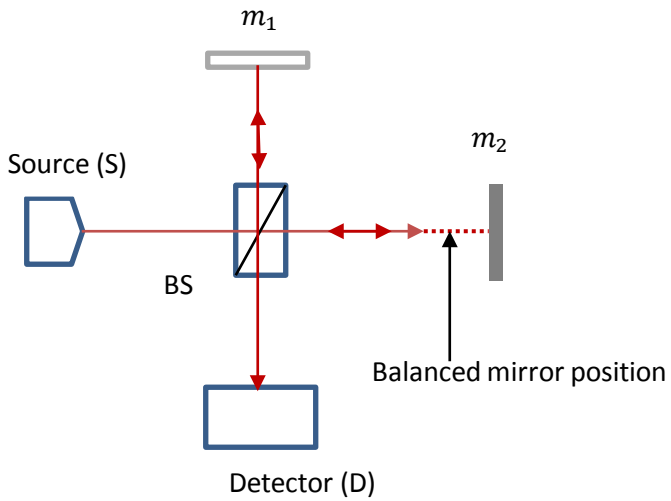

Figure 5.1: A schematic diagram of a typical Michelson interferometer; S is the optical source, BS is a beam splitter, while m_1 and m_2 are stationary and movable mirrors respectively.

In the case where there is a fibre under test (FUT) inserted before the interferometer, interference peaks appear at positions where the delay in the FUT is compensated by the delay in the moving arm of the interferometer.

Delays in the FUT are expressed as (Derickson, 1998);

$$\Delta\tau = \frac{2\Delta x}{c} \tag{5.3}$$

where c is the speed of light, $\Delta\tau$ is the delay time of the FUT and Δx is the displacement of the movable mirror from the balanced mirror position. The factor of 2 in equation 5.3 occurs because distance refers to one way excursion along the test wave guide but delay includes traveling both ways.

5.2.1 TINTY vs. GINTY

Both TINTY and GINTY operate on the general principles of the Michelson interferometer described above, but with some additions. In determining PMD of fibres, polarization effects have to be considered. Real fibres are mode coupled devices and there is constant coupling between modes during transmission resulting in a complicated interference waveform (Gisin, 1991; Gibbon, 2003). In principle there is not much difference between GINTY and TINTY. The major differences are the underlying assumptions and how the interferograms are obtained and analysed.

Firstly, TINTY assumes that the FUT is a randomly mode coupled device of infinite coupling ratio and the PMD is larger than the source coherence time. It calculates the interferogram (Gaussian) as a statistical average of all possible occurrences with a given conceptual PMD value (Gisin, 1991; Heffner, 1996). These tight assumptions affect the PMD calculations in the event where the interferogram from an FUT deviates from a Gaussian. In addition, TINTY was not considered suitable for long haul amplified links (IEC6280-4-4). According to Cyr, 2003 when components such as amplifiers, isolators or filters are added to a link some of the underlying conditions of the analysis of the interferograms are not met.

The GINTY technique, introduced by Cyr (2003, 2004), is devoid of such assumptions. The underlying theory is mathematically exact and ideal for all coupling regimes, irrespective of the shape of the interferogram. The only assumption that is retained is that of negligible polarization dependent loss (PDL). It is based on these arguments that we favoured to work

with GINTY. In the next section we present a brief background of the GINTY based on the account of Cyr (2004).

5.3 GINTY: Theory and principle of operation

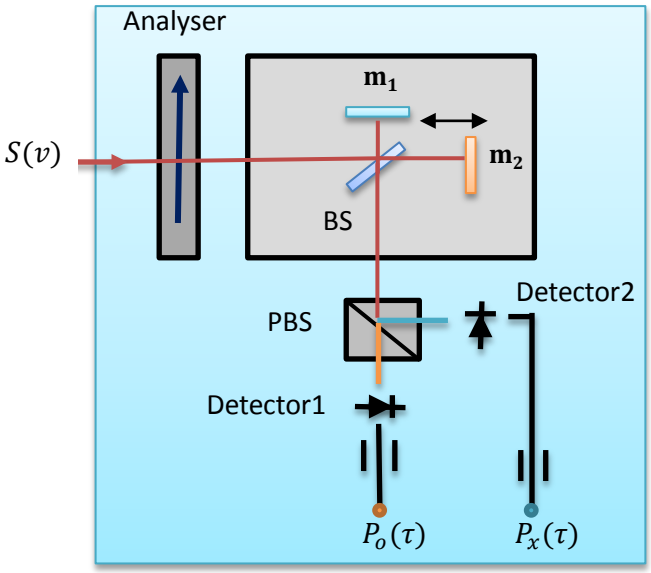

Figure 5.2: Schematic diagram of GINTY; PBS is a polarization beam splitter, which splits the interferograms into two orthogonal polarizations $P_o(\tau)$, $P_x(\tau)$ which are detected by detecctor1 and detector 2 respectively.

A schematic diagram of the GINTY (EXFO FTB 5500B) measurement technique is depicted in figure 5.2. The Michelson interferometer configuration is represented by the movable mirror (m_2), stationary mirror (m_1) and a polarization beam splitter BS. The detection system consists of a polarization beam splitter (PBS) and two separate detectors - polarization diversity detection. The interferogram from the Michelson interferometer is split into two by the (PBS) and then detected separately. The detected signals $P_0(\tau)$ and $P_x(\tau)$ have mutually orthogonal polarization states of polarizations (SOPs). If we consider a signal $s(v)$ emerging from a FUT and entering an analyser aligned at S_a, it emerges as a Fourier transform with a constant SOP independent autocorrelation part and a cross correlation (SOP dependent) part. The autocorrelation $(E_a(\tau))$ and cross correlation ($E_c(\tau)$) are calculated as the sum and difference between the two orthogonal pairs respectively as,

$$E_a(\tau) = |P_o(\tau) + P_x(\tau)| \tag{5.4}$$

$$E_c(\tau) = |P_o(\tau) - P_x(\tau)| \tag{5.5}$$

Equation 5.4 and equation 5.5 refer to a single envelope of input /output (I/O) pairs of states polarization. For an entire ensemble of (I/O) pairs such as in the case of polarization scrambling, averaging is recommended.

The PMD is calculated for the FUT from the cross and auto correlation by (TIA-455-124-A)

$$PMD = \sqrt{\frac{3}{2}(\sigma^2 - \sigma_0^2)} \tag{5.6}$$

where σ^2 is the root mean square (RMS) width of the cross correlation envelope and σ_o^2 is the RMS width of the autocorrelation envelope. The envelopes are given by

$$\sigma^2 = \frac{\int \tau^2 E_c^2(\tau) d\tau}{\int E_c^2(\tau) d\tau} \tag{5.7}$$

$$\sigma_o^2 = \frac{\int \tau^2 E_a^2(\tau) d\tau}{\int E_a^2(\tau) d\tau} \tag{5.8}$$

PMD measurements are sensitive to polarization and therefore in order to obtain an accurate knowledge of the PMD of an FUT, it is necessary to cover a good number of possible I/O SOPs. This procedure is known as polarization scrambling. Scrambling is performed to obtain an ensemble of PMD values upon which a reliable PMD value is obtained. Scrambling can be scan-to-scan or continuous. In scan-to-scan, the scramblers are varied independently for every interferometer setting. For continuous scrambling, it takes place while the interferometer is still scanning. Generally, the uncertainty of a single scan measurement is given by (Mankga, 2007);

$$\sigma_{single-scan} = \sqrt{\left((1 - \frac{8}{3\pi}) \frac{1}{\sqrt{1 + \frac{1}{4}(\frac{PMD_{mean}}{\sigma_A})^2}}\right)} \tag{5.9}$$

where σ_A is the RMS width of the autocorrelation of the light source and PMD_{mean} is the mean PMD calculated from an ensemble of SOP variations. For N number of I/O scan-to-scan measurements, the uncertainty (σ) incurred in this case is;

$$\sigma = \sigma\_(single - scan)/\sqrt{N} \tag{5.10}$$

5.3.1 Single-end measurements with GINTY

In this section single-end measurements based on GINTY are presented. Measurements were made on three different categories of FUTs. The optical broadband source was the EXFO–FLS 5800 and the GINTY analyser was the EXFO-FTB5500B. Both source and detector operate within the O (1260-1360nm), C (1530-1565nm) and L (1565-1625nm) bands of the optical spectrum. The analyser has a sensitivity of up to ~ (-45dB) and a dynamic range of about 50dB. It can measure PMD between 0-115ps. Such a dynamic range implies that the system can measure up to about 250km (for a fibre with 0.2bB/km). The uncertainty of this system is given by (Mudau, 2008);

$$\sigma = \pm(0.02 + 2\%PMD) \tag{5.11}$$

5.3.2 Experimental set-up

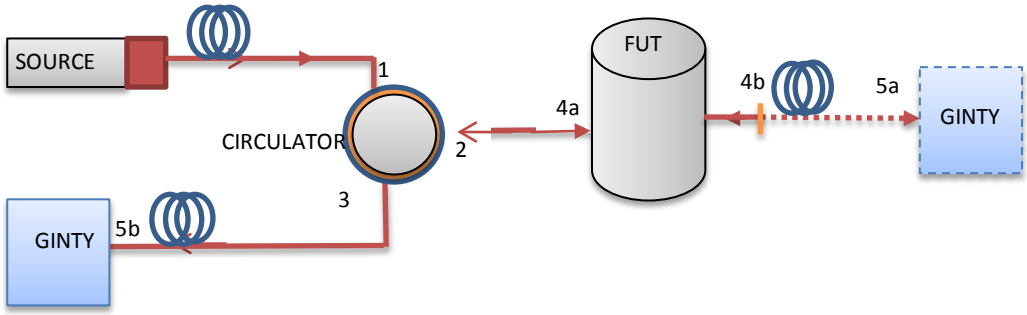

Figure 5.3. Set up for single-end and forward measurements using GINTY, the optical path for forward measurement is 1-2-4a-4b to 5a, and that for single-end is 1-2-4a-4b and back through 4a-2-3 to 5b.

Figure.5.3 shows the experimental scheme of how GINTY is adapted to measure in both single- end and forward configurations. A circulator with ports 1, 2, and 3 was used. Light travels through the ports in the directions 1-2 and 2-3. In the forward configuration the light travelled from the source through port 1-2, through points 4a-4b and then from 4b-5a. For a single-end measurement, the connection 4b-5a is eliminated and the GINTY is now connected at 5b via port 3 of the circulator. Light undergoes Fresnel reflection at the fibre end face at point 4b. The optical path for this configuration is therefore 1-2, 2-4a, 4a-4b and then back through 4a-2, 2-3 and then detected via 3-5b. To ensure stability and accuracy of measurements all patch cords were firmly fixed on the experimental bench. Measurements

were taken for both forward and single-end configurations without any significant disturbance of the set-up which could affect results.

5.3.3 Calculation of PMD

The magnitude of PMD which is the differential group delay (DGD) of two fibre sections with DGDs $\Delta\tau_1$ and $\Delta\tau_2$ can be estimated as Cyr (2004);

$$\Delta\tau_{tot} = \sqrt{(\Delta\tau_1^2 + \Delta\tau_2^2 + 2\Delta\tau_1\Delta\tau_2\cos\theta)} \tag{5.12}$$

where θ is the angle between three SOP axes on the Poincaré sphere indicating the coupling between the two fibres.

We consider our single-end measurement as a two-section device with DGDs $\Delta\tau_1 = \Delta\tau_2 = \Delta\tau$. That is, the signal travels to one end of the fibre and is coupled back into it. In this case equation 5.12 then becomes,

$$\Delta\tau_{tot} = \sqrt{(2\Delta\tau^2 + 2\Delta\tau^2\cos\theta)} \tag{5.13}$$

The value of $\Delta\tau_{tot}$ can then be estimated as

$$\Delta\tau_{tot} = \sqrt{2}\Delta\tau\left(\sqrt{1 + cos\theta}\right) \tag{5.14}$$

For a continuous wave system such as ours, Fresnel reflection is more dominant (Corsi, 1999) and so we consider the angle θ in the interval $0 < \theta < 90$ $(0 < \cos\theta < 1)$. Then we may expect $\sqrt{2}\Delta\tau < \Delta\tau_{tot} < 2\Delta\tau$. Moreover, for Fresnel reflection the relationship between the forward and single-end measurement is given by (Galtarossa, 2003, 2004; Corsi, 1999)

$$\Delta\tau_B = \frac{\pi}{2}\Delta\tau_f \tag{5.15}$$

where $\Delta\tau_B$ is the round trip (single-end) DGD and $\Delta\tau_f$ is the forward DGD measurement.

In the next sections we present results obtained for various FUTs. The experimental results obtained were compared with expected theoretical results according to equation 5.15.

5.3.4 Measurements on polarization maintaining fibres (PMFs)

Polarization maintaining fibres are specially made to retain a constant delay between the two orthogonal Eigen modes within the fibre. They are considered non-mode coupled if they are

not concatenated or coupled with other fibres. Measurements were made on two PMF fibres of length 1m and 2m respectively both in forward and single-end modes. The two fibres were then concatenated and measured again. Results are shown and summarised in figure 5.4 and Table 5.1 respectively.

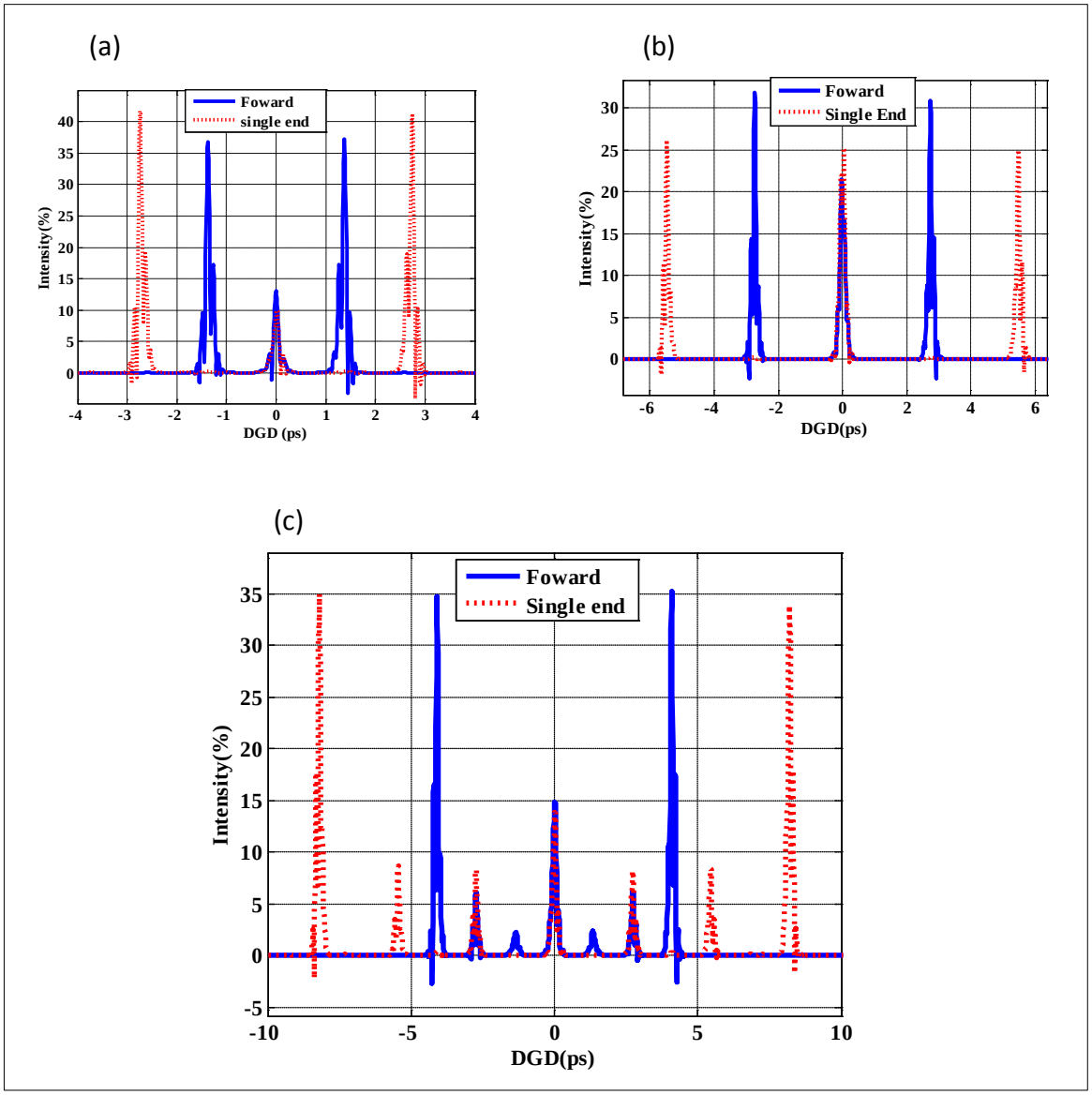

Figure 5.4: Interferograms for: (a) 1m PMF, (b) 2m PMF and (c) concatenation of 1m and 2m PMFs, Solid lines indicate forward measurements and dashed lines indicate single-end measurements.

Table 5.1: Delays for 1m PMF, 2m PMF and concatenation of the two segments. Uncertainty was calculated according to equation 5.11.

FUT	Forward $\Delta\tau_f(ps)$	Single- end $\Delta\tau_B\,(ps)$	Ratio	Uncertainty (Forward) $\pm\sigma_f$	Uncertainty (Single-end) $\pm\sigma_B$
1m PMF	1.38ps	2.74ps	1.99	0.05	0.07
2mPMF	2.73ps	5.48ps	1.99	0.07	0.11
2mPMF+1mPMF	4.10ps	8.20ps	2.00	0.08	0.18
Sum of PMF1n2	4.11ps	8.22ps	2.00	0.08	0.18

From figure 5.4, it was observed that the forward measurements of the 1m and 2m PMFs show one peak each on the left and the right of the central peak (solid curve). The distance between each peak to the centre is the DGD of the FUT. This is characteristic of none mode coupled devices with a constant delay (equation 5.3). The single-end measurement (red dashed curves) shifts the peaks to twice their original positions ($2\Delta\tau_f = \Delta\tau_B$). In figure 5.4(c) which is a concatenation of the two segments, both DGDs for the two lengths are present together with a total DGD due to the combination of the two segments. The single-end delay of the 1m PMF coincides with the forward delay for a 2m PMF. It thus behaves like a 2m PMF. It is also interesting to note that both the forward and single-end indicate three peaks representing the two individual sections and a combination of the two and in each case, the single-end is twice the forward. The values in table 5.1 agree very well with equation (5.14) when $\theta = 0$, with the reflected signal coupling back into the fibre along the same axes as the forward. Further since the three PMFs and their concatenations can be treated as non- mode coupled devices and operating in the short length regime, the DGD grows linearly with length unlike the long length regime where it scales as the square root of the length (see section 3.1.1 and 3.1.2 of chapter 3). Again the low uncertainty values (between ±0.05 and ± 0.18) in Table 5.1 confirms that the experimental results agree very well with theory.

5.3.5 Measurements on low PMD single mode fibres

PMD measurements were performed on three standard single mode fibres: fibre1, fibre2 and fibre3. Fibre1 and fibre 2 are two spools of standard single mode fibres of lengths 3km and

23km respectively while fibre3 is a 24km cabled fibre on a drum. Forward and single-end measurements were performed for an average of 10 I/O scrambling positions on the Poincaré sphere. A total of 50 scans were performed for each fibre, i.e. 5 averaged scans for each position.

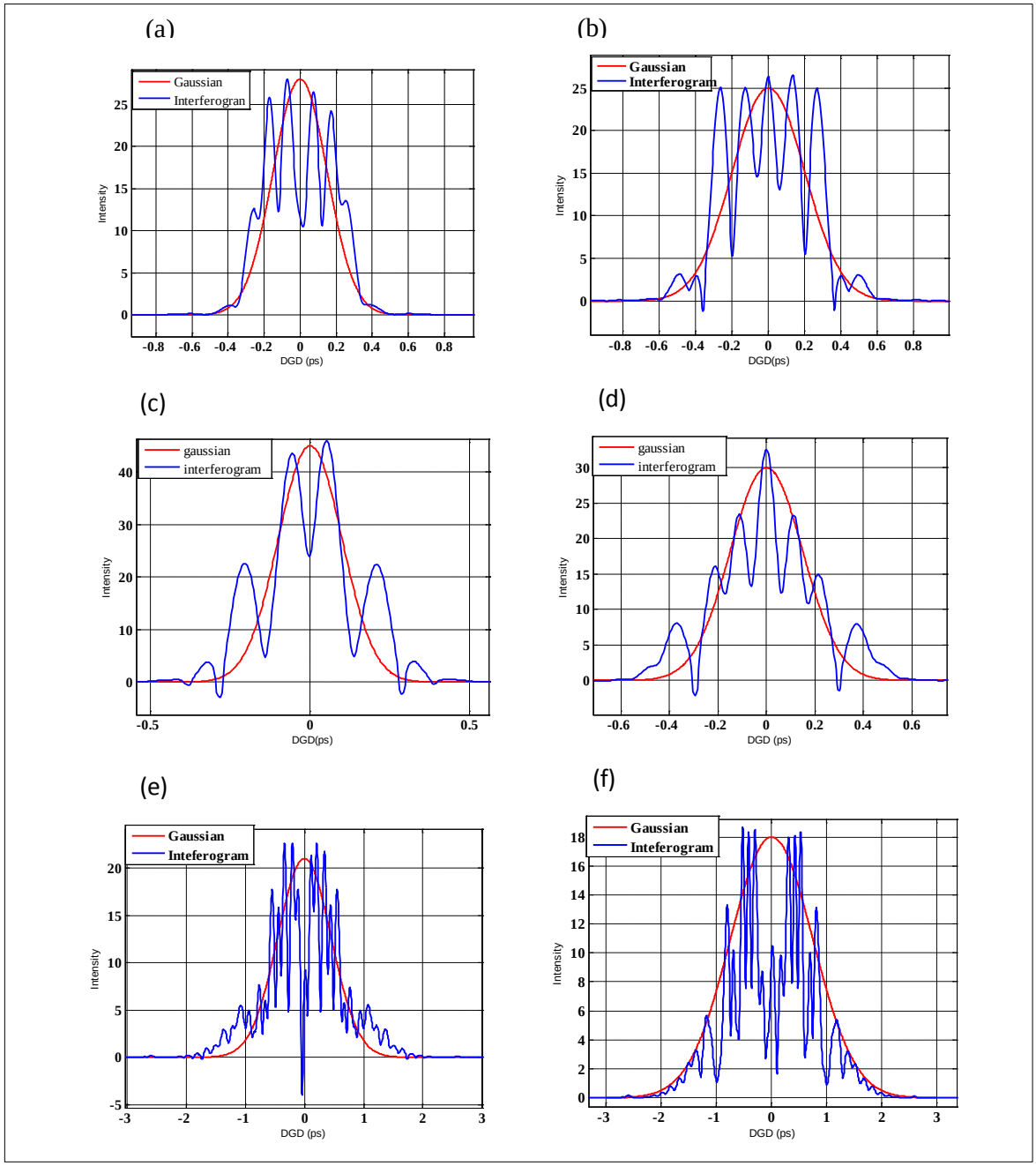

Figure 5.5: Some interferograms for the three weakly mode coupled fibres: (a), (c), (e) represents forward measurements while (b), (d), (f) represent single-end measurements for fibre1, fibre2 and fibre3, respectively. The DGD could be estimated from the FWHM of the Gaussian fits to the interferograms.

Figure 5.5 (on previous page) shows some interferograms for the three different fibres in both forward and single end configurations. Each interferogram represent an average of five scans. In the figure, (a) and (b) represent forward and single end configurations for fibre1 respectively, (c) and (d) for fibre 2 and (e) and (f) fibre 3. Figure 5.6 shows the scrambling positions on a Poincaré sphere and a plot of forward vs. single end DGDs for the three fibres. The results are summarised in Table 5. 2.

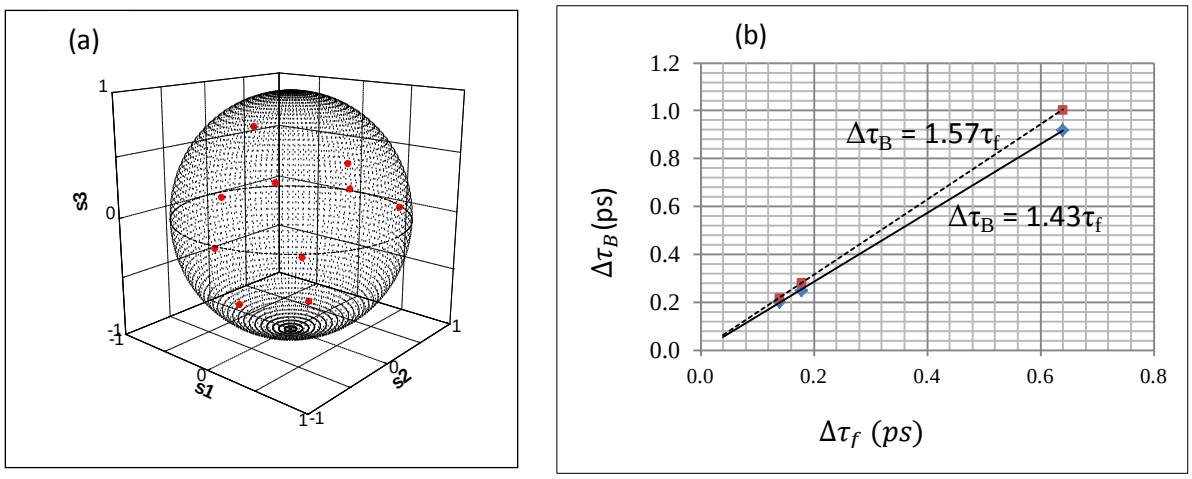

Figure 5.6: (a) A plot of I/O SOP scrambling positions on the Poincaré sphere; (b) A plot of forward measured DGDs $\Delta\tau_f$ (ps) vs. single-end DGDs $\Delta\tau_B$ (ps) for the three fibres, solid line represents experiment while dashed line represents theory.

Table 5.2: Forward and single-end measurements for the three fibres. Uncertainties were calculated according to equation 5.11.

FUT	DGD (forward) $\Delta\tau_f(ps)$	DGD (single-end) $\Delta\tau_B(ps)$		Uncertainty (forward) $\pm\sigma_B$	Uncertainty (single-end) $\pm\sigma_f$
		Expt.	Theory		
Fibre1	0.18	0.25	0.28	0.03	0.02
Fibre2	0.14	0.20	0.22	0.02	0.02
Fibre3	0.64	0.92	1.00	0.04	0.03

The I/O scrambling was done to indicate some of the possible polarization states of the light source as indicated on the Poincaré sphere in figure 5.6. In Table 5.2 it can be observed that fibre1 and fibre 2 which are uncabled have mean DGD values lower than fibre 3 which is cabled. This could be due to some induced birefringence introduced during the cabling process as explained under section 3.1.1 of chapter 3. Figure 5.6(b) indicates the relationship between forward and single end measurements. Solid lines represent experimental values while dashed lines represent theory. The ratio between the single-end the forward measurement is about 1.43 while the expected theoretical value is 1.57, indicating very good agreement between theory and experiment. The slight difference in the theoretical and experimental values is due to the effects of random mode coupling, which can act to reduce or increase PMD depending on the mode coupling angles (see section 3.1.2 of chapter 3). The maximum and minimum uncertainty for this set of measurements is 0.02 and 0.04 respectively. This implies that measurements are accurate and repeatable.

5.3.6 Measurements on High PMD fibres

Measurements were finally carried out on three highly mode coupled fibres comprising concatenations of single mode fibres and polarization maintaining fibres spliced together randomly. The interferograms in figure 5.8 reveals the nature of the mode coupling events and the resulting DGDs for these FUTs. A plot of the forward vs. single-end DGDs are presented in figure 5.7 together while summary of the results are presented in Table 5.3.

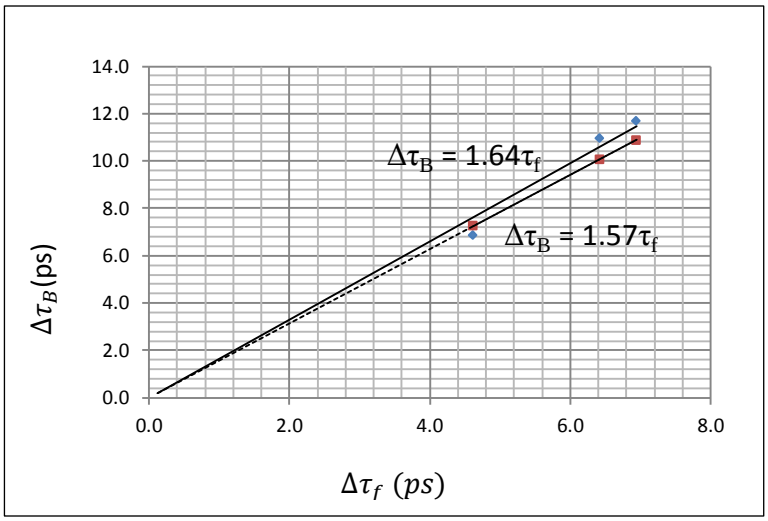

Figure 5.7: A plot of forward measured DGDs $\Delta\tau_f\,(ps)$ vs. single-end DGDs $\Delta\tau_B\,(ps)$ for three highly mode coupled FUTs. The solid line represents experiment while dashed line represents theory.

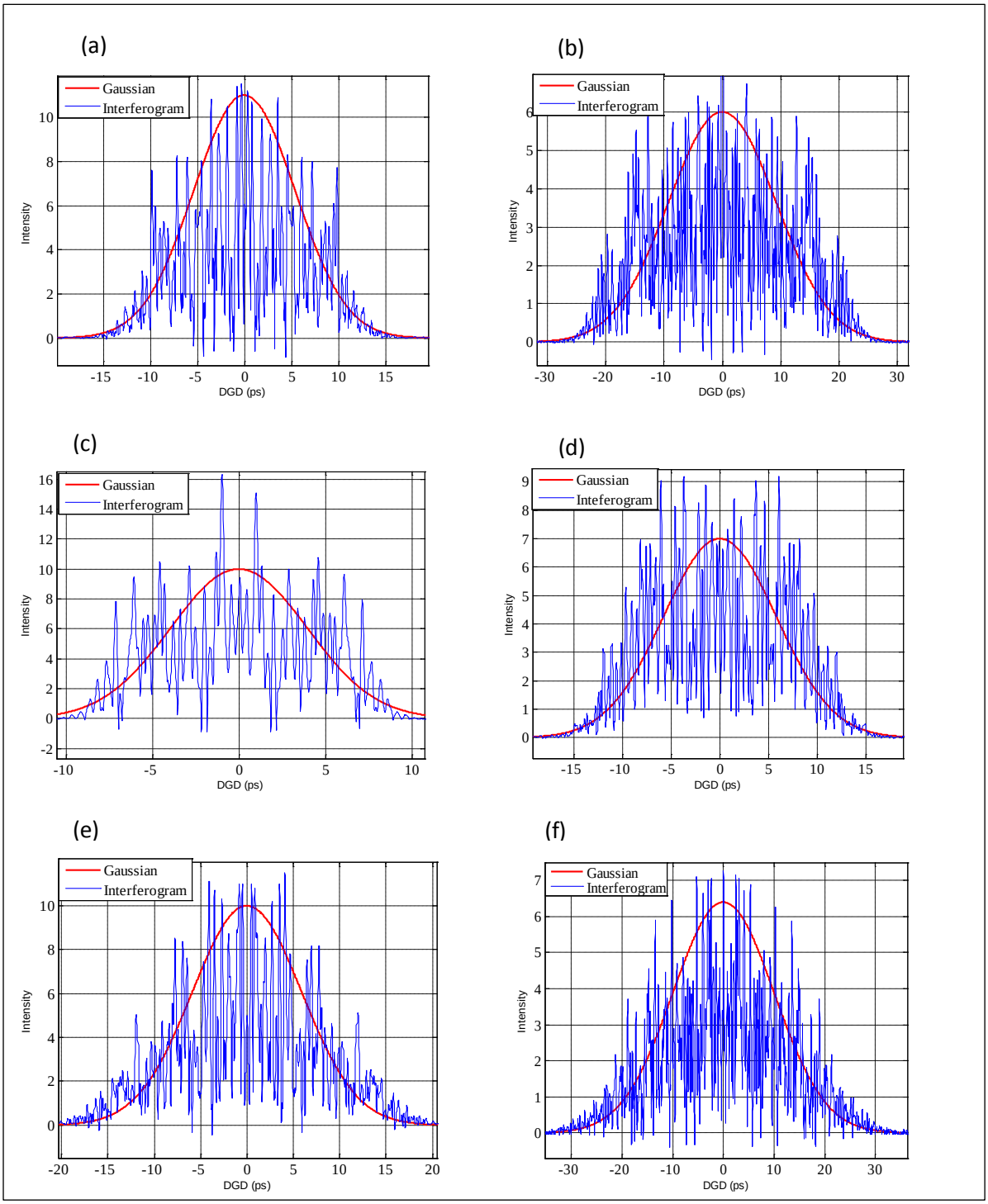

Figure 5.8: Some interferograms representing the three highly mode coupled FUTs: (a), (c) and (e) represents forward measurements for fibres 4,5and 6 while (b) (d) and (f) represent single end measurements. Each interferogram represents an average of five scans.

Table 5.3: Forward and single-end measurements for the three highly mode coupled FUTs. Uncertainties were calculated according to equation.5.11.

FUT	DGD (forward) $\Delta\tau_f(ps)$	DGD (single-end) $\Delta\tau_B(ps)$		Uncertainty (forward) σ_B	Uncertainty (single-end) σ_f
		Expt.	Theory		
Fibre4	6.42	10.96	10.10	0.15	0.24
Fibre5	4.62	6.84	7.25	0.11	0.15
Fibre6	6.94	11.65	10.90	0.16	0.26

The interferograms presented in figure 5.8 shows the nature of mode coupling in FUTs under consideration here, where the FUTs consists of PMF and single mode fibres (SMF) randomly spliced together. Each interference peak represents a delay between the two arms of the interferometer. The DGD values are a high due to the random mode coupling at the spliced points between the single mode fibres and the polarization maintaining fibre. In this case, there is random coupling between a high birefringence segment and low birefringence segment when the light travels from a PMF segment to a SMF segment. As has been explained earlier, the PMD of the PMF segments grows linearly with length while that of the longer SMF segments scale as the square root of the length. A combination of the two thus produces the observed results presented in figure 5.7, 5.8 and Table 5.3. It can be observed from Table 5.3 and figure 5.7 that the experimental values are still in very good agreement with the expected theoretical values. Here the ratio between the forward and the single-end is 1.64 which is falls within that of the high and low PMD fibres.

5.3.7 Discussions

The results from the above measurements show the difference between DGDs of different FUTs for both forward and single-end configurations using GINTY. For the non-mode coupled FUTs, the DGDs for the single-end measurements are twice that of the forward measurements. For these FUTs the single-end regime acts like the same fibre having twice the length. This is also because they are quite short and in the short length regime the PMD

grows linearly with length. For the three low PMD fibres (fibre1, fibre2 and fibre3), the ratio between the single-end and the forward measurements is about 1.4. In this case the fibres are considered to be in the long length regime and the PMDs scale as the square root of the fibre lengths (Derickson, 1998). Again the DGD can be viewed as the mean DGDs resulting from various mode coupling sites which could vary the total DGD depending on the coupling angles. For the high PMD concatenated fibres, the ratio between the single-end and forward measurements is about 1.64. This also falls within the expected range according to equation 5.14. The value is slightly higher than that of the low PMD fibres and lower than that of the PMFs. This is because the FUTs are a combination between the two fibre types and therefore should exhibit both characteristics. Random coupling between PMFs and single mode fibres act together to produce total PMD values which lie in between that of the different segments.

5.4 Summary

In this chapter single-end measurements have been applied to the general intereferometric method (GINTY). Three different types of FUTs were explored. The interferograms indicate the type of coupling regime. The PMFs have constant DGDs and could represent delays due to devices in a system. The low PMD FUTs show different interferograms with fewer peaks due to their stability and mode coupling regime. The characteristics of these FUTs are similar those used in stable environments, such as the laboratory (fibre1 & fibre2) and that of buried fibre (fibre3). The interferograms of the third category also reveal the random nature of the DGDs due to the random mode coupling. Their characteristics could be related to that of fibres in an unstable environment such as aerial fibres, which are very much affected by environmental conditions such as wind and temperature.

GINTY is a standard test method which is robust and suitable for almost all PMD measurements including aerial fibres, hence a single-end measurement technique based on it has a great potential. The only limitation to this method may be distance but even so, in principle, it should be able to measure distances close to 100km which may be adequate for measurements on metropolitan networks.

It has been demonstrated through experiment and theory that GINTY can be applied to measure PMD in single-end configuration. The key factor is to identify the FUT being measured and to choose the right ratios as discussed above in order to estimate the actual DGD. This novel method is cost effective, and simple to implement.

CHAPTER 6

CHARACTERIZATION OF SINGLE-MODE OPTICAL FIBRE USING P-OTDR TECHNIQUES

6.1 Introduction

An optical fibre can be characterized by its response to light. One of these characteristics is polarization mode dispersion. This effect is due to optical birefringence. The birefringence which can be extrinsic or intrinsic is a statistical phenomenon (Gisin *et al*, 1996; Galtarossa 2004b). Birefringence can be estimated by measuring the evolution of the states of polarization (SOP) or degree of polarization (DOP) of a signal as the light propagates through the fibre (Huttner 1999; Wai, 1996; Galtarossa, 2001). From the birefringence measurements, two important characteristics can also be estimated: the beat length and the correlation length. Thus a fibre can be completely characterized by determining the birefringence, beat-length, correlation length and eventually the polarization mode dispersion (PMD). In this chapter a polarization optical time domain reflectometric technique (P-OTDR) was applied to completely characterize four optical fibres. Birefringence, beat length and correlation lengths are determined statistically. PMD is again measured for the four fibres using the standard Jones matrix eigenanalysis (JME) method discussed under section 3.3.2 of chapter 3. The PMD values obtained from these two methods were then compared.

6.2 Background

Reflectometric measurements can be applied by either employing a continuous wave or a pulsed wave. A continuous wave permits easier experimental set-up but cannot perform local measurements. When a continuous optical wave is injected into a fibre, the total back scattered power is given by the sum of the contributions of the Rayleigh scattering and the Fresnel reflection at the fibre far-end face, with the contributions from the Fresnel reflection being the dominant power (Corsi *et al*, 1999a). On the other hand if a pulsed laser is applied, local measurements can be achieved, because the Rayleigh scattering accounts for the local birefringent effects within the fibre. This means that a CW system can only estimate the round -trip differential group delay (DGD) while a pulsed laser can estimate DGD at various sections of the fibre. The P-OTDR used in this experiment applies a pulsed laser to achieve local measurements.

The author acknowledges the support of Prof. Andrea Galtarossa and Dr. Luca Palmieri of the Department of Information Engineering, University of Padova, Italy, where this research work was conducted.

6.3 Local birefringence properties

The principle of the reflectometric technique is based on the relationship between the evolution of the states of polarization of the backscattered field and the fibre birefringence. The birefringence vector contains all the information about the perturbation acting on the fibre. It therefore characterizes all the polarization mode dispersion sources.

Let us assume an input signal $\hat{s}_0$ and the propagating signal $\hat{s}$. Then according to Galtarossa *et al* (2003, 2004a), the relationship between the two can be expressed by the Mueller/ Stokes formalism as:

$$\hat{s}(z) = R(z)\hat{s}_0 \tag{6.1}$$

where $R(z)$ is the Mueller matrix representing the fibre.

Taking the derivative of the above equation with respect to distance yields:

$$\frac{d\hat{s}}{dz} = \frac{dR}{dz}R^{-1}\hat{s} = \bar{\beta} \times \hat{s} \tag{6.2}$$

where $\bar{\beta} = (\beta_1, \beta_2, \beta_3)$ is the local birefringence vector according to Poole *et al* (1992). It summarizes all the perturbations causing PMD in the fibre.

Consider a launched pulse in a fibre, which propagates to a point, undergoes Rayleigh scattering and then propagates back to the launch point. Such propagation can be represented by:

$$\hat{s}_B(z) = R_B(z)\hat{s}_0 = MR^T(z)R(z)\hat{s}_0 \tag{6.3}$$

where $R_B(z)$ is the Mueller matrix representing the round-trip propagation. Making assumptions of reciprocity (Ulrich *et al*, 1979) and perfect reflection for a Rayleigh scattering (Corsi *et al* 1999a), the following differential equation results:

$$\frac{d\hat{s}_B}{dz} = \bar{\beta}_B \times \hat{s}_B \tag{6.4}$$

It can be showed that the 'round-trip' birefringence vector $\bar{\beta}_B$ is related to the fibre properties by the expression:

$$\bar{\beta}_B = 2MR^T(z)\bar{\beta}_L = 2MR^T(z)\begin{pmatrix}\beta_1\\ \beta_2\\ 0\end{pmatrix} \tag{6.5}$$

$$\left|\bar{\beta}_B\right| = 2|\beta_L| \tag{6.6}$$

where $\bar{\beta}_L = \begin{pmatrix}\beta_1\\ \beta_2\\ 0\end{pmatrix}$ is the linear component of the birefringence according to the random modulus model of birefringence (Wai *et al* 1996).

Equation 6.5 indicates that the modulus of $\bar{\beta}_B$ is twice the modulus of $\bar{\beta}_L$. This is due to the fact that M and R(z) are orthogonal matrices and the round trip birefringence does not depend explicitly on the third component of the birefringence vector.

Equation 6.4 has the same form as the evolution of the forward propagating SOP as a function of angular frequency(ω) (Corsi *et al*, 1999a). Since there is a dualism between frequency and distance, it is valid to apply eq.6.4 to any of the techniques used to measure PMD to measure the round-trip birefringence vector $\bar{\beta}_B$. One such method is the Mueller matrix method (Jopson *et a.l* 1999a), which does not require a complete knowledge of the input SOP, the only requirement being that the system suffers negligible polarization dependent loss. The above, local measurements were performed on four single-mode fibres using the experimental setup shown in figure 6.1.

6.3.1 Experimental setup

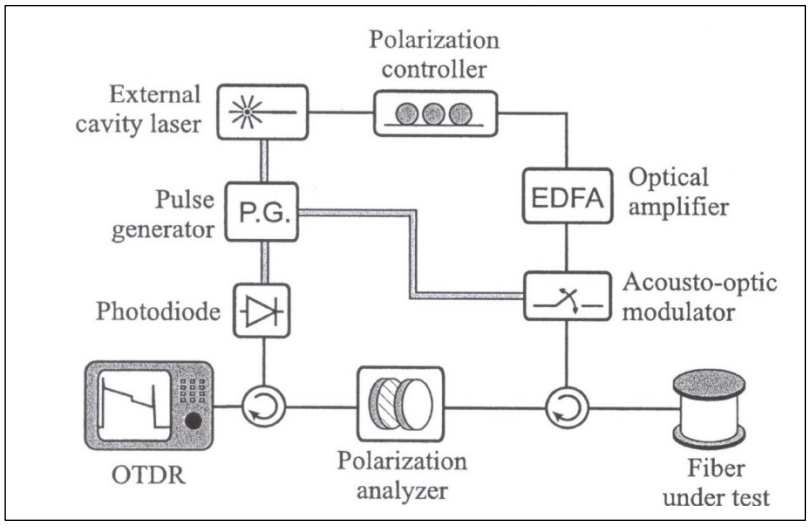

Figure 6.1: A schematic diagram of a P-OTDR (after Galtarossa et al., 2000)

The P-OTDR set up is similar to the standard OTDR except that an external cavity laser directly driven by an electric pulse generator acts as the probing signal in this case. In order to increase the dynamic range, the erbium-doped fibre amplifier (EDFA) amplifies polarized pulses emerging from a polarization controller. The acousto-optic modulator is employed to reduce effects of amplified spontaneous emission (ASE) from the EDFA, by opening a temporal window to allow the pulses to pass while stopping the ASE.

6.3.2 Experimental Procedure

The probe signal was set to 5ns and with peak power of 23dBm. This allowed a spatial resolution of 0.5m and an uncertainty 2% on the SOP measurements. The maximum measurement range is in the order of 20km. The input signal was launched into the fibre under test via a circulator/directional coupler. After backscattering the pulse passes through a quarter wave plate (to be rotated at any angle) followed by a fixed linear polarizer. Since the backscattered signal is polarized, the evolution of its polarization is converted into power fluctuations, detected and stored by the OTDR. Measurements were made for five different quarter wave plate orientations and the round SOPs, $\hat{s}_B(z)$. The information from the raw data was then analysed to calculate the evolution of the states of polarization in order to extract the birefringence as stated above. During the experiment the fibres were maintained firmly at a fixed position in order not to change their position with respect to the laboratory frame of reference. PMD measurements were performed using the standard JME technique. A wavelength window of 1500nm-1620nm in steps of 1 nm was used. Results are presented in the following sections.

6.4. Results for birefringence evolution

Figure 6.2 shows the evolution of the round-trip birefringence vectors along four 3.5km single-mode fibres retrieved from single P-OTDR measurements. In the figure, (a) shows the evolution along the total lengths while (b) shows a section of 500m between 1km and 1.5km sections of the same fibres. These local measurements were obtained due to the validity of equation 6.4.

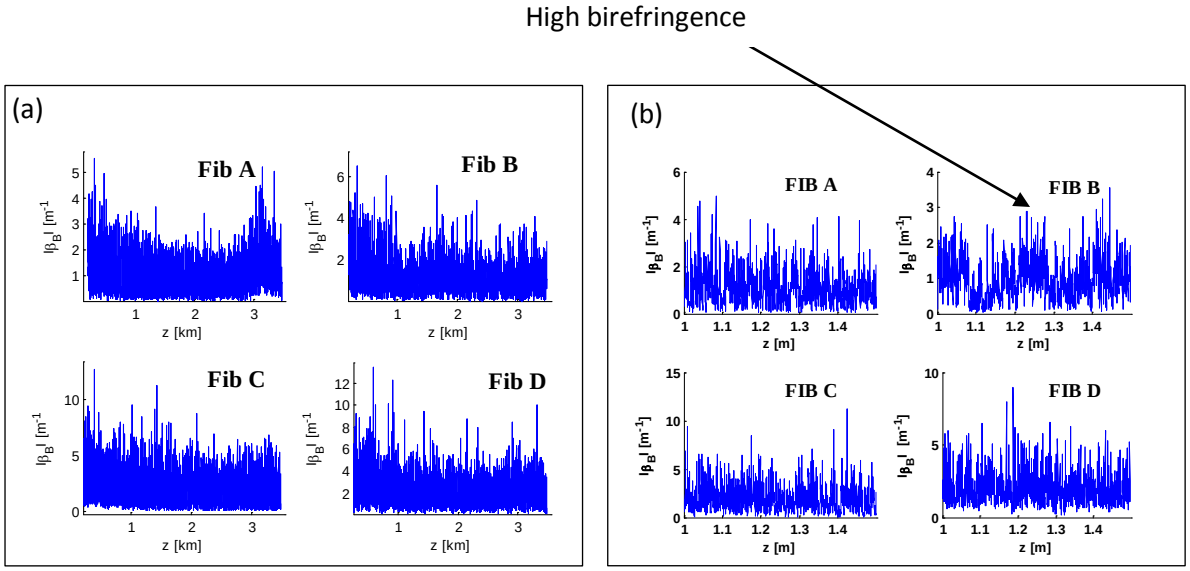

Figure 6.2: Modulus of the round-trip birefringence vector $|\bar{\beta}_B|\,[m^{-1}]$ vs. distance z [km] for the four single-mode fibres, A, B, C and D: (a) full length 3.5km, (b) 500m sections between 1km and 1.5km of the same fibres.

Figure 6.2 (b) also shows that the local properties of the link can be monitored by the P-OTDR technique, and that section by section analysis of birefringence is possible. The graph shows a plot of birefringence vs. distance (distributed/local).From such a birefringence distance plot, portions with high birefringence which contributes high PMD values to a link can be identified and replaced. This is thus a practical solution towards reducing the total PMD within a link. As an example, in the figure (6.2b), an area with high birefringence has been indicated with an arrow.

6.4.1 Birefringence models and statistics

Birefringence in optical fibres is random in nature and therefore it is necessary to study its statistical process and to represent it by some model. Generally three models have been suggested in literature. All of the models assume that there is no circular birefringence (β_3=0). In the first model, one component of the linear birefringence is constant and deterministic while, the second component varies as a white noise process giving rise to the random perturbations (Foschini, 1991). The second model proposed by Wai *et al.* (1996) assumes a constant modulus of the birefringence while its orientation varies as a Weiner process. The last model, known as the random modulus model (RMM) also proposed by Wai, assumes that the birefringence varies in both modulus and orientation. In RMM the first two components

of the local birefringence are considered as some random Gaussian processes which are statistically independent of each other, with zero mean and the same standard deviation. As a result the modulus of the linear birefringence (β_L) follows a Rayleigh distribution. Following the RMM, it has been shown that the autocorrelation function of the components of (β_L) is given by Galtarossa, (2004a&b):

$$r_\beta(z,u) = [\beta_i(z)\beta_i(z+u)] = \frac{8\pi}{L_B^2}\exp\left(-\frac{|u|}{L_F}\right) \tag{6.7}$$

where $L_B = {}^{2\pi}/_{\langle\beta_L\rangle}$ is the beat-length and L_F is the birefringence, correlation length.
The beat length describes the amplitude of the local birefringence vector.

6.4.2 Experimental results for statistical distribution of birefringence

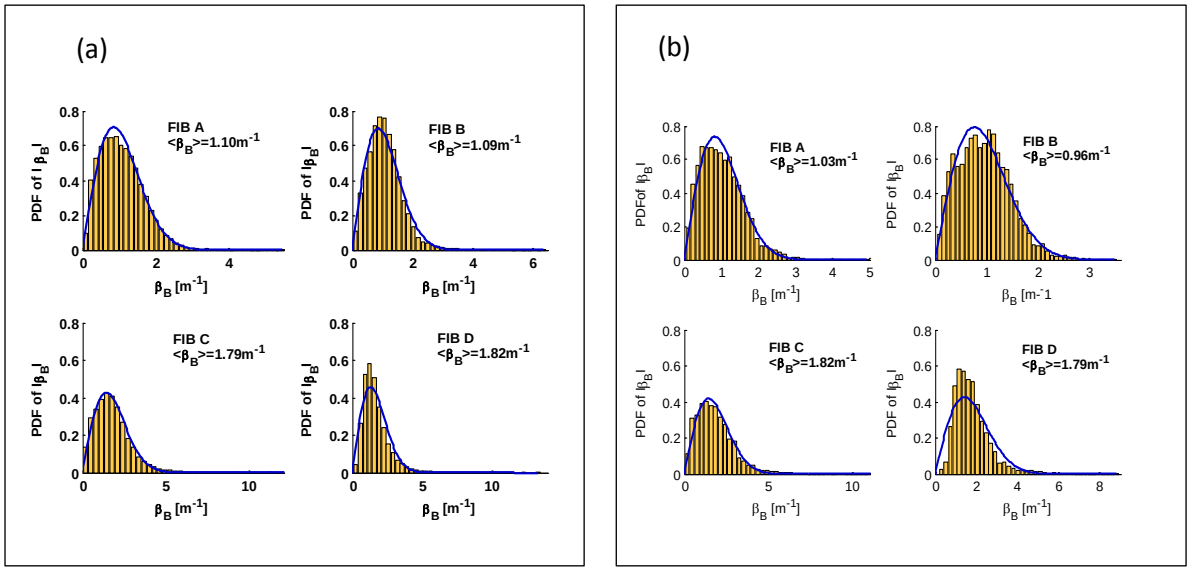

Figure 6.3: Probability density functions (PDF) for the round-trip birefringence vectors $\bar{\beta}_B$ of the four single-mode fibres: (a) for the full lengths of 3.5km (b) 500m section between 1km and 1.5km. Histograms represent experimental data while curves represent best theoretical fit.

Figure 6.3 shows the statistical distributions of the round-trip birefringence vector. The histogram represents experimental data while the smooth curve represents the theoretical best fit using the Rayleigh distribution given by (Galtarossa, 2004a):

$$f_{\beta_B} = \frac{\pi a}{2\langle\beta_B\rangle^2} exp\left(-\frac{\pi a^2}{4\langle\beta_B\rangle^2}\right), \quad a \geq 0 \tag{6.8}$$

In figure 6.3 the distributions of the round-trip birefringence vectors of the four fibres fit very well with the random modulus model. Figure 6.3(a) is for the entire lengths of the fibres and (b) is for the sections of 500m. In both cases the experimental data agrees very well with the theoretical fit. The mean values of the local birefringence are summarized in Table 6.1

Table 6.1.Mean values of the distributions of the round trip birefringence vectors $\langle \bar{\beta}_B \rangle$

Fibre	Full length 3.5km $\langle \bar{\beta}_B \rangle\, m^{-1}$	500m section $\langle \bar{\beta}_B \rangle\, m^{-1}$
Fib A	1.10	1.03
Fib B	1.09	0.96
Fib C	1.79	1.82
Fib D	1.89	1.79

From the table it can be observed that some of the mean values of the round-trip birefringence for the entire fibre lengths differ from those of the sections. This further confirms that birefringence is indeed localized.

6.5 Beat length measurement

Following the random modulus model and equation 6.7, it is evident that the beat length L_B can be estimated from the round trip birefringence vector. This is achieved by making use of the fact that the round-trip birefringence vector is twice the linear birefringence vector. The beat-length can also be calculated using other methods as described below.

6.5.1 Level crossing (LCR) method

The beat length could also be estimated from the power of the round-trip SOP signal s_B. This is known as the level crossing (LCR) method (Corsi et al 1999b, Galtarossa, 2000a; Poole *et al*. 1994). Using this approach the power of the signal is calculated as,

$$T(z) = \frac{1}{2}(1 + 3\langle \hat{s}_B(z) \rangle . \hat{s}_B(z)) \qquad (6.9)$$

where $\langle \hat{s}_B(z) \rangle$ is the average value of $\hat{s}_B(z)$ along z.

It has also been shown in the above reference that, the input SOP s_0, and the average round-trip vector $\langle \hat{s}_B(z) \rangle$ are related by, $\langle \hat{s}_B(z) \rangle = \frac{M\hat{s}_0}{3}$. This condition and eq.6.9 makes it possible to calculate explicitly the beatlength from 'level crossing' rate as (Galtarossa 2003, 2004a),

$$n(v) = \frac{2}{\pi}\langle \beta_L \rangle \sqrt{v} \text{ and } L_B = \frac{4\sqrt{v}}{n(v)} \qquad (6.10)$$

The level crossing rate (LCR) $n(v)$ is the mean number of times $T(z)$ a given level v.

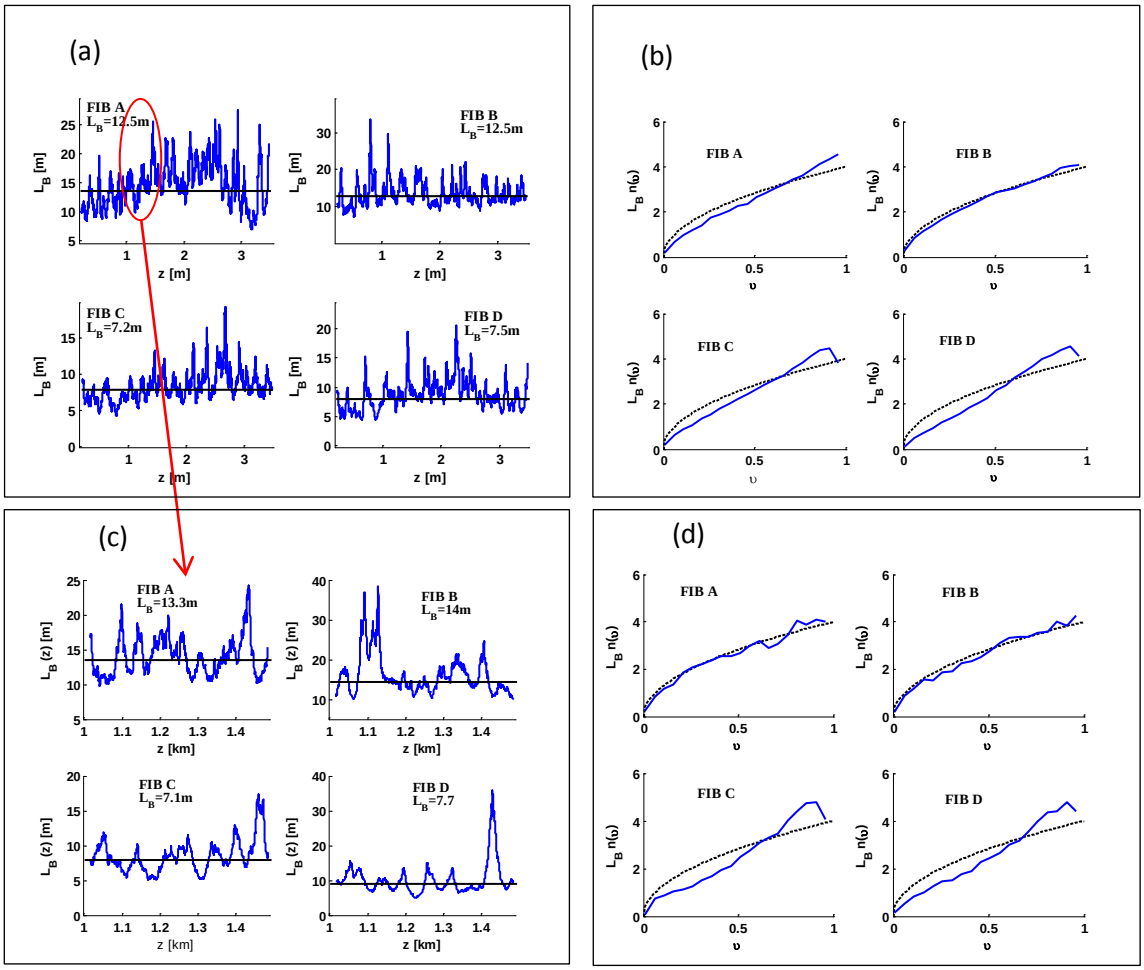

Fig.6.4: (a) Plots of beat-length $L_B\,[m]$ vs. distance $z\,[m]$ obtained by the level crossing method. (b) Plots indicating how the level crossing rate $L_B n(v)$ evolves with the level. Smooth curves represent experimental data while dashed curves represent theoretical fit; (a), (b) represents full length (3.5km) while (c) and (d) represent 500m section between 1km and 1.5km respectively.

Figure 6.4 (a) shows how the beat length changes along the fibre length. The figure indicates how various sections along the fibre links contribute to the total beat length of an entire link.

Sections with higher beat lengths correspond with sections with lower PMD according to equation 6.13. The plot of the evolution of beat length $L_B n(v)$ vs. level v in figure 6.4a validates equation 6.10, where the level rate, $L_B n(v)$ is proportional to the level. In the figure (c) and (d) corresponds to 500m sections between 1km and 1.5km of the fibres. The plots in figure 6.4(b) indicate a very good agreement between experiment and theory. It can thus be concluded that the level crossing method applied in the P-OTDR technique is a valid method for estimating the beat length of a fibre link.

6.5.2 Power spectral density (PSD) analysis

Another method for calculating the beat length via the spatial frequency power $T(z)$ is by evaluating the variance σ_B of the power spectral density (Galtarossa *et al*, 2004a; Heffner et al, 1996). Corsi *et al* (1999a) have proved that the variance of the power density is $\sigma_{\beta}^2 = 3\langle\beta_L^2\rangle/(4\pi^2)$. By applying Fourier calculus (Corsi *et al*, 1999b) and recalling that β_L is a Rayleigh distributed variable, the beat length L_B reads:

$$L_B = \sqrt{\frac{12}{\pi\sigma_{\beta}^2}} \qquad (6.11)$$

All the three methods for determining the beat length were applied to experimental data. The results will be summarized and presented in Table 6.2.

6.6 Birefringence correlation length measurement

The random modulus model also offers an opportunity to determine the birefringence correlation length L_F from the round trip birefringence vector. According to Huttner *et al.* (1998), the auto correlation function of the linear birefringence vector (β_L) is a bilateral exponential with a decay constant, L_F. Since the linear birefringence vector is related to the round-trip birefringence vector, it is possible to apply autocorrelation theory to the round-trip birefringence vector to determine, L_F from a P-OTDR measurement. The autocorrelation function of the round trip birefringence vector $\beta_{B,i}$ (i=1,2,3) is given by (Galtarossa 2001,2004a):

$$r_{\beta_B}(z,u) = E[\beta_{B,i}(z)\beta_{B,i}(z+u)]$$

$$= \frac{64\pi}{3L_B^2} exp\left(-\frac{|u|}{L_F}\right) \qquad (6.12)$$

Comparing equation 6.7 and equation 6.12, $r_{\beta}(z,u)$ and $r_{\beta_B}(z,u)$ have the same decay constant hence by measuring the correlation of the round-trip birefringence vector, it is possible to determine L_F and L_B .

The above derivations made use of stochastic differential equations and hold for the condition that, there is no circular birefringence.

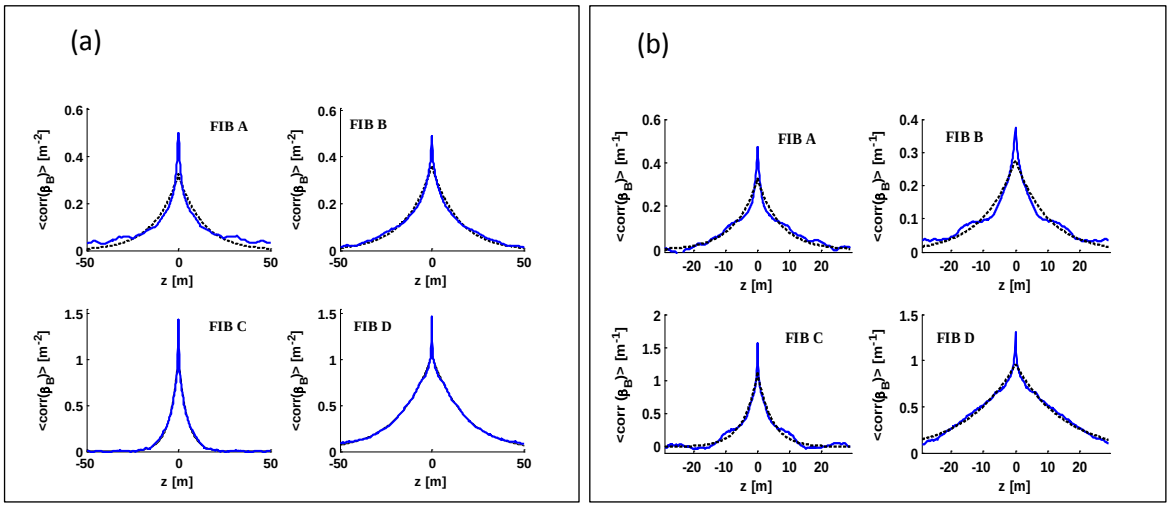

Figure 6.5: Autocorrelation correlation of the round-trip birefringence vector $\beta_B(z)$ for the four fibres: (a) is for the full lengths of 3.5km and (b) for a section of 500m, solid line indicates experimental values while dashed lines represent theoretical best fits.

Figure 6.5 show autocorrelation functions of the four fibres. The auto correlation function is the expectation of the signal multiplied by itself after a given instance in space. It thus reveals how quickly the signal decays exponentially and this happens very quickly. In the figure, it can be observed that the autocorrelation plots in (a) representing the entire fibre link are nearly identical to those in (b) which represents the 500m sections. This indicates that the fibre undergoes similar decays at the various sections and hence the determination of the correlation length using equation 6.12 is valid.

6.6.1 Measurement of differential group delay (DGD) $\langle \Delta\tau \rangle$

Following the determination of the correlation length L_F and the beat-length L_B, the mean differential group delay (DGD) can be calculated as (Wai,1996):

$$\langle \Delta\tau \rangle^2 = \frac{1}{3}\left(\frac{8\lambda L_F}{\pi c L_B}\right)^2 \left(exp - L/L_F + \frac{L}{L_F} - 1\right) \quad (6.13)$$

where L is the fibre length, λ is the wavelength of light and c the speed of light.

As a result of this the mean DGD can be evaluated from a single wavelength once the beat length and the correlation length have been estimated from the P-OTDR measurements.

Mean DGDs have been estimated for the four fibres, both for the full length and the 500m section. Mean differential delays were also measured using the standard JME technique (Heffner, 1992). Table 6.2 summarizes the results obtained for all the measurements.

Table 6.2: Summary of results: measured L_B ,L_F, and $\langle \Delta\tau \rangle ps$.

Measurements for full length (3.5km)							
Fibre	Measurements of $L_B[m]$ using;				$L_F\,[m]$	P-OTDR $\langle \Delta\tau \rangle\ ps$	JME $\langle \Delta\tau \rangle\ ps$
	β_B	LCR	PSD	$\langle L_B \rangle$			
Fib A	11.4	12.5	16.0	13.3	13.0	0.12	0.11
Fib B	11.5	12.5	15.1	13.0	14.5	0.13	0.18
Fib C	7.0	7.2	8.8	7.7	4.7	0.13	0.16
Fib D	6.7	7.5	8.9	7.7	17.9	0.24	0.33
Measurements for section (500m)							
Fib A	12.0	13.3	15.7	13.7	6.7	0.03	-
Fib B	13.0	14.0	17.0	14.7	9.9	0.04	-
Fib C	6.9	7.1	8.6	7.5	4.4	0.05	-
Fid D	7.1	7.7	9.1	8.0	12.9	0.07	-

Table 6.2 shows results obtained with the P-OTDR measurements. The table shows measurements for both full length of 3.5km and also for 500m segments of the links. The DGD was calculated via equation 6.13. The beat lengths were calculated using all three methods discussed above. The measurements show that the parameters of the fibre may vary

along its length. It is evident that the DGD varies according to the fibre's local parameters. This can be observed for Fib A in the table. The beat length and the correlation length for the entire 3.5km length are respectively 13.3m and 13.0m and for the 500m section, 13.7m and 6.7m respectively. These values obviously yield two different values of the differential group delay. Thus local DGD may vary from that of the entire fibre link. Since the methods used to determine the correlation length and beat-length have been validated, it follows that the calculated PMD values are valid.

6.7 Summary

P-OTDR technique has been applied to characterize completely four standard G652 optical fibres. The method has made it possible to evaluate the factors affecting polarization mode dispersion namely, birefringence, beat length and the correlation length. It can also be observed from equation 6.13 and Table 6.2 that the two parameters, L_B and L_F together with the fibre length determine the differential group delay (DGD). While the fibre length is constant, the parameters L_B and L_F vary along the fibre length. This is due to the statistical nature of the birefringence vector. To be able to characterize the birefringence, the random modulus model was adopted. Thus from a single measurement of the round-trip state of polarization (SOP) it was possible to evaluate completely the parameters characterizing the fibres.

The method also permitted one to characterize 500m subsections of the fibres. It was observed that the fibre characteristics vary at different sections of the fibre. As a consequence, the DGD also varies. From equation 6.13, two values of the DGD are possible; one value due to an accumulation from the input point to the subsection and the other due exclusively to the subsection (L=500m). In Table 6.2, the DGD for the 500m subsection is due exclusively to that subsection. It was not possible to measure the 500m subsection with the JME due to obvious reasons. The only way to do such a measurement is the destructive method of cutting that subsection.

In concluding, distributed measurements using a P-OTDR have been applied to characterize optical fibre properties. Differential group delay values calculated were in good agreement with standard measurement values. The method is non-destructive, repeatable and is capable of completely characterizing an optical fibre link.

CHAPTER 7

MEASUREMENTS OF INSTANTANEOUS AND ROOT-MEAN-SQUARE DIFFERENTIAL GROUP DELAY USING P-OTDR

7.1 Introduction

As has been discussed in the previous chapter, the birefringence vector information determined from the round-trip P-OTDR signal contains all the information about the fibre including the polarization mode dispersion. Special attention has been given to the measurements of differential group delay since it would allow bad sections of installed fibre to be identified. Until recently however, reflectometric measurements had been applied successfully to measure only the mean differential group delay (DGD). This was due to the assumptions made when establishing the measurements, such as no circular birefringence. Currently, it has become of interest to determine the instantaneous differential group delay in fibre links (Dong *et al*, 2007; Galtarossa *et al*, 2008; Fosuhene *et al.* 2010; Palmieri *et al.* 2011). The instantaneous value of the DGD may be useful in the real time monitoring of links.

In this chapter, the P-OTDR measurement technique such as described in the previous chapter is applied to determine the instantaneous and root-mean-square values of the DGD. A theoretical background is given which is validated by experimental results. Finally measurements made with the P-OTDR are compared to measurements made with the standard JME technique.

7.2 Determination of instantaneous differential group delay

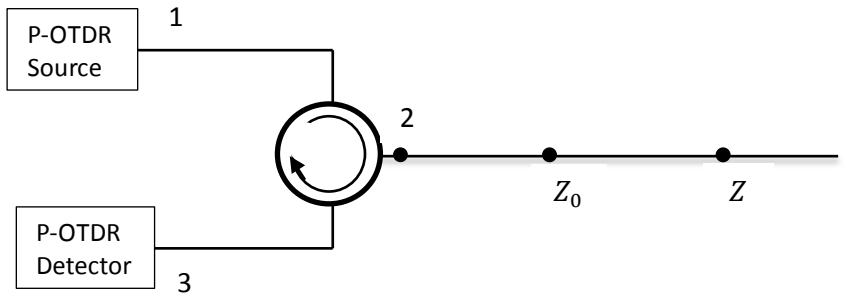

Figure 7.1: Schematic diagram showing optical path in a P-OTDR system.

Some of the results presented in this chapter have already been published by the author in references; Fosuhene et *al* 2010 (a), 2010(b).

Figure 7.1 depicts the optical path followed by a P-OTDR signal. The P-OTDR scheme is based on the one already described in chapter 6. It is assumed that the fibre is reciprocal and there is no polarization dependent loss in the system. The analysis is also restricted to the polarized components backscattered field since it contributes over 90% of the total backscattered power.

Under these conditions the polarization properties of an optical fibre can be described by the Stokes-Mueller formalisms. Let $\boldsymbol{F}(\boldsymbol{z_0})$ be the Mueller Matrix for a forward propagation vector from the P-OTDR source (point 1) to any arbitrary point Z_0 within the fibre link, $\boldsymbol{B}(\boldsymbol{Z_0})$ the back propagation vector from Z_0 to the P-OTDR detector (point 3) and $\boldsymbol{W}(\boldsymbol{Z_0};\boldsymbol{Z})$ be the forward propagation between Z_0 and Z.

The round-trip propagation from point 1 to z and back may then be represented by (Galtarossa *et al*, 2005):

$$\boldsymbol{R}(\boldsymbol{Z}) = \boldsymbol{B}(\boldsymbol{Z_0})\boldsymbol{M^T}(\boldsymbol{Z};\boldsymbol{Z_0})\boldsymbol{M}\boldsymbol{W}(\boldsymbol{Z};\boldsymbol{Z_0})\boldsymbol{F}(\boldsymbol{Z_0}) \tag{7.1}$$

where M=diag (1,1,-1) is a diagonal matrix.

All the matrices above are in general angular frequency dependent except **M.** For the forward propagation, the **W** dependence of distance (z) and angular frequency (ω) can be expressed as (Gordon *et al*, 2000):

$$\frac{\partial \boldsymbol{W}}{\partial Z} = \bar{\boldsymbol{\beta}} \times \boldsymbol{W} \tag{7.2}$$

$$\frac{\partial \boldsymbol{W}}{\partial \omega} = \bar{\boldsymbol{\Omega}} \times \boldsymbol{W} \tag{7.3}$$

where $\bar{\beta}(Z,\omega)$ is the birefringence vector and $\bar{\boldsymbol{\Omega}}(Z,\omega)$ is the polarization mode dispersion (PMD) vector.

Similarly, the R dependence on Z and ω describing the round-trip propagation is given by,

$$\frac{\partial \boldsymbol{R}}{\partial Z} = \bar{\boldsymbol{\beta}}_{\boldsymbol{B}} \times \boldsymbol{R} \tag{7.4}$$

$$\frac{\partial \boldsymbol{R}}{\partial \omega} = \bar{\boldsymbol{\Omega}}_{\boldsymbol{B}} \times \boldsymbol{R} \tag{7.5}$$

where $\bar{\boldsymbol{\beta}}_{\boldsymbol{B}} = 2\boldsymbol{B}(Z_0)\boldsymbol{M}\boldsymbol{W}^{\boldsymbol{T}}(Z;Z_0)\bar{\boldsymbol{\beta}}_{\boldsymbol{L}}(Z)$ represents the round-trip birefringence vector and $\bar{\boldsymbol{\Omega}}_{\boldsymbol{B}}(z)$ is the round trip PMD vector.

As discussed in the previous chapter, almost all the PMD information is contained in the birefringence vector. By assuming that the linear birefringence vector $\bar{\beta}$ is parallel to its ω derivative, Dong *et al* (2007) showed that in principle the instantaneous DGD can be calculated from $\bar{\beta}_B$, $\partial\beta_B/\partial\omega$, $\bar{\Omega}_B$ and $\partial R_B/\partial Z$. This assumption however was only applied using Fresnel reflection from the fibre far end. Consequently Galtarossa *et al*, (2008) provided an alternative solution using a distributed approach. Following this approach, consider propagation from a point $Z \geq Z_0$ to the detector of the P-OTDR. Such propagation can be described by the matrix $\boldsymbol{P}(\boldsymbol{Z}) = \boldsymbol{B}(\boldsymbol{Z_0})\boldsymbol{M}\boldsymbol{W}^{\boldsymbol{T}}(\boldsymbol{Z};\boldsymbol{Z_0})\boldsymbol{M}$ with a corresponding PMD vector reading,

$$\bar{\Pi}(Z) = \bar{\Pi}(Z_0) + B(Z_0)MW^T(Z;Z_0)\Omega(Z;Z_0) \tag{7.6}$$

where $\Omega(Z;Z_0)$ represents the forward propagation between Z_0 and Z.

The dependence of $\Pi(Z)$ on Z can be calculated as

$$\frac{\partial\bar{\Pi}(Z)}{\partial Z} = \boldsymbol{B}(Z_0)\boldsymbol{M}\frac{\partial\bar{\Omega}_{\boldsymbol{in}}}{\partial Z} = \boldsymbol{B}(Z_0)\boldsymbol{M}\boldsymbol{W}^{\boldsymbol{T}}(Z,Z_0)\frac{\partial\bar{\beta}}{\partial\omega} \tag{7.7}$$

where $\boldsymbol{\Omega_{in}}(Z;Z_0) = \boldsymbol{W}^{\boldsymbol{T}}(Z,Z_0)\bar{\Omega}(Z,Z_0)$ is the input PMD vector of the fibre portion between positions Z_0 and Z .

Assuming linear birefringence ($\bar{\boldsymbol{\beta}} = \bar{\boldsymbol{\beta}}_{\boldsymbol{L}}$) while applying the approximation ($\partial\bar{\boldsymbol{\beta}}_{\boldsymbol{L}}/\partial\omega = \bar{\boldsymbol{\beta}}_{\boldsymbol{L}}/\omega$), then

$$\frac{\partial\bar{\Omega}_{\boldsymbol{in}}}{\partial Z} = \frac{1}{2}\boldsymbol{M}\boldsymbol{B}^{\boldsymbol{T}}(Z_0)\bar{\beta}_B(\mathrm{Z}) \tag{7.8}$$

By integrating equation 7.8 and finding the modulus of $\bar{\boldsymbol{\Omega}}_{\boldsymbol{in}}(Z,Z_0)$, the instantaneous DGD between Z and Z_0 yields (Galtarossa et al ,2008),

$$\Delta\tau(Z,Z_0) = \frac{1}{2\omega}\left|\int_{Z_0}^{Z}\bar{\beta}_B(t)dt\right| \tag{7.9}$$

The above equation indicates that the DGD of any arbitrary section of the fibre link can be calculated by integrating the round-trip birefringence vector. This is quite significant since

the DGD can be calculated from a single P-OTDR measurement at a single frequency. This will be applied in section 7.3.2 where experimental data is analysed.

7.3 Determination of the root-mean-square differential group delay

As has been discussed so far, polarization mode dispersion is a statistical phenomenon due to the random nature of the optical birefringence that causes it. The different measurement techniques that are employed to measure the DGD use averaging either as the mean DGD or the root-mean-square (RMS) DGD (Gisin *et al,* 1991; Heffner *et al,* 1992, Pool *et al,* 1994). The averaging is either done over wavelength or over time. These measurement conditions impose limitations to the accuracy of measurement because the statistical representation of DGD implies that, the measurement is limited to a finite sample set. The only hope of improving accuracy is to expand the sample size by either increasing wavelength range or measurement time (Gisin et al, 1996). In practice however, the optical frequency range is limited by laser tunability and the dependence of modal birefringence on wavelength. In this section a single-end technique for estimating the RMS DGD from a single wavelength or optical frequency is developed and applied using P-OTDR. The technique also applies autocorrelation techniques to the component of the birefringence vector.

7.3.1 Derivation of RMS DGD

Proceeding from the previous section and using equation 7.9, the RMS DGD can be written as (Fosuhene *et al,* 2010; Palmieri *et al,* 2011);

$$\langle \Delta\tau^2(z_o, z; \omega)\rangle = \frac{1}{4\omega^2}\int_{z_o}^{z}\int_{z_o}^{z}\langle \beta_B^T(t)\cdot\overline{\beta}_B(\tau)\rangle d\tau dt \tag{7.10}$$

where $\langle \bar{\beta}_B^T(t)\bar{\beta}_B(\tau)\rangle$ is the autocorrelation function of the round-trip birefringence vector.

Essentially, the autocorrelation of a random signal is the expectation of the product of such a random signal with itself at two different points in a given space. It reveals how quickly the random process changes at different points and whether it has a periodic component and expected frequency.

For this analysis, the components of the round-trip birefringence vector are assumed to be asymptotically stationary with each other and have the same autocorrelation function

(Galtarossa *et al.*, 2001). The autocorrelation which is typically in the order of a few meters is comparable to the stationary regime.

Using the above requirement, the components of the birefringence vector $\bar{\beta}_B$ can be assumed to be stationary. Consequently applying autocorrelation theory results in the following,

$$\langle \bar{\beta}_B^T(t)\bar{\beta}_B(\tau)\rangle = 3r(\tau - t) \tag{7.11}$$

and making substitutions for $\tau = t + u$ into 7.11 yields

$$\langle \Delta\tau^2(z_o, z; \omega)\rangle = \frac{3}{4\omega^2}\left[\int_{z_o}^{z-u} dt \int_0^{z-z_0} r_\beta(u)du + \int_{z_o-u}^{z} dt \int_{z_o-z}^{0} r_\beta(u)du\right] \tag{7.12}$$

where, $r_{\beta,i}(u) = \langle \overline{\beta}_{B,i}(t) \cdot \overline{\beta}_{B,i}(t+u)\rangle, i = 1,2,3.$

Expanding equation 7.12 and simplifying gives,

$$\langle \Delta\tau^2(z_o, z; \omega)\rangle = \frac{3}{4\omega^2}\left[\begin{array}{l}(z - z_o)\left(\int_0^{z-z_o} r_\beta(u)du + \int_{z_o-z}^{0} r_\beta(u)du\right) + \\ \left(\int_{z_o-z}^{0} ur_\beta(u)du - \int_0^{z-z_o} ur_\beta(u)du\right)\end{array}\right] \tag{7.13}$$

By applying the identity $\int_a^b F(x)dx = -\int_b^a F(x)dx$, equation 7.13 becomes

$$\langle \Delta\tau^2(z_o, z; \omega)\rangle = \frac{3}{4\omega^2}\left[\begin{array}{l}(z - z_o)\left(\int_0^{z-z_o} r_\beta(u)du - \int_0^{z_o-z} r_\beta(u)du\right) + \\ \left(-\int_0^{z-z_o} ur_\beta(u)du - \int_0^{z_o-z} ur_\beta(u)du\right)\end{array}\right]$$

By applying the properties of auto correlation and making substituting for $u = -u'$, $du = -du'$ and using $r_\beta(u) = r_\beta(-u')$,

$$\langle \Delta\tau^2(Z_o, Z;\omega)\rangle = \frac{3}{4\omega^2}\left[\begin{array}{l}(z-z_o)\left(\int_0^{z-z_o} r_\beta(u)du - \int_0^{z-z_o} r_\beta(-u')du'\right)+\\ \left(-\int_0^{z-z_o} ur_\beta(u)du + \int_0^{z-z_o} ur_\beta(u')du'\right)\end{array}\right]$$

Making substitutions for $du = -du'$ to the previous equation and simplifying,

$$\langle \Delta\tau^2(Z_o, Z;\omega)\rangle = \frac{3}{4\omega^2}\left[(z-z_o)\left(\int_0^{z-z_o} r_\beta(u)du\right) - \left(\int_0^{z-z_0} ur_\beta(u)du\right)\right]$$

$$\Rightarrow \langle \Delta\tau^2(Z_0, Z;\omega)\rangle = \frac{3}{2\omega^2}\left[(Z)\left(\int_0^{Z} r_\beta(u)du\right) - \left(\int_0^{Z} ur_\beta(u)du\right)\right] \qquad (7.14)$$

where the substitution that $Z = z - z_o$ has been made. Physically, this implies that the RMS DGD between any arbitrary points Z_0 and Z, $Z > Z_0$ can be calculated. In equation 7.14 as $Z \to \infty$ the following results;

$$\langle \Delta\tau^2(Z_0, Z;\omega)\rangle = \frac{3}{4\omega^2}\left[(Z)\left(\int_0^{\infty} r_\beta(u)du\right) - \left(\int_0^{\infty} ur_\beta(u)du\right)\right]$$

Making substitutions and simplifying,

$$\sqrt{\left\langle \Delta\tau^2(Z_0, Z;\omega)\right\rangle} = \frac{3}{2\omega}\sqrt{(ZC_o - C)}$$

where $C_o = \int_0^{\infty} r_\beta(u)du$ and $C = \int_0^{\infty} u\, r_\beta(u)du$.

In the above discussions, both integrals, C_0 and C approach an asymptotically finite value as Z increases. The second term, C tends to be negligible with respect to the first because the first term C_0 increases linearly with the section length Z. Furthermore the auto correlation

function goes to zero in a length scale comparable to the auto correlation length. This implies that when Z is longer than a few meters, the second integral becomes negligible hence;

$$\sqrt{\langle \Delta\tau^2 \rangle} = \overline{\Delta}\tau \approx \frac{\sqrt{3}}{2\omega}\sqrt{(ZC_o)} \tag{7.15}$$

The above expression (equation7.15) can be used to estimate the squared DGD $\langle\overline{\Delta\tau}\rangle$ of the link. Following these results, Palmieri *et al*, (2011) have shown that the RMS can also be expressed in terms of the power spectral density PSD as;

$$\overline{\Delta\tau} = \sqrt{\overline{\Delta\tau^2}} \approx \frac{\sqrt{3}}{2\omega}\sqrt{\overline{R(0)Z}} \tag{7.16}$$

where $R(f)$ is the power spectral density, which is also the Fourier transform of the auto correlation function $r(u)$.

The auto correlation function is usually calculated as the inverse Fourier transform of the power spectral density which can be estimated from experimental data with different methods as the periodogram (Kay,1988), which may be rather complicated. It is therefore more practical to use equation (7.15).

7.3.2 Experimental determination of instantaneous and root-mean-square DGD

To test the proposed technique, the instantaneous and root mean squared DGD of four standard G.652 single mode fibres each of length 3.5km were measured. The values obtained were compared to the standard Jones-matrix eigenanalysis method. The fibres are labelled FibA-FibD.

The round trip-birefringence vector was measured using the same P-OTDR scheme described in chapter 6 (Galtarossa *et al*., 2001). The probe signal was set at 5ns with a peak pulse power of 23dBm. The spatial resolution of about 0.5m and SOP measurement uncertainty of 2% was achieved with a maximum measurement range of 20km. The instantaneous DGD and root mean square DGD were evaluated at a wavelength of 1536nm. Results are presented in Figures 7.1-7.4 and summarized in Table 7.1.

7.3.3 Instantaneous DGD

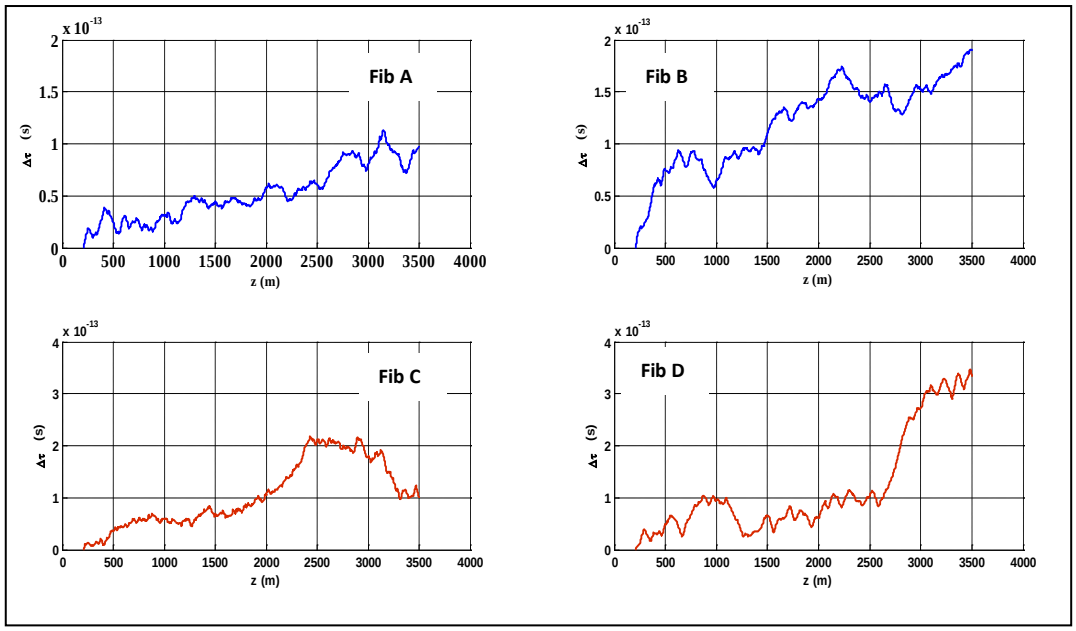

Figure 7.2: Instantaneous DGD as a function of fibre length cumulated along the four fibre links.

Figure 7.2 shows the instantaneous DGD as a function of distance, cumulated along each of the four fibres according to equation (7.9). The figure shows how the local DGD can be measured. This is remarkable considering the fact that measurements were done at a single wavelength. Though the DGD is a random phenomenon with statistical properties, this measurement reduces the limit imposed on its measurements due to spectral width.

While this technique is also limited by the bandwidth of the erbium-doped fibre amplifier (EDFA), it is still valid and eliminates wavelength averaging. From such a figure portions with high DGD along the link are easily identifiable for mitigation. This can be useful for real time monitoring of both installed links and for quality control during the manufacturing process.

7.4 Calculation of root mean square DGD

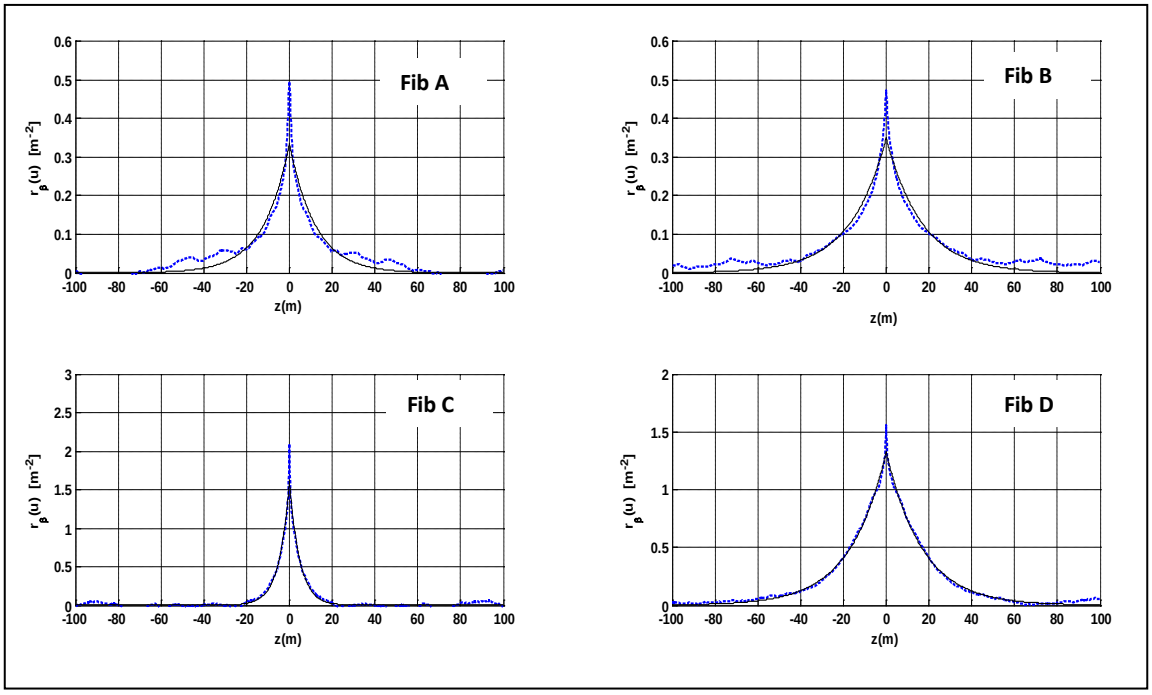

Figure 7.3: Estimate of the auto correlation functions of the round-trip birefringence, on the four fibres; solid lines indicate theoretical best fits while dashed lines indicate experimental data.

Figure 7.3 shows the autocorrelation functions (ACF) of the four fibres used to estimate the root-mean-square DGD. It can be observed that the functions tend to zero rapidly (a few meters). Further the ACFs approaches zero at different speeds for the fibres due to their different correlation lengths. This confirms the round-trip birefringence is asymptotically stationary and not correlated.

Figure 7.4 shows plots of the integral of the autocorrelation function in figure 7.3 with respect to length Z. For the same reasons stated above, the integral $\int_0^Z r_\beta\,(u)du$ approaches a constant value as Z increases. The constant asymptotic values were then applied to equation 7.14 to estimate the RMS DGD. The instantaneous DGD and RMS DGD values resulting from the P-OTDR measurements are summarized and compared to the JME measurements in Table 7.1.

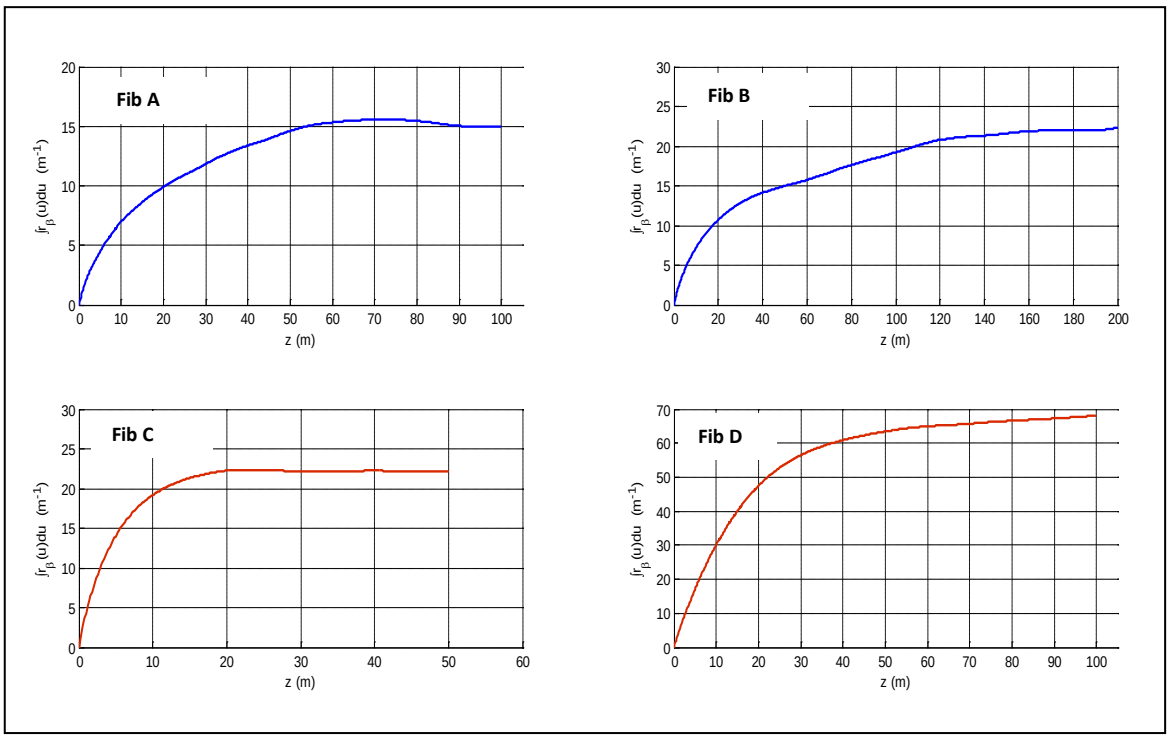

Figure 7.4: plots of $\int_0^Z r_\beta(u)du$ as a function of Z for each of the autocorrelation functions in figure 7.3; the asymptotic values are used to estimate the RMS DGD.

Figure 7.5 shows the JME measurements for the fibres. Measurements were performed within a wavelength window of 1500nm-1620nm in steps of 1 nm. The instantaneous DGD at 1536nm as well as their RMS DGD values are summarized and compared to the P-OTDR measurements in Table 7.1. In the JME case, the RMS value has been obtained by squaring and averaging the instantaneous DGD values. The uncertainty in the JME measurements were calculated using (Karlsson *et al*, 1999);

$$\sigma \approx 0.9\sqrt{\frac{\langle \Delta\tau \rangle}{\Delta\omega}} \tag{7.17}$$

where $\Delta\omega$ is the frequency range over which the instantaneous DGD was measured.

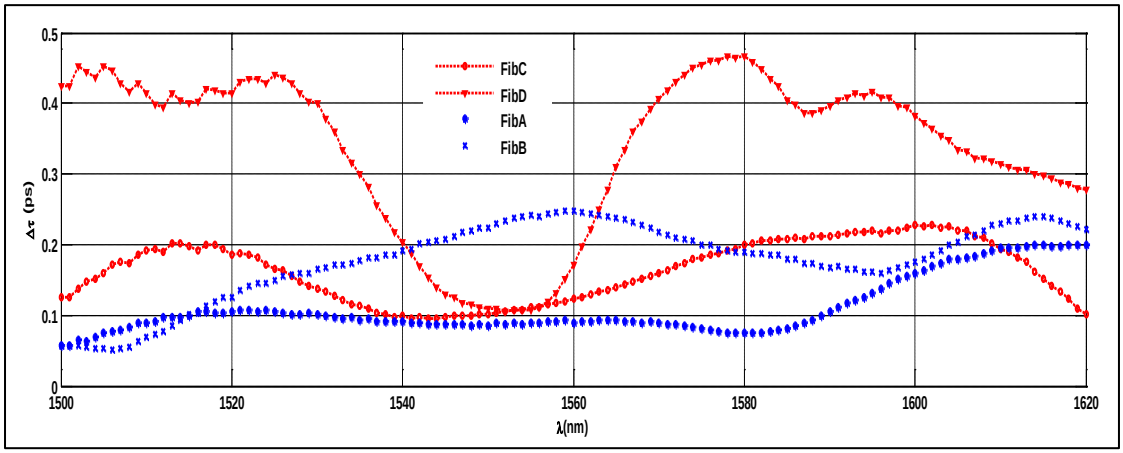

Figure 7.5: Plot of DGD vs. wavelength for the four fibres using the JME technique over a wave length span of 120nm in steps of 1nm.

Table 7. 1: Summary of results; comparing RMS and instantaneous DGD for P-OTDR and JME measurements

Fibre	Instantaneous DGD (λ =1536nm)		Root mean squared DGD		
	P-OTDR $\Delta\tau(ps)$	JME $\Delta\tau(ps)$	P-OTDR $\langle\Delta\tau^2\rangle^{\frac{1}{2}}(ps)$	JME $\langle\Delta\tau\rangle ps$	$\sigma(ps)$
Fib A	0.10	0.09	0.13	0.12	0.03
Fib B	0.19	0.18	0.16	0.18	0.04
Fib C	0.10	0.11	0.16	0.17	0.04
Fib D	0.33	0.28	0.28	0.35	0.06

The RMS and instantaneous DGD measurements shown in Table 7.1 indicates that there is a very good agreement between the two measurement techniques. The P-OTDR measurement technique uses a single wavelength to achieve these results while the JME measurement technique uses a wavelength range. Again due to the use of a single wavelength, it is possible to implement the P-OTDR technique on live fibre through multiplexing. This is not possible with the JME technique which uses a wavelength range, some of which may interfere with other channels in a multiplexed system. Table 7.1 further validates and confirms the repeatability of the P-OTDR technique. This is because the measurements were repeated on four different fibres, and all of these measurements are in very good agreement with the

standard JME technique. For these reasons, the P-OTDR technique is more suitable for field measurements.

7.5 Summary

In this chapter P-OTDR technique has been successfully applied to calculate the instantaneous and RMS DGD of optical fibre links. Theoretical analysis has been validated by experimental data. The technique has many advantages. Firstly it is single-end and therefore offers a practical application for field measurements. Secondly it utilizes a fixed wavelength of an optical source to achieve a high accuracy and therefore avoids the errors introduced by wavelength averaging methods. According to the analysis deduced, the method can be applied to any arbitrary subsection of a fibre link.

Another advantage is that the technique is based on birefringence measurements; hence real time monitoring of DGD may be achieved together with an assessment of the statistics of the PMD of an entire link. This means that the method can be applied to completely characterize the instantaneous DGD and RMS DGD of link (or subsection) at a fixed wavelength with a single P-OTDR measurement.

CHAPTER 8

CONCLUDIND REMARKS

With the growth in demand for high speed long haul optical communication links, polarization mode dispersion still remains a major limiting factor. Although improved fibre manufacturing techniques have reduced PMD in modern fibres, PMD still remains a challenge to legacy fibres. PMD compensation which is one solution to the problem is extremely challenging and difficult to implement. The most cost effective solution is to identify and eliminate high PMD sections within a link. During manufacturing, the later solution can be applied as a quality control method. It can also be applied to deployed fibres to mitigate PMD effects. In this PhD thesis, novel single-end measurement techniques capable of measuring the entire PMD of a link as well as locating sections with high PMD within a link have been investigated. The innovative experimental and analytical techniques developed and implemented in this thesis are cost effective ways of measuring and managing PMD in optical fibre links. Two single-end PMD measurement techniques were implemented in this thesis, the single-end interferometric (which is a modification to the generalized interferometric technique) and the polarization sensitive optical time domain reflectometric technique.

In Section 5.3.1, the standard generalized interferometric technique (GINTY-EXFO FTB 5500B) was modified to measure PMD in single-end configuration. This innovation was achieved by introducing a three-way coupler and polarization scramblers to form a round-trip set-up. The technique can measure values of PMD between 0-115ps, and a maximum link length of about 80km and above, at 0.2bB/km attenuation. The method was applied to measure different fibre types to test capabilities of the fibre. The ratios between the forward measurements and single-end measurements were calculated and compared with theory.

In order to test the agreement between theory developed in section 5.3.3, and experimental result, two PMF fibres were first measured in both forward and single-end configuration. According to the results presented in section 5.4, a factor of 2 was obtained as the ratio between the single-end measurement and the forward measurement. The same result was obtained when the PMFs were concatenated to form a single segment. It was therefore deduced that the single-end treats a single PMF section as two concatenated birefringent segments with no or little birefringence. In such a case the DGD is expected to grow linearly

with length. Thus the factor of 2 between the single-end and forward measurement was consistent with theory.

Next, three standard single mode fibres (two uncabled and one cabled) were measured in section 5.3.5. For these FUTs a ratio of ~1.4 between the single-end and forward configuration was obtained. There was a remarkable difference between the observed interferograms. The cabled fibre was characterised by closely packed interference peaks. The interferograms for the two uncabled fibres were quite broad with a few lobes. It was observed that the cabling process introduced some birefringence and mode coupling resulting in the nature of the observed interferogram for the cabled fibre. It was further observed that the factor ~1.4 falls within the theoretical expected range derived in section 5.3.3.

Finally, three fibres consisting of randomly spliced single mode and PMF were measured in section 5.3.6. A factor of, ~ 1.6 was obtained from the plot of single-end and forward measurements. The characteristics of these fibres were exhibited in their respective interferograms. The sharp closely packed interference peaks indicates the presence of both mode coupling and birefringence.

These three sets of results prove that the single-end interferometric technique is capable of measuring different types of optical fibres. The technique is thus suitable for measuring PMD in the field and the laboratory. The general interferometric technique is a standard PMD measurement technique which is robust and suitable for almost all PMD measurements including aerial fibres, hence a single-end measurement technique based on it possesses the same qualities. Although the single end-technique is limited in length compared to the forward technique, it can still be used to measure metropolitan networks (within 100km spans).

It was observed in literature that high PMD sections within an optical fibre link act to increase the total PMD of the link. For this reason, identifying and replacing such high PMD sections within a fibre link is an effective and cost effective way of countering the effects of PMD. Polarization sensitive optical time domain reflectometry (P-OTDR) techniques investigated in chapters 6 and 7 offer such a solution.

P-OTDR technique is a single-end reflectometric technique capable of completely characterizing an optical fibre in terms of the parameters responsible for PMD. Fibre PMD

occurs as a result of local birefringence effects. High birefringence indicates high PMD. It therefore follows that knowledge of the birefringence map within an optical fibre link provides useful information about its local PMD. The birefringence within a section of an optical fibre can be estimated by measuring the evolution of the states of polarization or degree of polarization of the signal as it propagates through a fibre.

Once the birefringence has been estimated, the beat-length and correlation length which are two important characteristic of the fibre can be estimated. Thus a fibre is completely characterized when these parameters are determined. The P-OTDR technique measures the round-trip birefringence of a fibre by monitoring the evolution of the states of polarization of the backscattered signal. The relationship between the round-trip birefringence and the SOP were presented in section 6.3. The information about the birefringence is contained in the optical power of the backscattered field as it propagates through a fibre. The technique is therefore able to retrieve birefringence information as a function of length. The P-OTDR used in this research work uses a pulse of 5ns with a peak power of 23dB. A spatial resolution of 0.5 was attained with an uncertainty of 2% on an SOP measurement. The maximum measurement range was in the order of 20km.

In section 6.4.1 various models for estimating the birefringence were discussed. Four standard single mode fibres were characterized. In section 6.4.2, it was observed that the statistics of the round trip birefringence vectors are Rayleigh distributed and fits well with the random modulus model. Following the determination of the birefringence vector, the beat length was estimated. Two other methods for determining beat-length were applied. Finally the correlation length was estimated from the autocorrelation of the round trip birefringence vectors. The mean DGD of the fibres were calculated from the already calculated beat-length and correlation lengths. To demonstrate the possibility of local measurements, subsections of lengths 500m each were also analysed and characterized. The estimated DGD values of the fibres were found to be in very good agreement with measurements made with the standard JME technique.

The estimated DGD values in chapter 6 represent the average DGD of the entire fibre or a sub section. In chapter 7, P-OTDR techniques were further explored to estimate the instantaneous DGD and root mean square DGD of the same set of fibres. In this section an

expression for estimating the root mean square differential group delay was derived and applied. This was done by applying autocorrelation theory to an expression involving the instantaneous DGD and the linear birefringence vector. Both of these measurements were implemented at a single wavelength. From the plots of instantaneous DGD vs. distance, the DGD accumulated within any segment of the fibre can be obtained. The root mean square differential, even though evaluated at a single wavelength, is still valid and represents the statistical mean of the fibre DGD. Both the instantaneous DGD and the root mean square DGD values measured with the P-OTDR technique agree very well with the standard JME technique.

Two novel single-end measurement techniques have been studied and implemented in this thesis. The advantages of these methods are that they are non-destructive, and cost effective. The interferometric technique is limited in terms of its inability to perform local measurement. However it is advantageous in terms of robustness, cost and higher PMD measurement range. The P-OTDR technique has many advantages. Firstly, it was able to characterizing fibre completely in terms of its birefringence, correlation length, beat length and DGD. From the instantaneous DGD plot, sections contributing particularly high DGDs can be identified and eliminated in order to reduce PMD. Since the P-OTDR operates at a single wavelength, it is possible to monitor or characterize live fibre via multiplexing. Both measurement techniques were found to be repeatable, accurate and agree with standard test measurements.

APPENDIX A

Polarization state	Jones vector	Stokes vector	Coherency matrix
Linear $\hat{x}$	$\begin{pmatrix}1\\0\end{pmatrix}$	$\begin{pmatrix}1\\1\\0\\0\end{pmatrix}$	$\begin{pmatrix}1 & 0\\0 & 0\end{pmatrix}$
Linear $\hat{y}$	$\begin{pmatrix}0\\1\end{pmatrix}$	$\begin{pmatrix}1\\-1\\0\\0\end{pmatrix}$	$\begin{pmatrix}0 & 0\\0 & 1\end{pmatrix}$
Linear at $\pm 45^0$	$\frac{1}{\sqrt{2}}\begin{pmatrix}1\\\pm 1\end{pmatrix}$	$\begin{pmatrix}1\\0\\\pm 1\\0\end{pmatrix}$	$\frac{1}{2}\begin{pmatrix}1 & 1\\1 & 1\end{pmatrix}$
Right-hand circular	$\frac{1}{\sqrt{2}}\begin{pmatrix}1\\j\end{pmatrix}$	$\begin{pmatrix}1\\0\\0\\1\end{pmatrix}$	$\frac{1}{2}\begin{pmatrix}1 & -j\\j & 1\end{pmatrix}$
Left-hand circular	$\frac{1}{\sqrt{2}}\begin{pmatrix}1\\-j\end{pmatrix}$	$\begin{pmatrix}1\\0\\0\\-1\end{pmatrix}$	$\frac{1}{2}\begin{pmatrix}1 & j\\-j & 1\end{pmatrix}$
Elliptical	$\begin{pmatrix}\cos\chi\\\sin\chi\, e^{j\phi}\end{pmatrix}$	$\begin{pmatrix}1\\\cos 2\varepsilon\cos 2\alpha\\\cos 2\varepsilon\cos 2\alpha\\\sin 2\varepsilon\end{pmatrix}$	$\begin{pmatrix}c^2 & e^{-j\phi}sc\\e^{j\phi}sc & s^2\end{pmatrix}$ $c=\cos\chi$ $s=\sin\chi$
Unpolarized	none	$\begin{pmatrix}1\\0\\0\\0\end{pmatrix}$	$\frac{1}{2}\begin{pmatrix}1 & 0\\0 & 1\end{pmatrix}$

All vectors are normalized to a Jones vector of unit length.

APPENDIX B

ACRONYMS

ASE	Amplified spontaneous emission
CD	Chromatic dispersion
CSRZ	Carrier suppressed return-to-zero
CW	Continuous wave
DFB	Distributed feed back
DGD	differential group delay
DOP	Degree of polarization
DPSK	Differential phase-shift keying
DQSK	Differential Quadrature phase-shift keying
DSF	Dispersion shifted fibre
DWDM	Dense wavelength division multiplexing
EDFA	Erbium doped fibre amplifier
FWHM	Full width at half maximum
FWM	four wave mixing
JME	Jones Matrix Eigenanalysis
LEAF	Large effective area fibre
LED	Light emitting diode
MMM	Mueller matrix method
NRZ	Non-return-to-zero modulation
OFDR	Optical frequency-domain reflectometry
OOK	On-off-keying
OSNR	Optical signal-to-noise ratio
OTDR	Optical time-domain reflectometry
P-OTDR	Polarization optical time-domain reflectometry

PC	Polarization controller
PCD	Polarization dependent chromatic dispersion
pdf	Probability density function
PDL	Polarization dependent loss
PMF	polarization-maintaining fibre
PMD	Polarization mode dispersion
PSK	phase shift keying
PSP	Principal states of polarization
RI	Refractive index
RMM	Random modulus model
RMS	Root-mean-square
RZ	Return-to-zero
SOP	State of polarization
VCSL	Vertical cavity-surface-emitting Laser
WDM	Wavelength division multiplexing
XPM	Cross-phase modulation

APPENDIX C
RESEARCH OUTPUTS

2012

Vitalis Musara, Winston T. Ireeta, **Samuel K. Fosuhene,** Lorinda Wu and Andrew W.R. Leitch 'Tunable polarization mode dispersion emulator: Fixed polarization maintaining fiber sections and rotatable polarization orientations,' Optik, vol.123, pp. 228-234 (2012).

2011

Vitalis Musara, **Samuel K. Fosuhene**, Winston T. Ireeta, Lorinda Wu and Andrew W.R. Leitch 'Emulator with inverse trend and in first-order and second-order polarization mode dispersion,' Optics Communications, vol. 284, pp. 2690-2694 (2011).

L. Palmieri, **S.K. Fosuhene**, A.W.R. Leitch and A. Galtarossa, 'Single-end measurement of root mean square Differential group delay in single mode fibres by polarization optical time-domain reflectometry,' IEEE Photonics Technology Letters, vol. 23, no.4, pp. 260-262 (2011).

Samuel. K. Fosuhene, Timothy B. Gibbon and Andrew W. R. Leitch, 'Single-end measurement of Polarization mode dispersion based on interferometry', proc., South African Telecommunications Network and Applications Conference, (SATNAC 2011), Premier Hotel, East London, South Africa (4^{th} to 7^{th} September 2011). Published in the conference proceeding, ISBN: 9780-0-620-50893-3, Paper 246.

2010

Samuel K. Fosuhene, L. Palmieri, A.W.R. Leitch and A. Galtarossa, 'Single-end measure of differential group delay in optical fibre links,' Proc.12th Southern Africa Telecommunication Networks and Applications Conference (SATNAC 2010), Spier Estate, Stellenbosch, South Africa (5^{th} to 8^{th} September 2010). Published in the Conference Proceedings, pp.256-260, ISBN: 978-0-620-47934-9.

Samuel K. Fosuhene, L. Palmieri, A.W.R. Leitch and A. Galtarossa, 'Single-end measurement of root mean square differential group delay in single mode fibres,'36^{th} European Conference on Optical Communications (ECOC 2010). Published in conference proceedings, ISBN: 978-1-42444-8535-2, IEEE catalogue number CFP10425-ART, paper P1.05.

Winston T. Ireeta, Vitalis Musara, **Samuel K. Fosuhene** and A.W.R. Leitch, “Determining the Rate of PMD Compensation in Deployed Aerial Optical Fibres Through SOP Monitoring,” Proc. 12th Southern African Telecommunication Network and Applications Conference (SATNAC), Spier Estate, Stellenbosch, South Africa (5th to 8thSeptember 2010). Published in the Conference Proceedings, ISBN: 978-0-620-47934-9, pp. 261-265.

Samuel K. Fosuhene, Vitalis Musara, Winston T. Ireeta, and Andrew W. R. Leitch, "Forward and Single-ended Polarization Mode Dispersion (PMD) Measurements on a Tunable PMD Emulator," Poster presentation at the 55th South African Institute of Physics (SAIP) Conference, CSIR, Pretoria, South Africa (27th September to 1st October 2010). Published in the Conference Proceedings, ISBN: 978-0-620-46211-2.

Vitalis Musara, Winston T. Ireeta, **Samuel K. Fosuhene**, Lorinda Wu, and A.W.R. Leitch," The Influence of High first-order Polarization Mode Dispersion Sections on Optical Network System Performance," Proc.12th Southern African Telecommunication Network and Applications Conference (SATNAC), Spier Estate, Stellenbosch, South Africa (5th to 8th September 2010). Published in the Conference Proceedings, ISBN: 978-0-620-47934-9, pp. 273-276.

REFERENCES

A

Akhmanov, S. A. and S. Yu Nikitin. 1997. 'Physical Optics' *Oxford press*.

Andersciani, D., F. Curti, F. Matera and B. Daino. 1987. 'Measurement of group-delay difference between principal states of polarization on low birefringent terrestrial fibre cable,' *Opt. Lett.12*: 844-846.

Androuchko, L., R. A. Butler and P. Morris. 1990. 'Optical fibre technology for developing countries-the advantages and disadvantages,' *proc., Second conference on rural telecommunications*, pp. 190-195.

B

Barnoski, M. K. and S. Jensen. 1976. 'Fibre waveguides: a novel technique for investigating attenuation characteristics,' *Appl. Opt*. 15: 2112-2115.

Brinkmeyer, E. 1980. 'Backscattering in single mode fibres,' *Electron. Lett.* 16:330-33.
Born, M. and E. Wolf. 1999. 'Principles of Optics', *Cambridge University Press*.

C

Cameron, J., L. Chen, X. Bao and J. Stears. 1998. 'Time evolution of polarization mode dispersion in optical fibres,' *IEEE Photon. Technol. Lett.* 10: 1265-1267.

Cameron, J., X. Bao and J. Stears. 1999. 'Field measurements of polarization mode dispersion,' *Fibre and Int. Opt.* 18: 49-59.

Corsi, F., A. Galtarossa and L. Palmieri. 1998. 'Polarization mode dispersion characterization of single mode fibre using backscattering technique,' *IEEE J. Lightwave Technol.* 16: 1832-1843.

Corsi, F., A. Galtarossa, L. Palmieri, M. Sciano and T. Tambosso. 1999a. 'Continuous-wave back-reflection measurement of polarization mode dispersion,' *IEEE Photon. Technol. Lett.* 11:451-453.

Corsi, F., A. Galtarossa and L. Palmieri. 1999b. 'Beat length characterization based on backscattering analysis in randomly perturbed single-mode fibres', *IEEE J. Lightwave Technol.* 17: 1172-1178.

Corsi, F., A. Galtarossa, and L. Palmieri. 1999c. 'Analytical treatment of Polarization mode-dispersion by means of backscattering signal,' *J. Opt. Soc. Am.* A 16: 574-58.

Cyr, N., A. Giard and G.W. Schinn. 1999. 'Stokes parameter analysis method, the consolidated test method for PMD measurements,' *Proc. 15th National Fibre Optics conference (NFOEC'99), Chicago IL*, p.280.

Cyr, N. 1999a. 'Equivalence of the Poincaré sphere and Jones matrix analysis for determination of PMD,' *5th Optical fibre Measurement conference (OFMC'99), Nantes France, Techn. Digest 4*, pp.597-598.

Cyr, N., B. Ruchet, R. Roberge, and P. Cantin. 2003. 'Interferometric PMD measurement of an amplified link,' *Proc. 29th European Conference on Optical Communications (ECOC 2003)*, paper Mo3.7.6, pp.68-69.

Cyr, N. 2004. 'Polarization-mode dispersion measurement: Generalization of the interferometric method to any coupling regime,' *IEEE J. Lightwave Technol.* 22:794-805.

D

Derikson, D**.** 1998**.** 'Fibre Optics tests and measurements', *Prentice Hall.*

Dong, Z., J. Yul., X. Tang, and W. Jian. 2011. '432Gbit/s O-OFDM QPSK signal transmission over 400km SMF-28 with EDFA-only amplification,' *proc. optical fibre Conference (OFC/NFOEC '11)*. pp.1-3.

Dong, H. and P. Shum. 2011. 'Single-end measurement of polarization mode dispersion in optical fibres with polarization-dependent loss,' *IEEE Photon Technol. Lett.* 23:185-187.

F

Foschini, G. J. and C. D. Poole. 1991. 'Statistical theory of polarization mode dispersion in single mode fibres,' *IEEE J. Lightwave Technol.* 9:1439-1456.

Fosuhene, S. K., T. B. Gibbon and A.W. R. Leitch. 2011. 'Single-end measurement of Polarization mode dispersion based on interferometry', *proc., South African Telecommunications Network and Applications Conference, (SATNAC 2011),* Paper .246.

Fosuhene, S. K., L. Palmieri, A.W. R. Leitch and A. Galtarossa. 2010. 'Single-end measure of differential group delay in optical fibre links,' *proc., Southern Africa Telecommunication Networks and Applications Conference (SATNAC 2010),* pp.256-260.

Fosuhene, S. K., L. Palmieri, A. W. R. Leitch and A. Galtarossa. 2010. 'Single-end measurement of root mean square differential group delay in single mode fibres'. *Proc. European Conference on Optical Communications, (ECOC 2010)*. paper P1.05.

Froggatt, M. E., D. K. Gifford, S. Kreger, M. Wolfe and B. J. Soller. 2006. 'Characterization of polarization maintaining fibre using high sensitivity Optical frequency domain reflectometry,' *IEEE J. Lightwave Technol.* 24:4149-4154.

G

Galtarossa, A., L. Palmieri, M Schiano and T. Tambosso. 1999. 'Single-end polarization mode dispersion measurement using a linear polarizer,' *IEEE J. Lightwave Technol.* 17: 1835-1842.

Galtarossa, A., L. Palmieri, M. Schiano and T. Tambosso. 2000a. 'Statistical characterization of fibre random birefringence,' *Opt. Lett.* 25:1322-1324.

Galtarossa, A., L. Palmieri, M. Schiano and T. Tambosso. 2000b. 'Measurement of beat length and differential group delay in installed fibres,' *IEEE, J. Lightwave, Technol.* 18:1389-1394.

Galtarossa, A., L. Palmieri, M. Schiano and T. Tambosso. 2000c . 'Measurements of beat length and perturbation length in long single-mode fibres,' *Opt. Lett.* 25:384-386.

Galtarossa, A., L. Palmieri, M. Shiano and T. Tambosso, 2001. 'Measurement of birefringence correlation length in long single-mode fibres,' *Opt. Lett*. 26 : 962-964.

Galtarossa, A. and L. Palmieri. 2003. 'Reflectometric measurements of PMD properties in long single-mode fibres,' *Opt. Fibre Technol.* 9:119-142.

Galtarossa, A. and L. Palmieri. 2004a. 'Reflectometric measurements of polarization properties in optical fiber links' *J. Trans. on Instrumentation and Measurement*. 53: 86-94.

Galtarossa, A. 2004b. 'First and second order PMD statistical properties of constantly spun randomly birefringent fibres,' *IEEE J. Lightwave Technol*. 22: 1127-1136.

Galtarossa, A. and L. Palmieri. 2004. 'Spatially resolved PMD measurements,' *IEEE J. Lightwave Technol*. 22:1103-1115.

Galtarossa, A. and L. Palmieri. 2005. 'Reflectometric measurements of polarization properties in optical fibre *links' in Polarization Mode Dispersion, A. Galtarossa and C.R. Menyuk Ed.*, Springer.

Galtarossa, A., D. Grosso, L. Palmieri and L. Schenato. 2008. 'Distributed polarization-mode-dispersion measurement in fibre links by polarization sensitive reflectometric technique,' *IEEE Photon. Technol. Lett.* 20:1944-1946.

Galtarossa, A., D. Grosso and L. Palmieri. 2009. 'Reflectometric measurement of strain induced optical activity coefficient in single-mode randomly birefringent twisted fibres,' *proc. European conference on optical communication (ECOC '09)*. Paper 4.1.4.

Ghatak, A. J. and K. Thyagarajan . 1998. 'Introduction to fibre optics,' *Cambridge University Press*.

Gibbon, T. B., A. B. Conibear and A.W.R. Leitch. 2005. "Polarization mode dispersion: characterization of optical fibre using cross-correlation interferometry", *Rev. of scientific Instrum*. 76:1-3.

Gibbon, T. B. 2007. 'Polarization Mode dispersion compensation in an optical fibre,' *PhD Thesis,* Nelson Mandela Metropolitan University.

Gisin, N., J. P. von der Weid and J. P. Pellaux. 1991 . 'Polarization Mode dispersion of short and long single mode fibres,' *IEEE J. Lightwave Technol*. 9:821-827.

Gisin, N., R. Passy and J. P von der Weid. 1994. 'Definitions and measurements of polarization mode dispersion: Interferometric versus fixed analyser methods,' *IEEE Photon. Technol. Lett*. 6:730-732.

Gisin, N., B. Gisin, J. P. Von der Weid and R. Passy. 1996. 'How accurately can one easure a statistical quantity like Polarization-mode dispersion?,' *IEEE Photon. Technol. Lett*. 8:1671-1673.

Gordon, J. P. and H. Kogelnik. 2000. 'PMD fundamentals : Polarization Mode dispersion in optical fibres,' *proc. National Academy of Sciences (PNAS)*. 97:4541-4550.

H

Hardy, A. P. 1980. 'The role of the telephone in economic development' *Telecommunications policy*, vol.4, pp.278-286.

Healey, P. 1985. 'Review of long wavelength single-mode optical fibre reflectometric techniques,' *IEEE J. Lightwave Technol*. LT-3:876-886.

Healey, P. 1986. 'Instrumentation principles for optical time domain reflectometry,' J.Phys. E: Sci. Instrum. 19:334-341.

Hecht, J. 1999. 'Understanding Fibre Optics,' *Prentice Hall*.

Hecht, E. 2002. 'Optics,' *Pearson Education Inc*.

Heffner, B. L. 1992. 'Automated measurement of polarization mode dispersion using Jones Matrix Eigenanalysis,' *IEEE Photon. Technol. Lett*. 4: 1066-1069.

Heffner, B. L. 1993. 'Accurate, automated measurement of differential group delay dispersion and Principal state variation using Jones matrix eigenanalysis,' *IEEE Photon. Technol. Lett.* 5:1066-1069.

Heffner, B. L. 1996. 'Influence of Optical source characteristics on the measurements of polarization mode dispersion of highly mode-coupled fibres' *Opt. Lett.* 21:113-115.

Hudson, H. E. 1987. 'Telecommunications and the developing world,' *IEEE Communications*. 25:28-33.

Huttner, B., B. Gisin and N. Gisin . 1999. 'Distributed measurements with a polarization-OTDR in optical fibres' *IEEE J. Lightwave Technol*, 17:1843-1848.

J

Jones, R. C. 1941. 'A New Calculus for the treatment of optical systems I: Experimental determination of the matrix' *J. Opt. Soc. Am*., 31:448-503.

Jopson, R. M., L. E. Nelson, H. K. Kogelnik. 1999. 'Measurement of Second-order Polarization-Mode Dispersion Vectors in Optical Fibers' *IEEE Photon. Technol. Lett.*11: 1153-1155.

K

Kaminow, I. P. 1981. 'Polarization in Optical Fibers', IEEE Journal of Quantum Electronics 17: 15-22.

Kao, C. K., and G. A. Hockham. 1966. 'Dielectric-fibre surface waveguides for optical frequencies,' *proc. IEE*. 133:1151-1158.

Kapron, F. P., D. B. Keck and R. D. Maurer. 1970. 'Radiation losses in glass optical waveguides,' *Appl. Phys. Lett*. 17: 423-425.

Karlsson, M., and J. Brentel. 1999. 'Autocorrelation function of the polarization-mode dispersion vector,' *Opt. Lett*. 24:939-941.

Kay, S. M. 1988. 'Modern Spectral Estimation- Theory & Application,' *Prentice-Hall*.

Keiser, G. 2000. 'Optical Fibre Communication,' *McGraw-Hill*.

Kogelnik, H .K., R.M Jopson and L. E Nelson. 2002. 'Polarization Mode Dispersion' *in Optical fibre Telecommunications IVB, I, Kaminow and T. Li, New York Academic Press.*

L

Li, M-J., P. Tandon, D. C. Bookbinder, S. R. Bickham, M. A. McDermott , R. B. Desorcie, D. A. Nolan, J. J. Johnson, K. A. Lewis, and J. J. Englebert. 2009. 'Ultra-low bending loss single mode fibre for FTTH,' *Proc. Optical fibre conference. (OFC/NFOEC)*. Paper PDO10.

Li, M-J., and D. A. Nolan. 2008. 'Optical transmission fibre design and Evolution', *IEEE J. Lightwave Technol*. 26:1079-1092.

M

Mankga, M. C. 2007. 'Field and Laboratory measurements of PMD using interferometric techniques,' *MSc.Thesis Nelson Mandela Metropolitan University*.

Mears, R. J., L. Reekie, L. Jauncy and D. N. Payne. 1988. 'Low noise erbium doped fibre amplifier at 1.54mm,' *Electron. Lett.* 23:1026-1028.

Miya, T.**, Y**. Terunuma, T. Hosaka, and T. Moyashita.1979. 'Ultimate low-loss single – mode fibres at 1.55mm,' *Electron. Lett*. 15:106-108.

Mudau, E. A., L. Wu, T. B. Gibbon and A. W. R. Leitch. 2007. 'PMD measurements on undeployed and deployed aerial optical fibre cables using the interferometric technique,' Proc. *Southern Africa Telecommunication Networks and Applications Conference (SATNAC '07)*. paper 122.

Mudau, E. A. 2008. 'Characterization of Polarization effects on Deployed Aerial optical fibre in South Africa,' *MSc. Thesis, Nelson Mandela Metropolitan University*.

N

Nakazawa, M. 1983**.** 'Theory of backward Rayleigh scattering in polarization-maintaining single-mode fibres and its application to polarization optical time domain reflectometry,' *IEEE J. Quant. Electron*. QE-19: 854-861.

Namihira, Y. and J. Maeda . 1992 . 'Polarization mode dispersion measurements in optical fibres,' *Proc. Symposium on Optical Fibre Measurements (SOFM'92)*. pp.145-150.

Nelson, L. E. and R. M. Jopson. 2005.'Introduction to polarization mode dispersion in optical fibre systems', *in Polarization Mode Dispersion, A. Galtarossa and C.R. Menyuk Ed., Springer*.

O

Oberson, P., K. Julliard, N. Gisin, R. Passy and J. P. Von der Weid. 1997. 'Interferometric polarization mode dispersion measurement with femtosecond sensitivity' *IEEE J. Lightwave Technol*. 15:1852-1857.

P

Palmieri, L., S. K. Fosuhene, A. W. R. Leitch and A. Galtarossa. 2011. 'Single-end measurement of root mean square Differential group delay in single mode fibres by polarization optical time-domain reflectometry,' *IEEE Photon. Technol. Lett*. 23:260-262.

Poole, C. D. and R. E. Wagner. 1986. 'Phenomenological approach to polarization mode dispersion in long single mode fibres,' *Electron. Lett*. 19: 1029-1030.

Poole, C. D., N.S. Bergano, R. E. Wagner and H. J. Schulte. 1988. 'Polarization dispersion and principal states in a 147km undersea lightwave cable,' *IEEE J. Lightwave Technol.* 6:1187-1190.

Poole, C. D. and C. R. Giles. 1988. 'Polarization-dependent pulse compression and broadening due to polarization dispersion in dispersion-shifted fibre,' *Opt. Lett.* 13:155-157.

Poole, C. D. and J. Nagel. 1997. 'Polarization effects in lightwave systems', *in Optical Fibre Telecommunication IIIA, I. Kaminow and T.L. Koch, New York Academic Press.*

Rashleigh, S. C. 1983. 'Origins and control of polarization effects in single mode fibers' *IEEE J. Lightwave Technol.* 1:312-331.

Rojers, A. J. 1981. 'Polarization-optical time domain reflectometry: a technique for measurement of field distributions', *Appl. Opt..*, 4:1060-1074.

T

TIA/EIA-445-124(FOTP-124), ITU Rec.G650.2 and IEC 607393-1-48. 2004. 'Polarization Mode dispersion measurement for single mode optical fibres by interferometry,' *Telecommunications Industry Association (TIA) std. Arlington, VA.*

V

Visser, J., M. Leblanc, R. Salmi, A. B. Conibear and A. W. R. Leitch. 2003. 'Locating bad PMD sections with an polarization-OTDR' *Proc. Southern Africa Telecommunication Networks and Applications Conference (SATNAC'03) conference*. pp. 195-200.

Von der Weid, J. P., R. P. Passy, G. Mussi and N Gisin. 1997. 'On the characterization of optical fibre network components with optical frequency domain reflectometry,' *IEEE J. Lightwave Technol.* 15: 1131-1141.

W

Wai, P. K. A. and C. R. Menyuk. 1996. 'Polarization dode dispersion, decorrelation, and diffusion in optical fibres with randomly varying birefringence,' *IEEE J. Lightwave Technol.* 14: 144-157.

Williams, P. A. 2005. 'PMD measurement techniques and how to avoid the pitfalls' *in Polarization Mode Dispersion A. Galtarossa and C.R. Menyuk Ed. Springer.*

Williams, P. A. 2004. 'PMD measurement techniques and how to avoid the pitfalls,' *J. Opt. Fibre Comm.* 1:84-10.

Wu, L, V**.** Musara, M. C. Mangka and A. W. R. Leitch. 2006. 'Making reliable PMD measurements: the importance of polarization scrambling,' *Proc. Southern Africa Telecommunication Networks and Applications Conference (SATNAC'06)*. paper 307.

Wuilpart, M. 2001. 'Measurement of the spatial Distribution of birefringence in Optical fibres,' *IEEE Photon. Technol. Lett.* 13:836-838.

Wuilpart, M., G. Ravet, P. Megret and M. Blondel, 2002. 'Polarization mode dispersion mapping on fibres with polarization-OTDR,' *IEEE Photon. Technol. Lett.* 14: 1716-1718.

Y

Yariv, A. 1997. 'Optical Electronics in Modern Communications' *Oxford University Press*.